

---

# Galaxy groups in the COSMOS survey:

cosmic laboratories for galaxy evolution and feedback

---

Stefania Giodini



München 2010



# Galaxy groups in the COSMOS survey: cosmic laboratories for galaxy evolution and feedback

DISSERTATION

der Fakultät für Physik der Ludwigs-Maximilians-Universität München  
zur Erlangung des Grades  
Doktor der Naturwissenschaften  
Dr. rer. nat.

vorgelegt von

Stefania Giodini  
aus  
Erba, Italien

München, den 14 März 2010

---

Erstgutachter: Prof. Dr. Hans Böhringer  
Zweitgutachter: Prof. Dr. Joseph Mohr  
Tag der mündlichen Prüfung: May 12th, 2010

# Galaxy groups in the COSMOS survey: cosmic laboratories for galaxy evolution and feedback

## Abstract

Groups and clusters of galaxies occupy a special position in the hierarchy of large-scale cosmic structures, being the largest and most massive ( $\sim 10^{13} M_{\odot}$  for groups and  $\sim 10^{15} M_{\odot}$  for clusters) objects in the universe evolved enough to reach a well defined equilibrium configuration. In particular, since the growth of structures proceeds in a bottom-up sequence, galaxy groups are thought to be the clusters' building blocks, thus they are important cosmic laboratories in which to investigate the physics of structure formation through time.

In this thesis I focus on the observational study of ordinary matter (baryons) in galaxy groups in the last 9 Gyr of the life of the Universe. The baryonic mass budget of galaxy groups consists mostly of stars and X-ray emitting hot gas. I use the unique multiwavelength database of the COSMOS 2 $\mu$ m survey to investigate the groups' baryonic content, and compare its properties to that of massive clusters of galaxies. In particular I address the following general questions: are galaxy groups scaled down versions of clusters? What is the role of galaxy groups in galaxy evolution? How important are non-gravitational processes in galaxy groups?

In the first part of the thesis I study 91 X-ray groups at redshift  $0.1 \leq z \leq 1$  selected from the COSMOS survey. This sample is complemented by 27 nearby massive clusters with a robust, analogous determination of the total and stellar mass. The final sample spans a range in total mass of  $\sim 10^{13}$ – $10^{15} M_{\odot}$ . I find that that the stellar mass fraction in galaxies is a decreasing function of the total mass of the group/cluster, constraining for the first time this relation in groups. *This shows that groups are not lower mass analogous of clusters.* Adding gaseous baryons to these considerations the baryonic budget of low mass groups does not add up to the value predicted by CMB observations. Thus groups are likely not closed systems, being more strongly affected by non-gravitational processes than clusters.

Searching for a cause of the baryon deficit in groups, I quantify the importance of the mechanical energy released by radio-galaxies inside galaxy groups. By comparing this energy output to the host groups' gravitational binding energy, I find that radio galaxies produce sufficient energy to unbind a significant fraction of the intra-group medium. *These results show that non-gravitational processes such as radio-galaxy feedback play a fundamental role in determining the properties of galaxy groups.*

Finally, I perform the analysis of the composite galaxy stellar mass function (GSMF) for 118 X-ray detected galaxy groups at  $0.2 < z < 1$  in the COSMOS field. I find a dip at intermediate masses in the GSMF for field and low mass groups at  $z < 1$  for both active and passive galaxies. The dip's amplitude depends on the environment, suggesting the presence of an excess of passive galaxies at intermediate mass ( $M \sim 10^{10} M_{\odot}$ ) in groups, likely as a product of environmental effects. At high redshifts the difference between the passive GSMF for the groups and the field (at  $M > 10^{10.1} M_{\odot}$ ) decreases, suggesting that the passive galaxies at  $M > 10^{11} M_{\odot}$  are already in place in all the environments. *Therefore a substantial evolution of galaxy properties has already taken place in galaxy groups, confirming their key role in the evolution of galaxies.*



---

## Zusammenfassung

Galaxiengruppen und -haufen nehmen in der Hierarchie der großräumigen Strukturen im Universum eine Sonderstellung ein, da sie die größten und massereichsten Objekte ( $\sim 10^{13} M_{\odot}$  für Gruppen und  $\sim 10^{15} M_{\odot}$  für Haufen) im Universum darstellen, deren Entwicklung zu einer wohldefinierten Gleichgewichtskonfiguration geführt hat. Insbesondere geht man davon aus, dass Strukturen von kleinen Skalen zu Großen Skalen sequenziell anwachsen und dass Galaxiengruppen somit die Bausteine für Galaxienhaufen darstellen. Galaxiengruppen sind deshalb wichtige kosmische Laboratorien, in denen man die Physik der Strukturbildung als Funktion der Zeit untersuchen kann. In dieser Doktorarbeit konzentriere ich mich auf die Beobachtungen normaler Materie (Baryonen) in Galaxiengruppen in den im Zeitraum der letzten 9 Gyr des Universums. Die baryonische Masse in Galaxiengruppen besteht hauptsächlich aus Sternen und heißem, im Röntgenlicht strahlendem Gas. Um diesen baryonischen Massenanteil zu untersuchen, verwende ich die einzigartige Multi-Wellenlängen-Datenbank des COSMOS 2 $\square$  Survey und vergleiche die Ergebnisse zu Galaxiengruppen mit denen von massereichen Galaxienhaufen. Insbesondere widme ich mich den folgenden Fragen: Sind Galaxiengruppen kleinere Versionen von Haufen? Welche Rolle spielen Galaxiengruppen in der Entwicklung von Galaxien? Wie wichtig sind “nicht-gravitativ” Prozesse in Galaxiengruppen?

Im ersten Teil dieser Arbeit untersuche ich 91 aus dem COSMOS-Survey ausgewählte Röntgengruppen mit Rotverschiebungen von  $0.1 \leq z \leq 1$ . Diese Auswahl wird durch 27 nahe, massereiche Haufen ergänzt, deren Gesamt- und Sternmasse analog bestimmt wird. Damit umfasst die Stichprobe einen Massebereich von  $\sim 10^{13}$ – $10^{15} M_{\odot}$ . Ich stelle fest, dass der stellare Massenanteil in Galaxien eine abnehmende Funktion der Gesamtmasse der Gruppe bzw. des Haufens ist, womit diese Relation in Gruppen zum ersten Mal bestimmt wurde. *Dies zeigt, dass Gruppen nicht nur weniger massereichen Analogien von Haufen sind.* Selbst wenn man die gasförmige Baryonische Materie bei diesen Überlegungen berücksichtigt, so erreicht der Anteil an Baryonen in massearmen Gruppen nicht den Wert, der mit Hilfe von CMB-Beobachtungen vorhergesagt wird. Gruppen sind deshalb wahrscheinlich keine geschlossenen Systeme, da sie stärker von nicht-gravitativen Prozessen beeinflusst werden als Haufen. Bei der Suche nach dem Ursprung dieses Baryonendefizits in Gruppen quantifiziere ich die Bedeutung der mechanischen Energie, die von Radiogalaxien in Galaxiengruppen freigesetzt wird. Wenn ich diesen Energieausstoß mit der gravitativen Bindungsenergie der Gruppen vergleiche, so stellt sich heraus, dass die Radiogalaxien genügend Energie produzieren, um einen signifikanten Anteil des Intra-Gruppen-Mediums freizusetzen. *Diese Ergebnisse zeigen, dass nicht-gravitativ Prozesse wie die Energieausstoß von Radio-Galaxien eine grundlegende Rolle spielen, um die Eigenschaften von Galaxiengruppen festzulegen.*

Abschließend analysiere ich die zusammengesetzte stellare Massenfunktion der Galaxien (GSMF) für 118 im Röntgenbereich nachgewiesene Galaxiengruppen mit  $0.2 < z < 1$  im COSMOS-Feld. Bei mittleren Massen finde ich einen Abfall in der GSMF für Feld- und massearme Gruppen mit  $z < 1$  sowohl für aktive als auch passive Galaxien. Die Größe des Abfalls hängt von der Umgebung ab, was darauf hindeutet, dass in Gruppen mehr passive Galaxien mit mittlerer Masse ( $M \sim 10^{10} M_{\odot}$ ) vorhanden sind, wahrscheinlich aufgrund von Umgebungseinflüssen. Bei hohen Rotverschiebun-

---

gen wird die Differenz zwischen der passiven GSMF in Gruppen und für Feldgalaxien (at  $M > 10^{10.1} M_{\odot}$ ) kleiner, was darauf hinweist, dass passive Galaxien mit  $M > 10^{11} M_{\odot}$  bereits in allen Umgebungen vorhanden sind. *Damit fand bereits zu früher Zeit eine wesentliche Entwicklung der Eigenschaften von Galaxien in Galaxiengruppen statt, was ihre Schlüsselrolle in der Evolution von Galaxien zeigt.*

# Contents

<b>1</b>	<b>Introduction</b>	<b>1</b>
1.1	Galaxy Groups . . . . .	1
1.2	X-ray properties of galaxy groups . . . . .	2
1.3	Cool Cores . . . . .	5
1.4	X-ray scaling relations . . . . .	7
1.5	AGN Feedback . . . . .	8
1.6	Optical Properties of galaxy groups . . . . .	10
1.6.1	Richness of Galaxy Groups . . . . .	10
1.6.2	The color of Galaxies . . . . .	11
1.6.3	Galaxy Classification . . . . .	12
1.6.4	The morphology–density relation . . . . .	14
1.6.5	The Galaxy Luminosity Function . . . . .	17
1.6.6	Galaxy Stellar Mass and the Galaxy Stellar Mass Function . . . . .	18
1.7	The baryon mass fraction . . . . .	22
1.8	Surveys of Galaxy Groups . . . . .	23
1.8.1	The COSMOS survey . . . . .	24
1.8.2	The COSMOS photometric catalogue . . . . .	25
1.8.3	X-ray galaxy groups in the COSMOS field . . . . .	25
<b>2</b>	<b>Stellar and total baryon mass fraction in groups and clusters since <math>z=1</math></b>	<b>29</b>
2.1	Introduction . . . . .	30
2.2	The sample . . . . .	32
2.2.1	The COSMOS survey of galaxy groups . . . . .	32
2.2.2	COSMOS X-ray-selected groups: total mass estimate . . . . .	34
2.2.3	Multiwavelength photometry and photometric redshifts . . . . .	36
2.2.4	Nearby clusters . . . . .	37
2.3	Data Analysis . . . . .	38
2.3.1	Galaxy stellar mass function: completeness and extrapolation . . . . .	38
2.3.2	Total stellar mass (in galaxies) . . . . .	40
2.4	Results . . . . .	42
2.4.1	Stellar mass budget (galaxy component) . . . . .	42
2.4.2	Evolutionary considerations . . . . .	46

## Contents

---

2.4.3	The total baryon mass fraction . . . . .	47
2.4.4	Comparison with WMAP . . . . .	49
2.4.5	Impact of systematic effects . . . . .	51
2.5	Discussion . . . . .	54
2.5.1	The stellar mass fraction . . . . .	55
2.5.2	The total baryon mass fraction . . . . .	55
2.6	Conclusions . . . . .	56
	Bibliography . . . . .	58
<b>3</b>	<b>Radio galaxy feedback in X–ray selected groups from COSMOS</b>	<b>63</b>
3.1	Introduction . . . . .	64
3.2	The samples . . . . .	65
3.2.1	Radio galaxies in X–ray detected groups . . . . .	65
3.2.2	The comparison sample of massive clusters . . . . .	66
3.3	Analysis of the COSMOS group sample . . . . .	67
3.3.1	Mechanical energy input by radio galaxies in groups . . . . .	67
3.3.2	Binding energy of the intra–group medium . . . . .	68
3.4	Analysis of the galaxy cluster sample . . . . .	70
3.4.1	Mechanical energy input by radio galaxies in massive clusters . . . . .	70
3.4.2	Binding energy of the intra–cluster medium . . . . .	71
3.5	Results . . . . .	72
3.5.1	The balance of radio–input and binding energy . . . . .	72
3.5.2	Can radio galaxies offset radiative cooling in galaxy groups? . . . . .	72
3.5.3	Impact of systematic effects . . . . .	74
3.6	Discussion: the entropy in X–ray groups . . . . .	76
3.7	Conclusions . . . . .	80
3.8	Radio Images . . . . .	81
	Bibliography . . . . .	86
<b>4</b>	<b>The Galaxy Stellar Mass Function of COSMOS X–ray detected groups</b>	<b>91</b>
4.1	Introduction . . . . .	92
4.2	The sample . . . . .	93
4.2.1	Galaxy groups in the COSMOS field . . . . .	93
4.2.2	Galaxies in the COSMOS groups . . . . .	94
4.3	Analysis . . . . .	97
4.3.1	Consistency with the result from the deep fields . . . . .	97
4.3.2	Galaxy stellar mass function of COSMOS groups . . . . .	99
4.4	Results . . . . .	99
4.4.1	The shape of the galaxy stellar mass function . . . . .	99
4.4.2	Environmental Dependence . . . . .	102
4.4.3	Evolution . . . . .	105
4.5	Discussion . . . . .	107
4.5.1	Passive galaxies: environmental dependence . . . . .	107
4.5.2	Active galaxies: environmental dependence . . . . .	110
4.5.3	Evolution . . . . .	111

4.6 Summary . . . . .	111
Bibliography . . . . .	112
<b>5 Final Remarks and Future Outlook</b>	<b>117</b>
<b>Acknowledgements</b>	<b>121</b>
<b>CV</b>	<b>123</b>
<b>Publications</b>	<b>125</b>



# Introduction

## 1.1 Galaxy Groups

Not too long after the first telescopes were used, astronomers realised that the galaxy distribution in the sky was not uniform. Already in 1781, Charles Messier reported in a note that 16 of the first 91 “nebulae” of his catalogue happen to lie in the small region of the sky at the north-western edge of the constellation of Virgo and overlapping with Coma Berenices. These “clumps” of galaxies are now known as two of the innumerable clusters of galaxies that populate the Universe, each of them including hundreds to thousands of galaxies.

Our current cosmology explains the presence of these structures as the product of the evolution of the Universe. In the standard picture, we live in an expanding Universe that originated 13.8 billions of years ago from a phase of extremely high density and temperature in the Big Bang. 300,000 years later, small fluctuations of the order of  $\sim 10^{-5}$  present in the almost uniform density field, started growing due to gravitational instability. Theoretical work and simulations have shown that primordial density fluctuations eventually cease expanding with the Hubble flow once they achieve a critical overdensity, and successively collapse and virialize<sup>1</sup>.

Furthermore, we know that roughly 85% of the gravitational mass involved in the growth and dynamical evolution of the structures consists of a weakly interacting, collisionless form of matter. Because of its properties, this matter has so far escaped direct detection through effects other than gravity, and has been named “dark mat-

---

<sup>1</sup>For a virialized structure holds the virial theorem, which states that for a bound, self-gravitating, spherical distribution of mass the total kinetic energy of the objects is equal to minus 0.5 times the total gravitational potential energy. Knowing the velocity dispersion and size of the system is therefore possible to compute a total mass, which is called “virial mass”. The “virial radius” is the radius enclosing the virial mass.

## 1 Introduction

---

ter”.

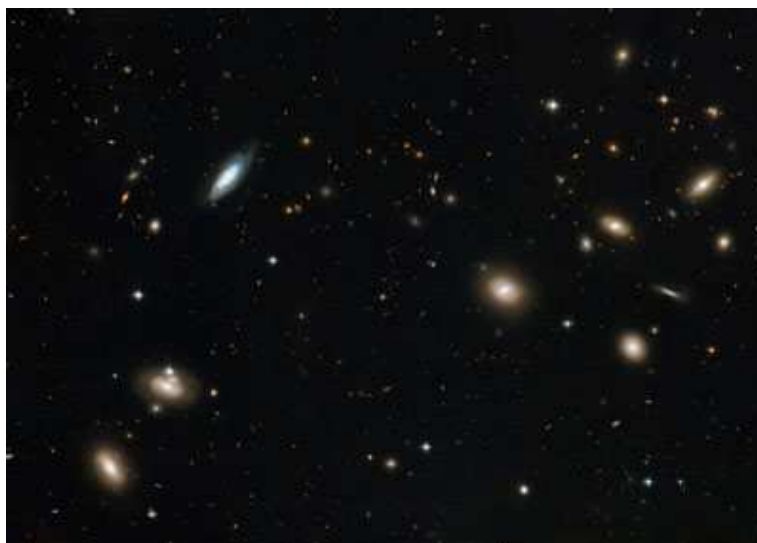
Gravity creates a huge variety of cosmic structures, but most galaxies are found in groups of no more than a few dozens members and with a total mass content of  $\sim 10^{13} M_{\odot}$ . Groups ranges from loose associations a few times denser than their surroundings to galaxy clusters, which are the largest virialized structures in the Universe, with a total mass of  $\sim 10^{15} M_{\odot}$ . However clusters are rare objects, containing only 1% of all galaxies, while gravitationally bound groups contain up to 70% of the galaxies in the universe. In the scenario of an inhomogeneous Universe, rich clusters of galaxies act as nodal points in the filamentary structure, while groups of galaxies lie like beads within the filaments.

Furthermore, groups are an unstable environments, since while galaxy formation is ongoing, the group itself may merge with other groups to build a large structure. In the current picture, dark matter cluster formation proceeds in a hierarchical bottom-up sequence: virialized haloes of small mass form first, and then grow by accretion and merging. In this sense galaxy groups are the “building blocks” of galaxy clusters.

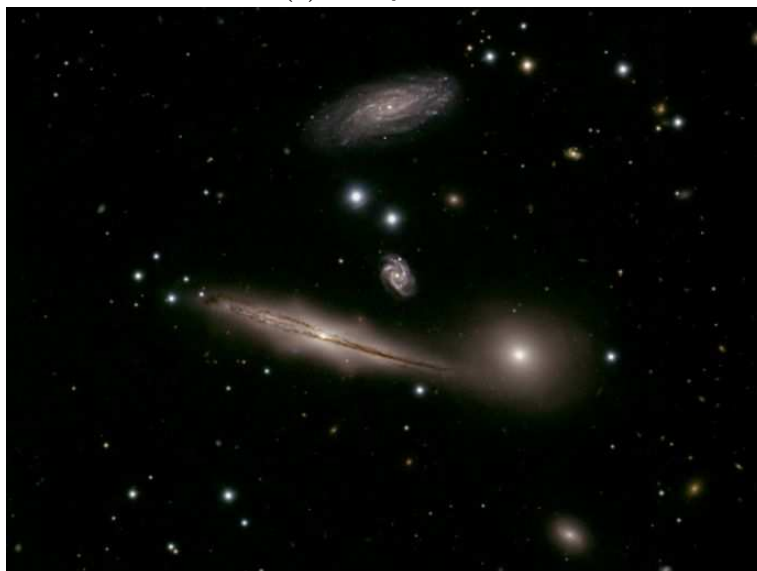
Galaxy groups are important laboratories to investigate the evolution of galaxies and the large scale structure formation. Galaxy evolution appears to be a complex, drawn-out process, involving the collapse of a matter overdensity, accretion of gas and dark matter, outright merging of distinct galaxies, gas outflows enriched with metals by supernova and active galactic nuclei (AGN) activity. Most galaxies conduct these transitions in the group environment: indeed, while 70% of the cluster galaxies are “red and dead” elliptical galaxies, the group population is a mixed bag of morphologies, suggesting that galaxy evolution is still ongoing in groups while the same evolution in clusters happened at earlier epochs ( $z > 1.0$ ). Also, the velocity dispersion in groups is lower than in clusters and comparable to that of individual galaxies, thus processes such as galaxy-galaxy merging are more prevalent in groups than in clusters.

### 1.2 X-ray properties of galaxy groups

Galaxy clusters are detected as bright, extended sources in the X-ray sky. Indeed massive clusters have internal line of sight velocity dispersion of  $500\text{--}1000 \text{ km s}^{-1}$ , and they contain a large amount of gas. Since the gas and the galaxies share the same potential, it is possible from simple arguments to estimate the temperature of the gas, which is heated at temperatures of  $10^7\text{--}10^8 \text{ K}$ . Gas at these temperatures radiates primarily in the X-ray part of the spectrum due to thermal bremsstrahlung (and some line emission), with characteristic energies of few kilo-electronvolts. The X-ray hot



(a) Galaxy Cluster



(b) Galaxy Group

Figure 1: (a) The Coma cluster is one of the richest clusters of galaxies in the Local Universe. Its total mass is  $\sim 10^{15} M_{\odot}$ . This image from the Hubble telescope is 9 arcmin across and encloses only the central part of this rich cluster. (b) HCG 87 is a nearby compact galaxy group composed of only 4 galaxies. This image by the Gemini telescope is 4 arcmin across.

gas can reach up to 15% of the total system mass. The typical X-ray luminosity of galaxy clusters is  $\sim 10^{44} - 10^{45} \text{ erg s}^{-1}$ .

In the 1990s, thanks to the launch of two important X-ray telescopes, ROSAT and ASCA, it has been firmly established that also many less massive groups of galaxies emit X-rays. However the spectral nature of the X-ray emission in galaxy groups is

## 1 Introduction

---

somewhat different than in clusters: since groups have a lower velocity dispersion, thus a lower temperature, the abundant elements are not fully ionized, and part of the flux is due to line emission. The typical X-ray luminosity of galaxy groups is  $\sim 10^{41}\text{--}10^{43}$  erg s $^{-1}$ .

There is a considerable range of morphologies in the X-ray appearance of observed groups. Most X-ray luminous clusters and groups ( $L_X > 10^{43}$  erg s $^{-1}$ ) tend to have somewhat regular morphologies, where the peak of the emission is usually coincident with a luminous early-type galaxy, which tends to be the optically brightest member of their system (BCG). In this case, the position of the central galaxy defines then the centre of the potential well, so that it lies at the dynamical centre of the system. At lower luminosities, instead, more irregular X-ray morphologies are often found, and the X-ray emission is not centred on one particular galaxy, but rather distributed around several galaxies.

The extent of the hot gas, as estimated by tracing the X-ray surface brightness profile of the system until it approaches the background value, reaches approximately the virial radius of the system. Traditionally, the surface brightness profile of a cluster is described by a hydrostatic isothermal model (“ $\beta$ -model”, e.g. Jones and Forman 1984). By analogy, this model is also adopted for groups, though this may be a coarser approximation, especially for those with an irregular morphology. However, since the sound crossing time in groups is short compared to the Hubble time<sup>2</sup>, the intra-group medium should generally be in hydrostatic equilibrium to a good approximation. With King’s (1962) analytic approximation to the isothermal sphere, the X-ray surface brightness at a projected radius  $R$  is then given by:

$$S(R) = S_0 \left[ 1 + \left( \frac{R}{r_c} \right)^2 \right]^{(-3\beta+0.5)} \quad (1)$$

where  $r_c$  is the core radius of the gas distribution and  $\beta$  is derived by the ratio of the specific energy in galaxies to the specific energy in the hot gas and depends on the temperature<sup>3</sup>. This profile can then be converted to a gas density profile by geometric deprojection and under the assumption of spherical symmetry. If the only source of heating of the gas is gravitational and there is no efficient cooling, it is true that the gas temperature is a direct measure of the potential depth, and therefore of the total mass.

---

<sup>2</sup>The Hubble time provides an estimate for the age of the universe by presuming that the universe has always expanded at the same rate as it is expanding today.

<sup>3</sup>This is a theoretical profile (Cavaliere & Fusco-Femiano 1976) and the definition of  $\beta$  is motivated by the assumption made in the model. Observations, however, indicate that there is a discrepancy between the value of  $\beta$  predicted by this model and that estimated from the fit to the X-ray surface brightness distribution. This is nowadays still a matter of debate (e.g. Bahcall & Lubin 1994).

In particular, when the conditions of hydrostatic equilibrium and spherical symmetry are met, the total mass interior to any particular radius is a simple function of the gas temperature and gas density. Thus it is possible to obtain the hydrostatic mass estimation within a given radius ( $R$ ) as:

$$M(< R) = -\frac{kT(r)r}{\mu m_p G} \left( \frac{d \ln \rho}{d \ln r} + \frac{d \ln T}{d \ln r} \right) \quad (2)$$

where  $k$  is the Boltzmann's constant,  $T$  is the gas temperature at the radius  $R$ ,  $G$  is the gravitational constant,  $\mu$  is the mean molecular weight,  $m_p$  is the proton mass and  $\rho$  is the gas density. All the parameters of this equation may be computed directly from X-ray observations.

The typical group mass is approximately  $10^{13} M_\odot$  (one hundreds time less massive than a cluster like Coma).

Clusters and groups do not have a sharp, well defined boundary. The extent of a galaxy system is usually defined in terms of the radius within which the mass density of a group/cluster is equal to  $\Delta$  times the critical density of the Universe ( $R_\Delta$ ). X-ray mass estimates can generally be applied out to  $R_{500}$ , which is  $\sim 70\%$  of the virial radius. Beyond that, the gas density profile is not well constrained, due to the difficulty of detecting low emissivity of the X-ray gas in the cluster outskirts by past and present X-ray telescopes.

Another important property of the hot gas is the gas fraction. Groups have lower gas mass fractions within  $R_{2500}$  when compared to clusters (e.g. Sun et al. 2008). Since the gas fraction in simulated groups and clusters is directly linked to the strengths of cooling and star formation (e.g. Kravstov et al. 2005), a small value at the groups regime may imply that these processes are more efficient there. The enclosed gas fraction may also be modified by AGN feedback (Puchwein et al. 2008), thus bearing the imprint of the whole intra-cluster gas heating history.

### 1.3 Cool Cores

Early X-ray observations revealed that the intra-cluster medium in the centre of many clusters is so dense that the cooling time of the gas is much shorter than the Hubble time (e.g. Fabian & Nulsen 1977). Indeed a large fraction of systems shows a sharp X-ray brightness profile and a temperature drop in the inner  $\sim 100$  kpc.

These observations led to the development of the cooling-flow model. In this model the intra-cluster medium (ICM) at the centre of clusters with dense cores hydrostatically cools, so that the cool gas is compressed by the weight of the overlying gas

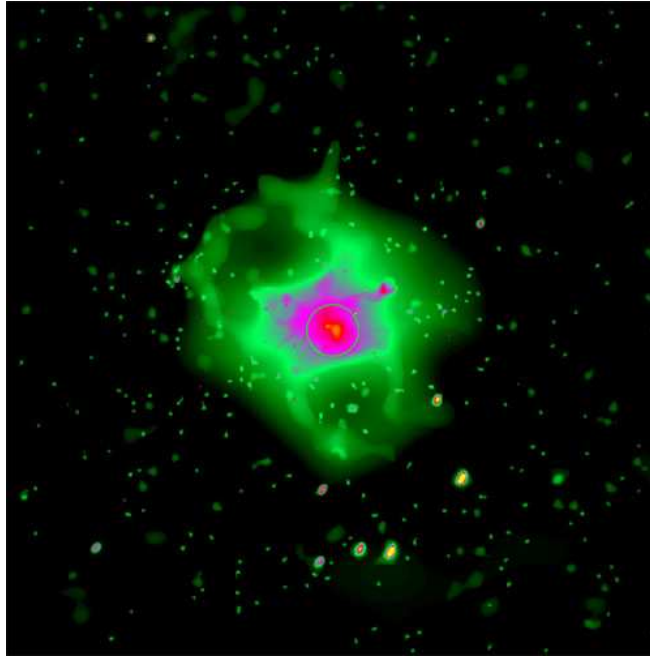


Figure 2: Chandra image of HCG 62, a galaxy group with  $L_X \sim 10^{43}$  erg s $^{-1}$  [Credit: Chandra Archive]

layers. Hot gas from the outer regions of the ICM flows in to replace the compressed gas, generating a cooling flow. However, this model predicted a large amount of star formation to happen in the centre of clusters when the gas cooled below  $10^4$  KeV, which failed to be detected with optical observations (e.g. McNamara & O’Connell 1989). More recent grating spectra from XMM-Newton (e.g. Peterson et al. 2001; Kaastra et al. 2001) have revealed that the gas in the clusters’ central region does not cool below one third of the virial temperature, or only to an amount about 1-2 orders of magnitude below the expectation. This implied the necessity of a fine-tuned heat source which would provide just enough heat to prevent all but a few percent of the central ICM from cooling out of the X-ray band. Since the cooling flow problem exists in a broad class of objects ranging from individual elliptical galaxies to the most massive clusters, the heating mechanism must be able to operate at vastly different scales. The heating mechanism must be quasi-continuous (on the time scales much longer than the cooling time) and self-tuning to the properties of a given object.

Different heating models have been invoked to explain current observations, such as: conduction (Zakamska & Narayan 2003), central AGN heating via cosmic ray-ICM interaction (Mathews et al. 2006), heating by soundwaves (Ruzkowski et al. 2004), relativistic plasma bubble injection and turbulent motion (Churazov et al. 2002; Den-

nis & Chandran 2005), mechanical heating by AGN driven bubbles (e.g. Birzan et al. 2004; Birzan et al. 2008). The failure of the classical cooling flow model has changed the nomenclature of these centrally dense clusters to cool-cores (Molendi & Pizzolato 2001).

Many groups and clusters have large and dense cool cores (e.g.  $\sim 50\%$  in the HI-FLUGCS sample, Chen et al. 2007) but it is still a matter of debate whether or not this percentage is strongly dependent on the redshift (Vikhlinin et al. 2007; Santos et al. 2008). Cool core systems are generally more dynamically relaxed when compared to non cool core ones. Furthermore observations of cool core clusters and groups at radio wavelengths have shown that a large percentage of those systems has a central radio galaxy interacting strongly with the surrounding plasma (Blanton et al. 2004; Boehringer et al. 2004; Fabian et al. 2006, Forman et al. 2006).

## 1.4 X-ray scaling relations

Clusters of galaxies, being the outcome of the process of structure formation, are mostly ruled by the physics of gravitation. In a universe with a density close to the closure density <sup>4</sup>, the amplitude of the initial density fluctuations is approximately a power law function of the length scale. So these perturbations are scale free (Kaiser 1986). Neglecting dissipation, no additional physical scale is introduced into the problem up to the gas infall into the potential wells, therefore the gas distribution in groups and clusters will also be scale-free. This condition is named “self-similarity”.

Self-similar models predict simple scaling relations between basic cluster properties and the total mass. In particular, three important correlations are the X-ray luminosity-temperature ( $L_X$ - $T$ ), mass-temperature ( $M_\Delta$ <sup>5</sup>- $T$ ) and entropy<sup>6</sup>-temperature ( $S$ - $T$ ) relations. In formulas:

$$L_X \propto T^2 \quad M_\Delta \propto T^{1.5} \quad S \propto T \quad (3)$$

These relations are of great importance for the investigation of groups and clusters of galaxies and are important diagnostics for the astrophysics of the ICM. The  $M$ - $T$  relation constrains the scale of a system. It gives a direct measurement of the system mass when its X-ray temperature is known. The  $L_X$ - $T$  relation is a proxy for the structural regularity of galaxy clusters. Since the X-ray luminosity depends on the baryon mass

<sup>4</sup>The mass density of the universe which just stops the expansion of space, after infinite cosmic time has elapsed. The closure density is the boundary value between universe models that expand forever (open models) and those that recollapse (closed models).

<sup>5</sup> $M_\Delta$  is the total mass computed at the overdensity  $\Delta$ .

<sup>6</sup>defined as  $S = \frac{kT}{n_e^{2/3}}$  where  $n_e$  is the electron density, and  $k$  the Boltzmann constant.

## 1 Introduction

---

and the temperature on the total mass, the  $L_X$ – $T$  relation can trace variations in the gas fraction. Finally, the  $S$ – $T$  relation reflects the thermodynamic and the accretion history of the ICM.

However, while clusters of galaxies seem to be mostly well behaved along these relations, observational studies of galaxy groups report deviations from self similarity for systems below 4 keV. In particular the slope of the  $M$ – $T$  ( $S$ – $T$ ) relation is consistent with the theoretical predictions only for high temperature clusters and steepens (gets shallower) for low temperature ones (e.g. Finoguenov et al. 2001; Arnaud et al. 2005; Pratt & Arnaud 2003; Ponman et al. 2003). Also, the slope of the  $L$ – $T$  relation obtained from observations is considerably steeper than the theoretically predicted one for all systems ( $L_X \propto T^3$  from soft X–ray band observation), indicating that the gas fraction depends on the temperature.

It is exactly such deviations that give us a precious diagnostic to study the thermodynamical history of the ICM. These findings indicate that non–gravitational processes may interfere with the groups physics, such as pre–heating during the systems collapse (e.g. due to star formation or shocks), radiative cooling and AGN activity.

### 1.5 AGN Feedback

It is now widely believed that supermassive black holes ( $M > 10^6 M_\odot$ ) are present in most if not all galaxies with a bulge component and that their masses are correlated with the stellar properties of their host galaxies (e.g. Ferrarese & Merrit 2000; Kormendy & Richstone 1995). The existence of these relations suggests that black holes interact strongly with their surroundings, and this interaction is called “feedback”.

Observational and theoretical considerations suggest that different channels of AGN feedback exist. At high redshift, mergers of gas rich galaxies happen frequently and funnel large amounts of cold gas towards the central region of galaxies, which can be accreted onto the black hole at high rates. The radiation energy associated with the accretion can support the enormous luminosities of a class of observed AGN called quasars. Quasars produce high velocity winds, which affect the properties of the surrounding galaxies and gas (Silk & Rees 1998; Chartas 2003).

Another channel of feedback is associated with bubbles of relativistic plasma. Such bubbles are created by the supermassive black hole and move through the thermal gas, driven by the buoyancy force. Signatures of such bubbles are observed both in radio and in X–rays (since the passage of the bubble leaves a cavity in the X–ray surrounding gas). A spectacular and well studied example is the Perseus Cluster ( Figure 4).

A unified model that accounts for the different modes of black hole feedback in a

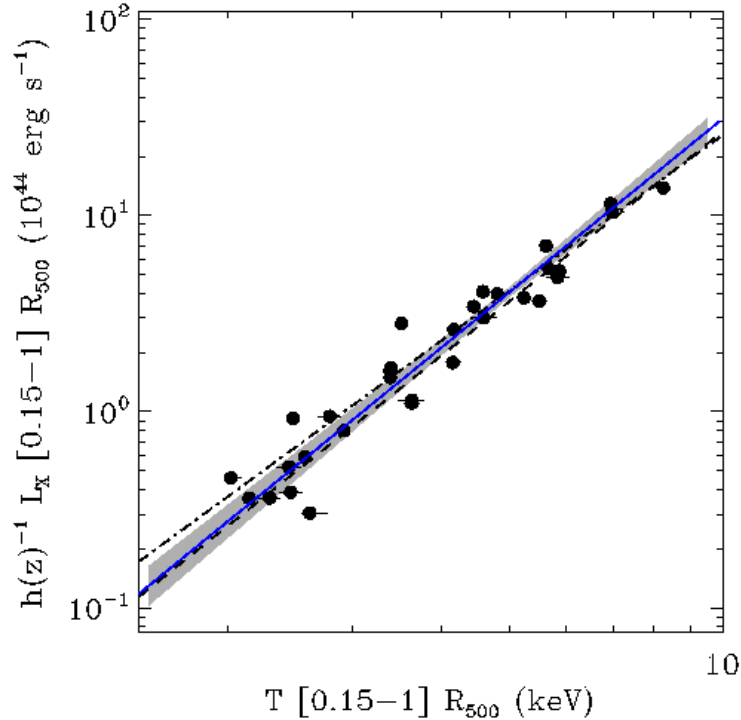


Figure 3:  $L_X$ - $T$  relation for the REXCESS galaxy cluster sample presented in Pratt et al. (2009). The quantities are computed in an aperture of  $0.15R_{200} < R < R_{200}$  to avoid the contribution of the cool core (see section 1.3) and reduce the scatter in the relation.

cosmological framework has been proposed, by analogy with observational finding on X-ray binaries (Fender et al. 1999; Gallo et al. 2003). Indeed X-ray binaries switch between a low/hard state, where a radio jet is present and the observed spectrum is hard, and a high/soft state, in which the jet shuts off and a softer X-ray spectrum is observed. This dichotomy has been interpreted with a differently radiatively efficient accretion. In a similar fashion, a “two-mode” model has been proposed to explain AGN feedback in clusters (Sijacki et al. 2007): for high-accretion rates a quasar-like feedback occurs, while for states of low accretion feedback via mechanical bubbles applies (radio-mode).

Simulations show that the bulk of the BH growth occurs at high accretion rates, corresponding to radiatively efficient AGN activity, while the relative importance of the radio mode grows towards late times, and becomes large in clusters of galaxies at  $z < 1$  (Sijacki et al. 2007; Puchwein et al. 2008).

This simple model, currently intensively discussed in the literature, assumes that an outflow of relativistic plasma from the supermassive black hole is responsible for transferring the energy to the thermal gas. Cavities, shocks, ripples in the distribution of

## 1 Introduction

---

the thermal gas are now observed in many clusters with cool cores, clearly showing that the mechanical interaction of the radio plasma with the thermal gas is strong and that the gas is disturbed by the activity of the nucleus. Furthermore, bubbles of relativistic plasma, created by the supermassive black hole, move through the thermal gas, driven by buoyancy forces. Therefore, supermassive black holes are a very attractive solution as a source of heating, since they can provide large amounts of energy, extracted from the gravitational energy of accreting matter. The Eddington luminosity<sup>7</sup> for a  $10^9 M_{\odot}$  black hole is of the order of  $10^{47} \text{ erg s}^{-1}$ . This energy is more than enough to offset the gas cooling losses in the strongest cooling flows, even if one considers a moderate efficiency of the heating mechanism. Moreover a self-tuning of the energy release is possible through the modulation of the accretion rate onto the black hole (e.g. Nulsen 2004, Böhringer et al. 2004b, Chandran 2005). Indeed AGN feedback is a self-regulated mechanism, which can be understood with a simple toy model (Churazov 2002): the ICM responds to the AGN heating by expanding and thus lowering the gas density and the accretion rate. The latter regulates the AGN energy output, lowering it. As the gas radiates away the energy, the atmosphere around the AGN contracts, and thus the accretion rate rises again, starting another cycle of AGN activity.

### 1.6 Optical Properties of galaxy groups

When observed with optical telescopes, galaxy groups appear as definite, localised overdensities of galaxies, with up to a few tens of galaxies concentrated in the plane of the sky. Groups of galaxies are classified by their optical properties: richness (number of members), galaxy content (spiral-rich, spiral-poor, or elliptical-rich), member galaxies' color, stellar mass. When considering the optical properties, galaxy groups provide a natural and continuous extension to lower richness, mass, size, and luminosity from the rich and rare galaxy clusters.

#### 1.6.1 Richness of Galaxy Groups

Abell (1958) produced a first catalogue of several thousands clusters and groups detected through visual inspection of optical plates from the Palomar All Sky Survey. He also introduced a first classification based on richness, i.e. the approximate number of galaxies composing the system. This was estimated as the background-corrected number of galaxies brighter than  $m_3 + 2$  (where  $m_3$  is the magnitude of the third

---

<sup>7</sup>The Eddington luminosity is defined as the point where the gravitational force inwards equals the radiation force outwards, assuming hydrostatic equilibrium and spherical symmetry.

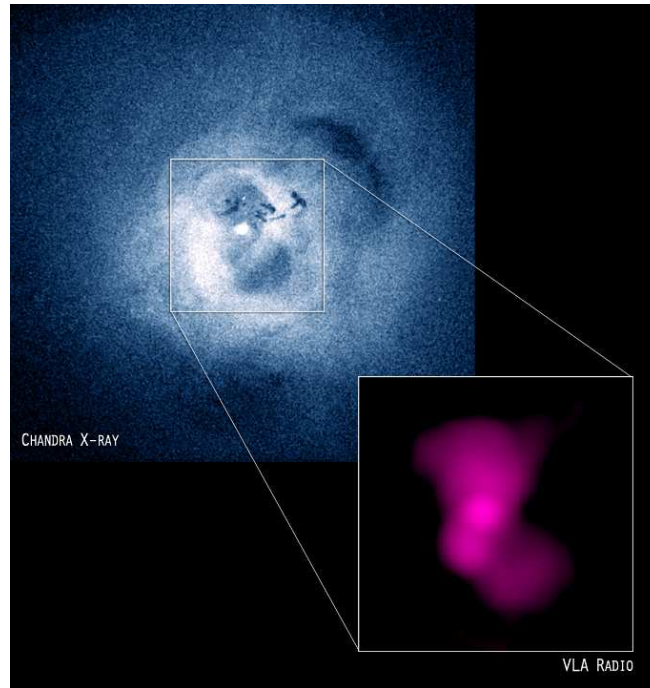


Figure 4: The CHANDRA image of the Perseus Cluster along with the radio emission from the central regions. The radio emission fits neatly inside the cavities in the X-ray emission. (Image courtesy CHANDRA)

brightest cluster member) within a radius of  $R=1.5h^{-1}$  Mpc of the system’s center. By this definition everything that contains more than 50 galaxies above this threshold is classified as a galaxy clusters.

### 1.6.2 The color of Galaxies

When we image a galaxy with an optical telescope, the observable quantity we can directly obtain is the flux emitted in a certain wavelength, which then can be translated into magnitude. Imaging a galaxy with filters centred at different wavelengths enable us to reconstruct its spectral energy distribution (SED), which is usually dominated by starlight in the UV to near-infrared wavelength domain, with a small fraction of the light coming from glowing interstellar gas. The difference between the magnitude in two filters is called “color”. Depending on the relative contribution of different stellar populations to the SED, a galaxy may be classified as “red” or “blue”. In general galaxies with a high contribution of cool stars (which emit at visual/infrared wavelengths) and a low contribution of hot stars (which emit at shorter wavelengths) are

## 1 Introduction

---

classified as “red”. Since the galaxy color is linked to the presence of star-formation activity, often red galaxies are referred to as passive, and blue galaxies as active. The former have older and more metal-rich stellar population with respect to the latter. Absorption and scattering of stellar light by interstellar dust modify the intrinsic stellar SED, thus can bias the color classification of a galaxy. Dust consists of fine particles and molecules, mostly made of O, C, Mg, Si, Fe and N, produced during the evolution of stars. The size of the particles ranges between 0.1 and 1  $\mu\text{m}$ , in general, which gives the wavelength dependence of the extinction. Thus, very dusty star forming galaxies can exhibit very red colors.

In order to avoid misinterpretation, the absorption by dust is somehow modelled (e.g. Calzetti et al. 2001) when analysing a galaxy SED.

Another effect that must be taken into account is that the cosmological redshift both shifts and stretches the SED: for example, the blue light emitted by a galaxy at  $z=1$  is seen only in a red filter since its intrinsic blue emission has been redshifted into the red part of the optical spectrum. Thus, an accurate classification of galaxies at high redshift on the basis of their SEDs requires a very wide spectral coverage.

In general the occurrence of galaxies of a certain color depends strongly on the environment that hosts them. In rich galaxy clusters a large fraction of the galaxies are red. In particular, when representing the galaxies of a cluster on a color-magnitude diagram, many of those define a roughly linear sequence at a well defined red color: this feature is called “red-sequence”. The red sequence can be reproduced by a model assuming that the bright red galaxies have roughly the same stellar age but a metallicity that diminishes at decreasing luminosity (Kodama & Arimoto 1997). Since the red sequence can be rather well predicted by such models, it has been used as an indication of the cluster’s redshift (e.g. Gladders & Yee 2000).

A red sequence is present also in galaxy groups, but seems to be formed later: while the galaxy cluster’s red sequence is in place at  $z\sim 1$  that of groups is still building up (Tanaka et al. 2005). In general galaxy groups contain more red galaxies at a fixed stellar mass than the field (see Figure 5).

### 1.6.3 Galaxy Classification

The optical luminosity of galaxy groups comes mostly from that of the individual galaxies, and the amount of flux emitted at a particular wavelength is determined mostly by the properties of the stars within the galaxies. In general the properties of the stellar populations correlate with the morphology of the galaxy itself. In the observed universe there exist a variety of galaxies’ morphological types, whose schematic description can be summarised in the so-called “fork-diagram” compiled by E. Hubble

## 1.6 Optical Properties of galaxy groups

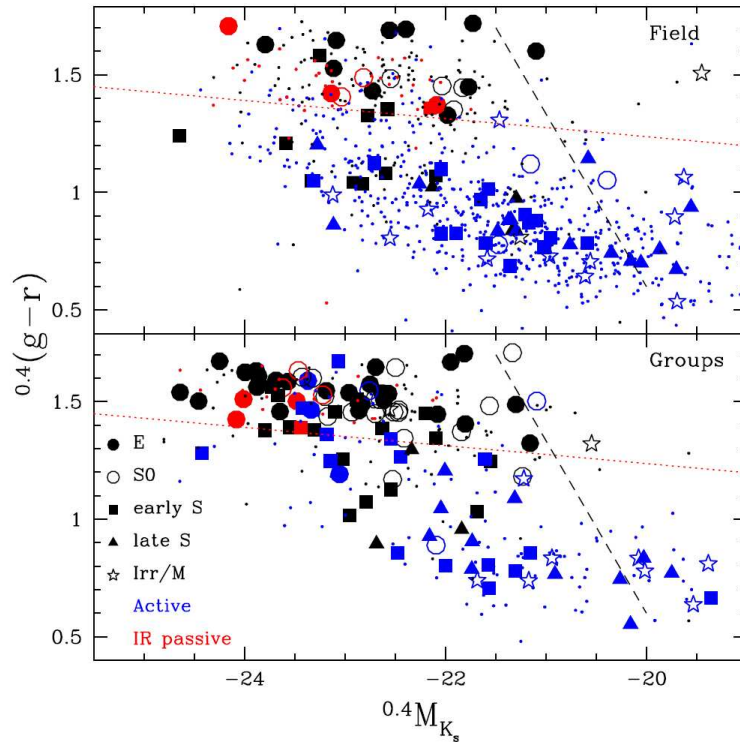


Figure 5: A color–magnitude diagram for groups and the field at  $z=0.25\text{--}0.55$  from Balogh et al. (2009). Galaxy groups contain more red galaxies than the field at a fixed stellar mass (traced by the K–band magnitude on the x axis). This picture also shows that the field does not have a defined red sequence.

(1926). The Hubble classification recognizes four principal types of galaxies: elliptical, lenticular, spiral and irregular.

Essentially the Hubble classification scheme is based on the relative proportions of the two major structural parts of the luminous component of galaxies, namely the bulge and the disk.

The bulge is generally made of a relatively old and evolved stellar population, and is shaped like an ellipsoid with various degrees of flattening and oblateness (no flattening or oblateness means we are dealing with a sphere). In general bulges at  $z=0$  contain no appreciable amount of dust and gas, and therefore host no star formation activity; when star formation ends the luminosity of a galaxy is dominated by the light of low mass stars, which emit at red and infrared wavelength<sup>8</sup>, and therefore bulges are characterized by red colors.

<sup>8</sup>Stars are optically thick spheres of plasma, emitting light as a black body from the surface (photosphere). Therefore, a star of a given mass (temperature) emits light at a peak wavelength for the photospheric temperature which can be calculated by Wien's law i.e.  $\lambda_{peak}=bT^{-1}$ .

## 1 Introduction

---

The disk is composed by a mixture of old and young stars and by gas and dust, and it is frequently site of star formation activity. Its colors are generally bluer than those of the bulge, because massive stars on the red sequence dominate the spectral energy distribution at blue wavelengths. The most visually striking feature of the disk is the frequent presence of spiral arms: these are produced by density waves excited by the differential rotation of the disk and contain active regions of star formation.

From the point of view of dynamics, the bulge usually shows very little amount of rotation, and stars in it have large thermal motions whereas the motion of stars in the disk is governed by its rotational velocity, and self-gravity and centrifugal force balance each other.

In this sense, the Hubble diagram is not only a classification of galaxy morphology but it reflects some important physical properties of galaxies, such as the age and the dynamics of their stellar population.

Elliptical galaxies are composed by a spheroidal-like bulge and have no disk. Lenticulars are essentially elliptical galaxies with a very thin disk which gives them the shape of a lentil. Spiral galaxies have a central bulge surrounded by an extended disk with a pattern of spiral arms. In barred spiral galaxies the arms emerge from the ends of what looks like a rigid bar, or elongated ellipsoid of stars and luminous material that straddles the central nucleus. The Milky Way belongs to this category. Irregulars tend to resemble disk galaxies where the spiral arms are not regularly defined, or absent.

The galaxies that occupied the left part of the Hubble diagram have been named “early-type”, while those on the right side “late-type”. Hubble took these terms from spectral classification of stars to signify a sequence related to complexity of appearance, albeit based on images, not spectra (see Baldry et al. 2008 for a review on Hubble’s nomenclature). Such nomenclature has remained, and today it is common to refer to ellipticals and lenticulars as early-type galaxies, and to spirals and irregulars as late types galaxies.

### 1.6.4 The morphology density relation and environmental effects in galaxy groups

The census of the morphology of galaxies within galaxy groups has shown a striking difference when compared to the field. In particular early type galaxies tend to populate galaxy clusters and groups, while the contribution of spiral galaxies to the total galaxy budget (spiral fraction) increases when moving towards less dense environment (Oemler 1974; Dressler 1980).

This finding reflects the so-called morphology–density relation, which expresses the link between the occurrence of specific Hubble types and the local density. Since the

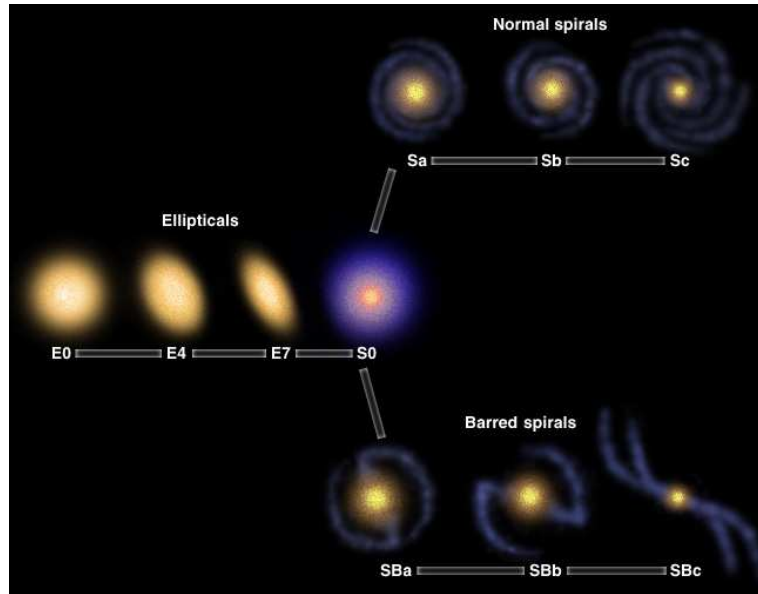


Figure 6: The “tuning fork” diagram compiled by E. Hubble. (Courtesy University of Texas, McDonald Observatory)

color is tightly bound to the galaxy morphology and to the level of star formation activity, red and passive galaxies are more frequent in high density environments, while blue and actively star forming objects populate mostly low density ones.

This relation, however, evolves with redshift, and recent studies conducted with HST have shown larger spiral fractions in higher redshift galaxy clusters (Dressler 1994; Dressler 1997).

The evidence of high occurrence of actively star forming galaxies in distant clusters has been found from photometric studies which analysed the distribution of blue galaxies at different redshifts (Butcher & Oemler 1978; Kodama & Bower 2001). The same studies show that the galaxies with red colors in distant clusters contain very old stellar populations formed at  $z > 2$ , and evolved passively since then (Ellis 1997).

The existence of such relations suggests that the environment of a galaxy may have significantly affected its evolution. To understand how the environment shapes galaxy evolution is of crucial importance in the framework of the hierarchical formation and evolution of structure. Indeed, while structures grow, galaxies experience different environmental conditions throughout the cosmic history. In particular the environmentally driven processes which are usually considered to be influential on the evolution of galaxies are the following:

## 1 Introduction

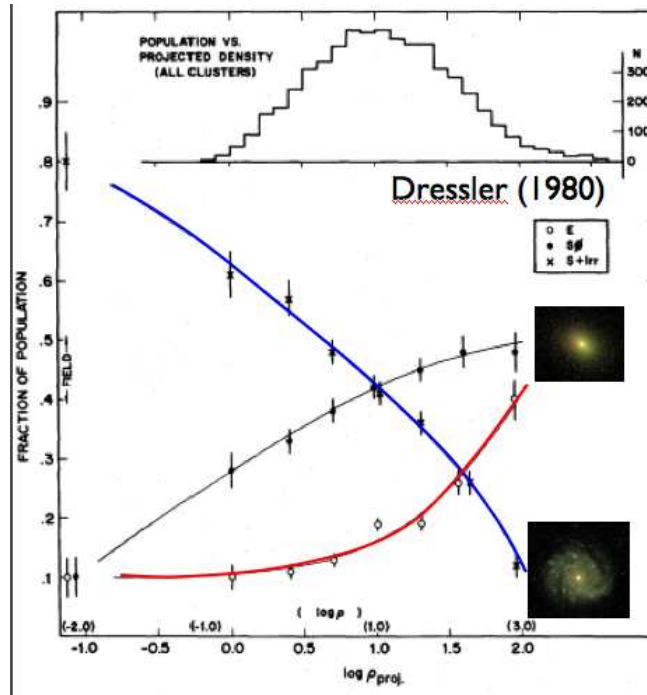


Figure 7: The morphology–density relation found by Dressler (1980) in galaxy clusters. The fraction of early–type galaxies increases with increasing density, while the fraction of late–types decreases.

1. *Mergers*: strong interactions between galaxies and merging are more efficient when the relative velocity among galaxies is low, therefore in groups of galaxies rather than in clusters (Toomre & Toomre 1972).
2. *Harassment*: the cumulative effect of the gravitational interactions in high velocity encounters truncates the galaxy star formation in  $\sim 10^7$  years (Moore et al. 1995).
3. *Gas Stripping*: The interaction between galaxies and the intergalactic medium. The stripping of the gas is mostly due to the effect of the ram pressure which is efficient in very dense environments, and when the relative velocity of galaxies is high. These conditions are achieved in the core of rich galaxy clusters (Gunn & Gott 1972).
4. *Strangulation*: the removal of the galaxy cold gas supply happens when the galaxy fall in a more massive dark–matter halo. This process inhibits the star formation, which dies out on a timescale of  $\sim 10^9$  years.

### 1.6.5 The Galaxy Luminosity Function

One very powerful tool to describe quantitatively the properties of galaxies is a statistic called the “luminosity function”, which provides information on the relative frequency in space of galaxies with a given luminosity (Binggeli 1988).

The reason of coupling together the luminosity and the abundance of galaxies is that this reflects an important set of physical properties. The luminosity of the galaxies is a measure both of their stellar content and of their star formation activity: the former is generally correlated with the total mass of the galaxy, the star formation and merging history, while the latter provides the rate at which the stellar content of a galaxy is increasing. On the other hand, the volume density of galaxies is a prediction of the theory of structure formation through gravitational instabilities, and is tightly linked to the cosmological parameters  $\Omega$  and  $\Omega_\Lambda$ <sup>9</sup>. Thus by coupling together the information on the luminosity and numerical abundances of galaxies, the luminosity function provides synthetic information on the formation and evolution of both the star formation history of galaxies and the cosmological parameters.

The luminosity function of local galaxies has been measured with good accuracy: it shows that fainter galaxies are much more numerous than brighter ones. The shape of the luminosity function was predicted for the first time by Fritz Zwicky in 1942: thermodynamical considerations naturally lead to the existence of a large number of low mass, faint galaxies, and consequently a steeply rising luminosity function towards low luminosities. Nowadays the most popular parametrization of the luminosity function is the so-called Schechter function (Schechter 1976):

$$\frac{dN}{dL} \propto L^{-\alpha} \exp(-L/L^*) \quad (4)$$

where  $L^*$  is  $\sim 10^{10}L_\odot$  and  $\alpha \sim 1-1.5$ , depending on the galaxy selection criterion. The characteristic luminosity  $L^*$  indicates the maximum luminosity at which galaxy formation is efficient, while the slope  $\alpha$  describes the relative contribution of low mass galaxies. This relation has been found empirically, but Press & Schechter (1974) show that the mass distribution of the underlying dark matter haloes exhibits a Schechter form: since baryons fall into dark matter haloes and produce stars one might expect a Schechter function to hold for the galaxy mass distribution (which is related to the luminosity distribution).

---

<sup>9</sup>The cosmological parameters  $\Omega$  and  $\Omega_\Lambda$  measure the total mass content of the universe and the contribution to the total density of the cosmological constant (which describes the accelerated expansion of the Universe). Their combined value decides if the universe will evolve in continuous expansion, or it will turn around and collapse. Together with the Hubble constant, these two parameters determine the age of the universe.

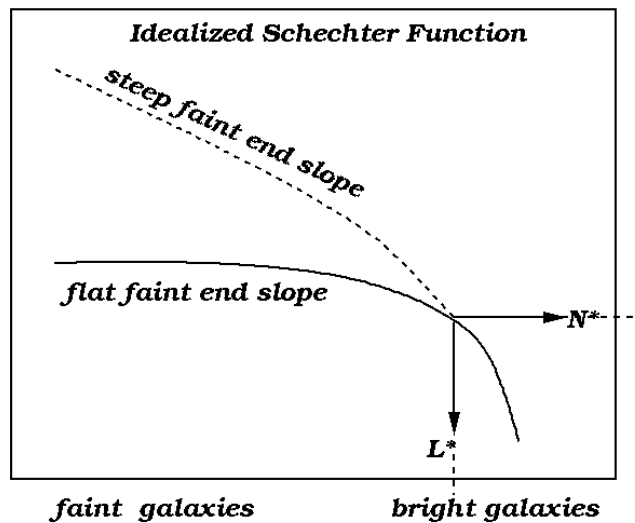


Figure 8: The Schechter function.[Credit:<http://zebu.uoregon.edu/>]

### 1.6.6 Galaxy Stellar Mass and the Galaxy Stellar Mass Function

While luminosity is the most straightforward observable, the stellar mass of galaxies is more tightly linked to the physics of star (and then galaxy) formation: this makes the galaxy stellar mass function (GSMF) an even more valuable statistics than the luminosity function.

The origin and evolution of early type galaxies seem to follow different ways and timescales as a function of their stellar mass, the so-called “downsizing scenario” (e.g. Cowie et al. 1996). As recognised by Brinchmann & Ellis (2000), to put tight constraints on the models of galaxy formation, an independent “accounting variable” is needed, which is capable of tracking the likely assembly and transformation of galaxies. A comprehensive picture has been obtained on its evolution in the interval marked by  $0 < z < 1$ . The luminosity and emission-line characteristics are transient properties and poorly suited for this purpose: during their evolution, galaxies transform from one kind to another, and their optical luminosity changes drastically during the phases of mergers. The stellar mass, instead is either conserved or slowly increasing, and is therefore an obvious choice.

Thus, reliable stellar mass estimates enable us to move beyond luminosity measurements and apply comprehensive tests to the cosmological paradigm by comparing the expected hierarchical assembly of dark matter haloes to the observed assembly his-

## 1.6 Optical Properties of galaxy groups

---

tory of the galaxy stellar mass. However, to obtain robust galaxy stellar masses, deep infrared photometry is a basic requirement. Indeed the observed infrared flux (e.g. K-band) best traces the old stellar populations, which make most of the mass of a galaxy, and is therefore a good measurement of its total stellar mass (e.g. Kauffman & Charlot 1998). Moreover, the infrared flux is only weakly affected by extinction.

The stellar mass can be derived from the direct conversion of the K-band luminosity by means of a stellar mass-to-light ratio supplied by stellar population evolutionary synthesis models. Another method is based on the combination of multi-band optical and infrared photometry, and entails the fit of the observed photometric points with a grid of synthetic galaxy templates (SED-fitting). The outcome of the SED-fitting is a set of best-fitting parameters which describe several properties of galaxies within a certain confidence; among these parameters stellar mass, photometric redshift and stellar spectrophotometric type are the most valuable.

The conversion of the infrared light into mass is an efficient method, but suffers from the lack of information on the galaxy spectral type, on which the mass-to-light ratio depends. On the other hand, the SED fitting is computationally very expensive in large surveys. A combined approach, as the one undertaken in the COSMOS survey, entails obtaining the galaxy type from the SED and then convert the K-band luminosity using a type dependent mass-to-light ratio.

Given the longer observational effort required to estimate the stellar mass of a galaxy, the galaxy luminosity function is better known than the galaxy stellar mass function. Because of their bound nature, X-ray galaxy groups and clusters are best places to perform studies on the environmental dependence of the GSMF. A crucial aspect of such investigation is whether the shape of the galaxy stellar mass function depends on the global properties of the system, such as its total mass, and if it differs from the GSMF of the field. Different studies performed on the luminosity function have investigated its dependence on the environment, concluding that the optical luminosity function of galaxies in rich clusters is universal, and there is little variation between the field and clusters (e.g. Popesso et al. 2005; De Propris & Christlein 2009). Furthermore, when separating the galaxy types, star-forming galaxies have the same luminosity function in all the environments, while quiescent ones show a significant difference, in that clusters contain a population of dwarf ellipticals which is missing in the general field (Lewis et al. 2002, Christlein & Zabludoff 2003; De Propris et al. 2003, 2004; Gomez et al. 2003; Balogh et al. 2004; Popesso et al. 2006). However, when comparing the K-band luminosity function of galaxy groups to that of rich clusters, Lin et al. (2004) show that there is a marked decrease in the number density of galaxies fainter than  $M^*$  as one moves to more massive clusters and, in addition, extremely luminous galaxies

## 1 Introduction

---

are more populated very massive clusters. The previous discussion refers to the galaxy luminosity and stellar mass function shape (see also Popesso et al. 2006).

This of course leaves several questions open: is there any significant difference between the GSMF of field and clusters, owing to their different densities and galaxy merging histories? Are groups more similar to the field or to rich clusters? What is the role of the groups in galaxy evolution?

By measuring the GSMF of galaxies in high redshift systems, and comparing to well established GSMF at low redshift, it is possible to determine how the distribution of stellar mass throughout the system's population has evolved. Ellis & Jones (2004), for example, study the K-band luminosity function of rich clusters, finding it to be consistent with purely passive evolution<sup>10</sup>. Recent results from the deep field show a weak evolution of the GSMF up to redshift  $\sim 1$  for passive galaxies, followed by a strong evolution in number density between  $z=1$  and 1.5 (Ilbert et al. 2010). Up to now no investigation of the role of groups in the build up of the GSMF exist at redshift  $> 0.1$ .

Another debated issue is the shape of the galaxy stellar mass function. Generally, Schechter fits to the galaxy stellar mass function with a faint end slope  $\alpha \sim 1$  have been found adequate to describe the galaxy population (even separated morphologically, by star-formation activity and color; e.g. Pannella et al. 2009). Recently, however, a steepening of the slope of the luminosity function at low luminosities ( $M_i < 17$ ) has been detected in the local universe, when considering galaxies belonging to clusters (e.g. Popesso et al. 2006), groups (e.g. Gonzalez et al. 2006) or the field (Blanton et al. 2005). Moreover Baldry et al. (2008) find that the local GSMF steepens as well below  $\text{Log}(M/M_\odot) \sim 9.5 M_\odot$ . From the theoretical point of view, a steep mass function of galactic halos is a robust prediction of currently popular models of hierarchical growth for cosmic structure (e.g. Kauffmann et al. 1993; Cole et al. 1994). Nevertheless hierarchical models predict that the ratio of low mass halos to massive halos is larger in low-density regions, such as the field, than in the dense cluster regions. Furthermore, a more complicated behaviour of the galaxy luminosity function has been detected in galaxy groups: there is a lack of galaxies at intermediate luminosities ( $M_B = -18$ , Miles et al. 2004)

Lately the deviation from a simple Schechter function of the luminosity/stellar mass function has been interpreted as a bimodality in galaxy properties, according to which the mass function consists of the sum of two components. However, which bimodal

---

<sup>10</sup>In the traditional monolithic collapse picture of galaxy formation (Eggen et al. 1962) all the stars in an elliptical galaxy are formed in an initial burst, and thereafter the galaxy evolves only in a passive, quiescent manner as its stars make their journey out of the main sequence. This results in a gradual dimming of the stars, and consequently the galaxy.

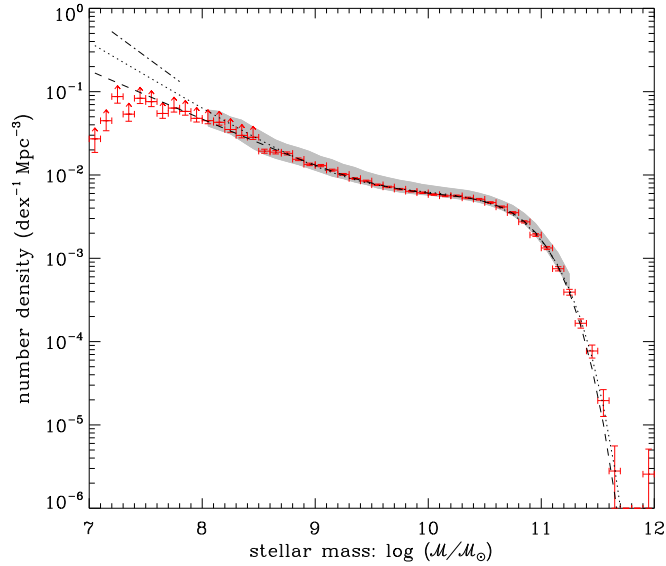


Figure 9: The galaxy stellar mass function based on  $\sim 50000$  galaxies from SDSS (Baldry et al. 2008). It shows evidence for an upturn at the low mass end, and it is fitted with a double Schechter function (dashed line).

galaxy properties can explain the observed behaviour is still a matter of debate (Bolzonella et al. 2009; Faltenbacher et al. 2010).

It has to be reminded that the major difficulties in constructing a galaxy luminosity or mass function in groups and clusters are (1) to avoid contamination from fore/background galaxies (2) to have a sufficient number of member galaxies. The best way to avoid contamination is to measure the redshift of galaxies from their spectra (spectroscopic redshift). This technique provides a precision on the measure of the distance of  $\sim 14$  Mpc comoving (limited by the cluster velocity dispersion,  $\sim 1000$   $\text{km s}^{-1}$ ), greatly reducing the contamination. Moreover it is impossible to have spectroscopy complete down to faint magnitudes. However spectroscopy is much more time consuming when compared to imaging, and taking spectra of a statistically significant number of galaxies takes long time. Other studies based on imaging data (e.g. Popesso et al. 2006), and without redshift information, have used a statistical subtraction of the background to produce the luminosity function in clusters; contamination, remains anyway a problem. In conclusion, one needs to find a trade-off between a good enough estimate of the distance and the size of the galaxy sample. The photometric redshift technique offers the best solution at the moment, since redshifts are determined from multiwavelength broad band photometry. The photometric redshift of a galaxy is estimated from the comparison of the observed SED with synthetic or observed spectra

## 1 Introduction

---

at a reference redshift. Its precision is much reduced when compared to spectroscopic redshifts (the typical precision is 0.1 compared to 0.0001 for spectroscopic redshifts), but a fairly good and inexpensive measure can be obtained for large sample of galaxies. Furthermore redshifts for galaxies that are too faint for spectroscopy can be obtained in this way. The use of photometric redshifts has greatly improved our ability of producing luminosity and mass functions out of multi-wavelength data.

### 1.7 The baryon mass fraction

Galaxy clusters can be used to study the mix of baryonic and dark matter on a scale that is representative of the matter content of the Universe. Indeed, galaxy clusters form from density fluctuations on a scale of  $\sim 10$  Mpc, and no mechanism is known to easily segregate the matter on these scales. Therefore, it is often argued that the baryonic fraction within rich galaxy clusters should reflect the universal baryon fraction  $f_b = \Omega_B/\Omega_M$ , where  $\Omega_B$  is the density parameter<sup>11</sup> for baryonic matter and  $\Omega_M$  that of all clustered matter.

An independent measure of the baryonic fraction can be obtained from primordial nucleosynthesis constraints on the light-elements abundance. When the universe was about three minutes old, the initial protons and neutrons formed helium (at a mass fraction of  $\sim 22$ – $25\%$ ), together with some traces of deuterium,  $^3\text{H}$  and  $^7\text{Li}$ , and these primordial light-element abundances depend only on the cosmic baryonic density. In particular, the deuterium abundance is most sensitive to  $\Omega_B h^2$ , and that can be estimated by observing quasar absorption lines.

Also, observations of the Cosmic Microwave Background (CMB) power spectra constrain very precisely the baryon-to-photon ratio by both the ratios of the odd and even acoustic peaks and by the Silk damping tail (Hu & White 1996, 1997). This information, together with the knowledge of the exact temperature of the CMB, fixes the value of  $\Omega_B$ .

Therefore, combining the value of  $f_b$  from cluster measurements with primordial nucleosynthesis constraints and measurements of the CMB yields an estimate of the cosmological density parameter  $\Omega_M = \Omega_B/f_b$ . This argument has been used by White et al. (1993) to prove that  $\Omega_M < 1$ , requiring to abandon one of the basic tenets of the theories of structure formation at that time.

The two known baryonic components in galaxy groups and clusters are stars and gas. The total mass of stars in the galaxies may be estimated by converting the total

---

<sup>11</sup>In general the density parameter is the ratio of the density of the given component to the critical density of the universe.

light with an appropriate mass-to-light ratio, or by adding up the stellar masses of individual galaxies. The mass in galaxies in X-ray groups is typically in the range  $3 \times 10^{11} - 2 \times 10^{12} h_{100}^{-1} M_{\odot}$  (Mulchaey 2000). The mass of the ICM can be estimated by model fitting to the X-ray surface brightness profile and X-ray spectroscopy.

However, the exact value of the baryonic fraction from galaxy clusters and groups and its agreement with the CMB measurements is still a matter of debate. Many attempts at estimating the baryon mass fraction in clusters have reported smaller values than the expected ones (Ettori 2003; Lin et al. 2003; Biviano & Salucci 2006; McCarthy et al. 2007). In addition, the discrepancy appears to be larger for groups than for rich clusters (Lin et al. 2003).

Then, some interesting questions are still open: are galaxy clusters and groups representative of the baryon content of the universe? If not, why?

## 1.8 Surveys of Galaxy Groups

Although most of the galaxies reside in galaxy groups, their identification is more difficult than for rich galaxy clusters. The reason is straightforward: groups are fainter at all wavelengths. Galaxy groups contain a lower number of galaxies than rich clusters, therefore they are less well defined in the sky, and more affected by contamination from fore/background galaxies. Therefore deeper galaxy surveys are required to identify groups, especially at non local redshifts. Also, they often show a more complicated morphology than clusters, and it is more difficult to conduct an automated search in large galaxy catalogues. The largest optical catalogue of galaxy groups is the one compiled from the *Sloan Digital Sky Survey* (SDSS; Yang et al. 2007), which contains  $\sim 8000$  groups with more than 3 galaxies at  $z < 0.2$ .

However, the most robust way to identify gravitationally bound groups is via detection of their extended X-ray emission. X-ray information enables us to easily obtain an estimate of the total mass of the systems, and thus to define a physically motivated radius to characterise a cluster/group (the virial radius, or  $R_{\Delta}$ ). However, since X-ray groups have a luminosity which is  $\sim 10-100$  times lower than that of rich clusters and that X-ray flux suffers from a large dimming effect with redshift, a robust identification of groups requires a deep X-ray survey on an area which is representative of the large scale structure of the universe at different redshifts ( $\sim 100 h^{-1} \text{Mpc}$ ; 1 degree at  $z \sim 1$  corresponds to  $\sim 40 h^{-1} \text{Mpc}$ ).

Currently, the largest catalogues of X-ray selected systems at masses lower than  $10^{14} M_{\odot}$  do not contain more than a few tens of systems (e.g. RASSCALs Mahdavi et al.

## 1 Introduction

---

2000; Heldson & Ponman 2000). The number decreases drastically at high redshift (e.g. AEGIS Jeltema et al. 2007; Gonzalez et al. 2007; CNOC2 Finoguenov et al. 2009).

In order to perform a complete study of galaxy groups, the X-ray data should also be supplemented by:

- optical data with a sufficient depth to enable the study of the evolution of galaxies within X-ray detected groups ( $i_{AB} > 23$ );
- a multiwavelength coverage to enable the reconstruction of galaxy SEDs and a robust measurement of the galaxies' photometric redshift and stellar mass;
- high resolution imaging ( $< 0.1$  arcsec), in order to reveal the galaxy morphology also at high redshift.

The only survey, up to now, which combines a large area, deep X-ray data, deep multi-wavelength information and high resolution imaging is the Cosmic Evolution Survey (COSMOS; Scoville et al. 2007).

### 1.8.1 The COSMOS survey

COSMOS is the largest survey ever made using the Hubble Space Telescope (HST). It covers 2 square degrees (a square field  $1.4^\circ$  on a side), with an exposure in I band obtained by a single orbit down to  $I_{AB} = 27$  mag. The whole survey consists of data from 640 orbits, over a period of 2 years.

The coverage of such a large area enables the sampling of the large scale structure of the universe, and reduces the cosmic variance as a source of systematic error. Indeed large scale structures as voids, filaments, groups or galaxy clusters occur on scales up to 100 Mpc comoving, and the COSMOS field can adequately map the galaxy evolution for a large range of environments. The COSMOS survey samples  $\sim 2 \times 10^6$  galaxies with  $I_{AB} < 27$  mag

The field is centred at RA= $10^h:00^m:28.6^s$ , DEC= $+02^\circ:12':21.0''$  (J2000). Here galactic extinction is exceptionally low and uniform ( $< 20\%$  variation; Sanders et al. 2007), but the infrared background is higher than in dark fields like the Lockman Hole (Scoville et al. 2006a), which are not equatorial. On the other hand, it can be observed by telescopes located both in the northern and in the southern hemisphere.

The power of COSMOS resides in coupling the unique imaging resolution of HST (0.05 arcsec) with a multiwavelength coverage from both ground and space based facilities. In particular it guarantees a full spectral coverage, with X-ray (*Chandra*

& XMM-Newton), UV (GALEX), optical (SUBARU), near-infrared (CFHT), mid-infrared (Spitzer), sub-millimetric (MAMBO) and radio (VLA) imaging. In particular the X-ray information provided by the 1.5 Msec observation time with XMM-Newton (53 pointings on the whole field, 50 ksec each) and the additional 1.8 Msec observations with *Chandra* in the central square degree enable a robust detection of galaxy groups down to  $z \sim 1.2$  (Finoguenov et al. 2007). The imaging survey is complemented by a spectroscopic program (zCOSMOS; Lilly et al. 2007) which provided 20000 spectroscopic redshifts down to  $i_{AB}=22.5$ .

Such a wealth of information is an asset for a study of the coupled evolution of stellar populations, AGN and dark matter throughout an amount of cosmic time which correspond to  $\sim 75\%$  of the age of the universe.

### 1.8.2 The COSMOS photometric catalogue

The COSMOS photometric catalogue (Capak et al. 2007; 2009) includes photometric information for  $\sim 2 \times 10^6$  galaxies in the entire field. The position of the galaxies has been extracted by the deep  $i$ -band imaging obtained with Suprime-Cam mounted on the SUBARU telescope (Taniguchi et al. 2007), and the number of galaxies is in agreement with the number counts in the same band obtained in other surveys. A limit of 80% completeness is achieved at  $i_{AB}=26.5$ . The catalogue contains the estimated magnitude for each galaxy in 30 bands, from UV to infrared, and various parameters measured by the fitting of the spectral energy distribution, such as the photometric redshift (from the SED fitting) and the guess of the galaxy spectral type (early-type; Sb/Sc; Starburst; Irregular). The availability of 30 photometric points to constrain the SED, and the use of deep infrared information, enables us to get a typical photometric redshift error of  $0.01 \times (1+z)$  ( $1\sigma$ ). The galaxy stellar mass in the catalogue is measured by the conversion of the K-band magnitude, using mass to light ratio computed in Arnout et al. (2007), and depending on the galaxy type. The typical error on the galaxy stellar mass is  $\sim 30\%$ .

### 1.8.3 X-ray galaxy groups in the COSMOS field

From a composite mosaic of the XMM-Newton and *Chandra* X-ray data, it has been possible to detect and measure the flux of extended sources (i.e., groups and clusters) down to a limit of  $10^{-15}$  erg s $^{-1}$  cm $^{-2}$ , as described in the corresponding catalogue (Finoguenov et al. 2007, in preparation).

Extended source detection was based on a wavelet scale-wise reconstruction of the

## 1 Introduction

---

image, as described in (Vikhlinin et al. 1998b), employing angular scales from  $8''$  to  $2.1'$ . Clusters and groups of galaxies were effectively selected by the spatial extent of their X-ray emission, following the approach of Rosati et al. (1998), Vikhlinin et al. (1998b), and Moretti et al. (2004).

The cluster detection algorithm consists of:

1. removal of the background;
2. detection of point-like sources (i.e. AGN);
3. removal of AGN flux from the large scale;
4. search for extended emission.

As a result, a total of  $\sim 300$  X-ray extended sources were identified in the redshift range  $0 < z < 1.6$ ; they span the rest-frame 0.1–2.4 keV luminosity range  $10^{41} \leq L_X \leq 10^{44}$  erg s $^{-1}$ , which is typically populated by groups and poor clusters.

Quality flags tag individual systems. Flag 1 is assigned to objects whose center corresponds to the X-ray peak of the source, while flag 2 objects have their spectral extraction region redefined to include only their robust association with a unique optical system. A redshift was assigned to each candidate X-ray group/cluster, corresponding to the mean of the photometric redshift (photo- $z$ ) distribution of the red-sequence galaxies as identified in Tanaka et al. (in preparation), if present, and lying within the X-ray overdensity contour region. This redshift is checked against the available spectroscopic redshifts mostly provided by the  $z$ COSMOS spectroscopic survey Lilly et al. (2007). The presence of a red-sequence is not required for the group/cluster detection: if no overdensity of red sequence galaxies is found in the photo- $z$  space, the spectroscopic data only are checked for the presence of a galaxy overdensity in the same area. Flag 3 is assigned to high- $z$  groups ( $z > 1$ ) which are not spectroscopically confirmed. Flag 4 is assigned when multiple optical counterparts are present within the X-ray overdensity contour region.

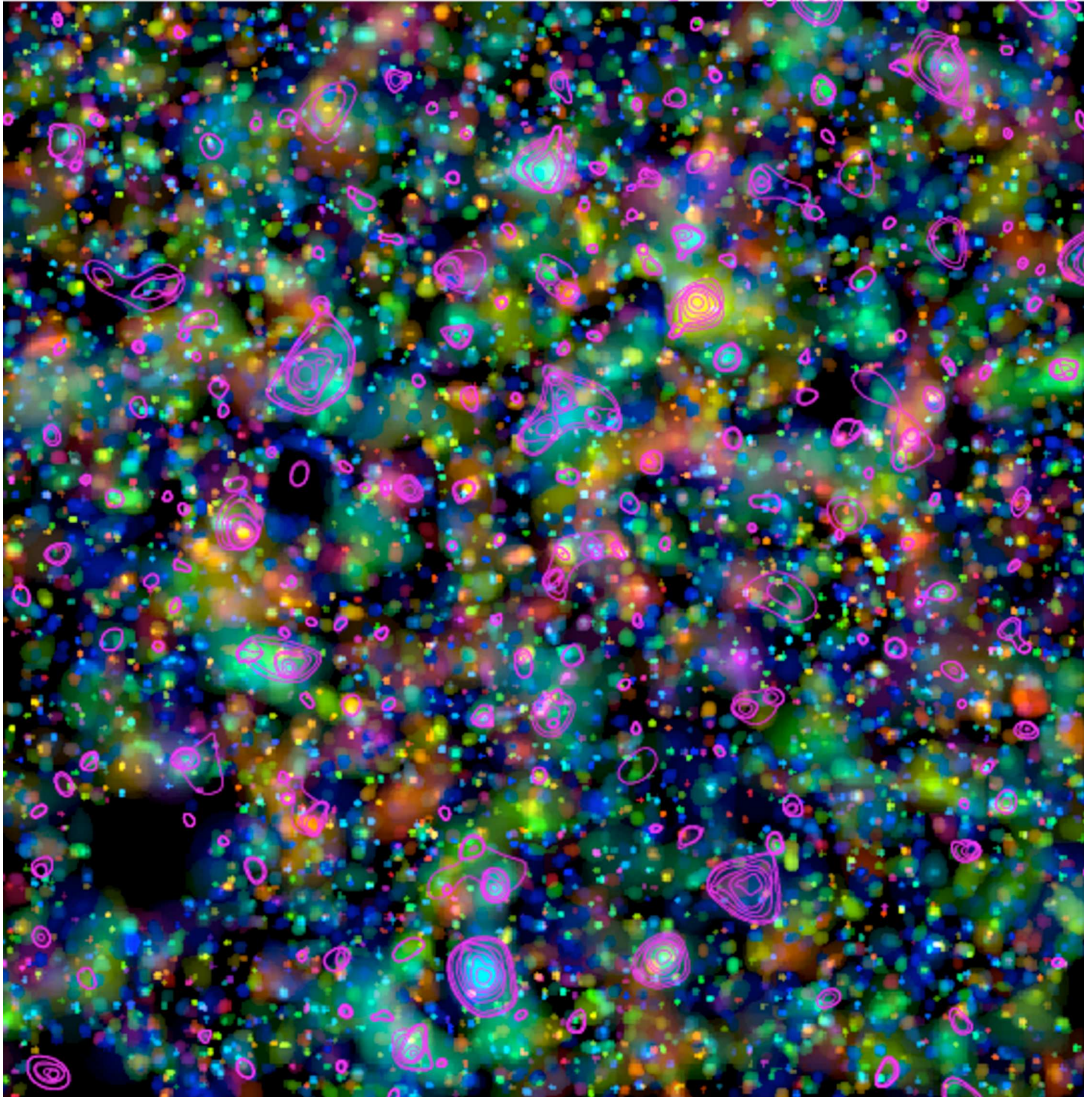


Figure 10: The wavelet reconstruction of the early-type galaxy concentrations searched in the photometric redshift catalogue is color coded according to the average redshift: blue, 0.2; cyan, 0.4; green, 0.6; yellow, 0.8; and red, 1.0. The magenta contours outline the area of the X-ray emission associated with  $\sim 300$  extended source. The image is  $1.5^\circ$  on a side [Credit: A. Finoguenov].

# 1 Introduction

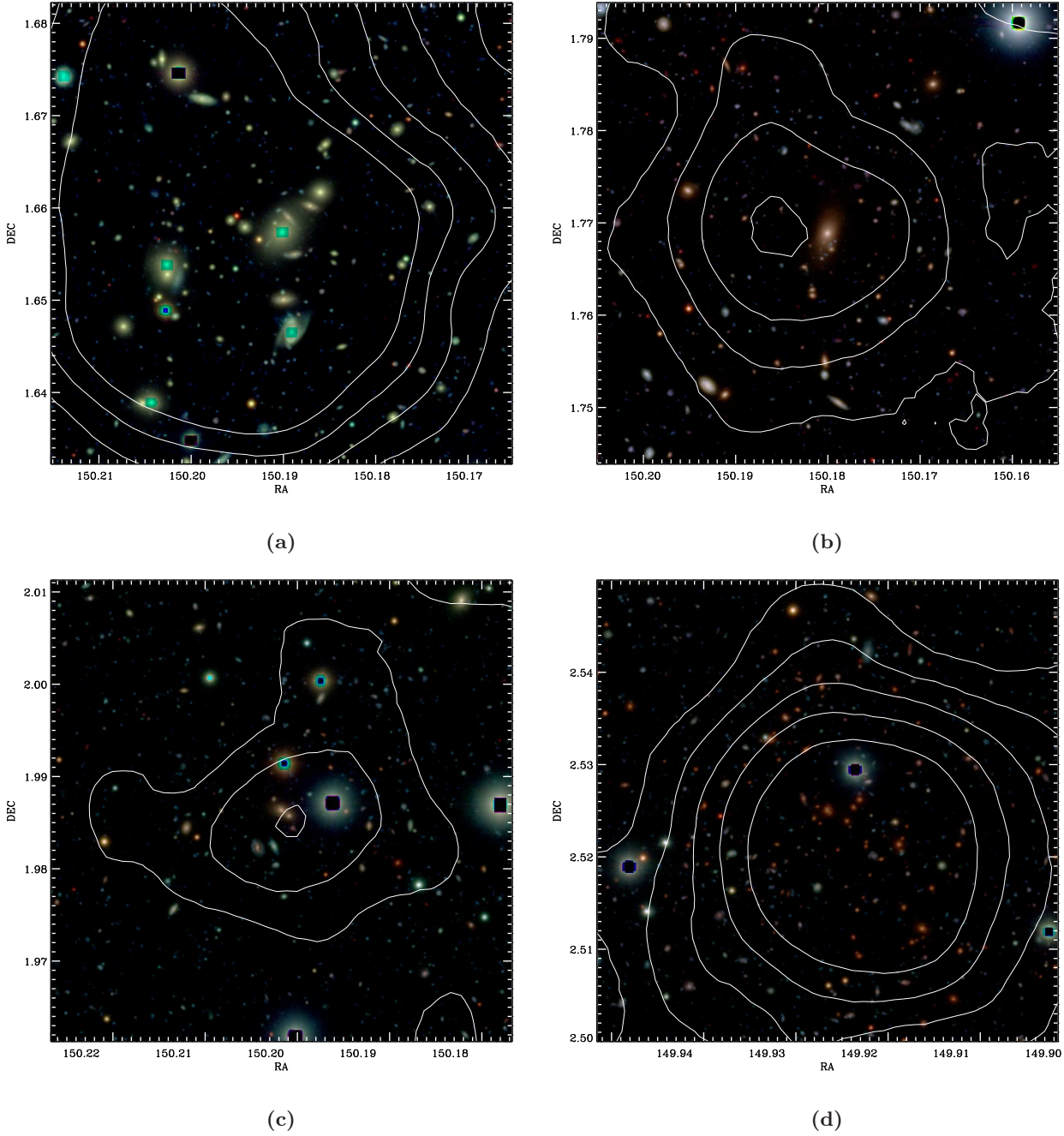


Figure 11: Three-color images for a selection of 4 groups in the COSMOS field. The images are produced using the B-V-Z filters from SUBARU. Images are 3x3 arcmin and centered on the group center. The white line shows the contours of X-ray flux significance. The contours correspond to [3, 9, 15, 21, 27]  $\sigma$  X-ray flux significance. (a) XID11 at  $z=0.22$ ,  $M_{200}=1.5 \times 10^{14} M_{\odot}$  (b) XID29 at  $z=0.35$ ,  $M_{200}=6 \times 10^{13} M_{\odot}$  (c) XID64 at  $z=0.43$ ,  $M_{200}=3 \times 10^{13} M_{\odot}$  (d) XID220 at  $z=0.73$ ,  $M_{200}=2 \times 10^{14} M_{\odot}$  is the most massive system in the survey

# Stellar and total baryon mass fraction in groups and clusters since $z=1$

*S. Giodini, D. Pierini, A. Finoguenov, G.W. Pratt, H. Boehringer, L. Guzzo, P. Capak, M. Elvis, G. Hasinger, O. Ilbert, J. Kartaltepe, A. Leauthaud, S.J. Lilly, H.J. McCracken, M. Salvato, D.B. Sanders, N.Z. Scoville, S. Sasaki, Y. Taniguchi*

*The Astrophysical Journal, Volume 703, Issue 1, pp. 982-993*

## Abstract

We investigate if the discrepancy between estimates of the total baryon mass fraction obtained from observations of the cosmic microwave background (CMB) and of galaxy groups/clusters persists when a large sample of groups is considered. To this purpose, 91 candidate X-ray groups/poor clusters at redshift  $0.1 \leq z \leq 1$  are selected from the COSMOS 2 deg<sup>2</sup> survey, based only on their X-ray luminosity and extent. This sample is complemented by 27 nearby clusters with a robust, analogous determination of the total and stellar mass inside  $R_{500}$ . The total sample of 118 groups and clusters with  $z \leq 1$  spans a range in  $M_{500}$  of  $\sim 10^{13}$ – $10^{15} M_{\odot}$ . We find that the stellar mass fraction associated with galaxies at  $R_{500}$  decreases with increasing total mass as  $M_{500}^{-0.37 \pm 0.04}$ , independent of redshift. Estimating the total gas mass fraction from a recently derived, high quality scaling relation, the total baryon mass fraction ( $f_{500}^{\text{stars+gas}} = f_{500}^{\text{stars}} + f_{500}^{\text{gas}}$ ) is found to increase by  $\sim 25\%$  when  $M_{500}$  increases from  $\langle M \rangle = 5 \times 10^{13} M_{\odot}$  to  $\langle M \rangle = 7 \times 10^{14} M_{\odot}$ . After consideration of a plausible contribution due to intra-cluster

## 2 Baryon mass fraction in groups and clusters

---

light (11–22% of the total stellar mass), and gas depletion through the hierarchical assembly process (10% of the gas mass), the estimated values of the total baryon mass fraction are still lower than the latest CMB measure of the same quantity (WMAP5), at a significance level of  $3.3\sigma$  for groups of  $\langle M \rangle = 5 \times 10^{13} M_{\odot}$ . The discrepancy decreases towards higher total masses, such that it is  $1\sigma$  at  $\langle M \rangle = 7 \times 10^{14} M_{\odot}$ . We discuss this result in terms of non-gravitational processes such as feedback and filamentary heating.

### 2.1 Introduction

The baryon mass fraction is a parameter which can be constrained by the primordial light element abundance set by the nucleosynthesis at very early times. It has been measured to a very high precision from the 5 years *Wilkinson Microwave Anisotropy Probe* (WMAP5) observations of the Cosmic Microwave Background (CMB), giving a value of  $f_b^{\text{WMAP5}} = 0.171 \pm 0.009$  (Dunkley et al., 2009)<sup>1</sup>. An independent measure of this quantity can also be achieved with galaxy clusters. These structures are large enough to be representative of the baryon content of the universe, which exists mainly in the form of X-ray emitting gas and stars. In the absence of dissipation, they are expected to provide a baryon mass fraction  $f_b$  comparable to the one measured from the CMB (White et al., 1993; Evrard, 1997).

Galaxy systems appear in a wide range of masses, from  $\sim 10^{13}$  to  $\sim 10^{15} M_{\odot}$ . In a hierarchical scenario (White & Frenk, 1991) the less massive ones, ( $M < 10^{14} M_{\odot}$ , referred as groups) are the building blocks for the most massive ones (clusters). However, the vast majority of the attempts to estimate the baryon mass fraction in nearby clusters have reported smaller values than expected (Ettori, 2003; Lin et al., 2003; Biviano & Salucci, 2006; McCarthy et al., 2007). In addition this discrepancy appears to be larger for groups than for clusters (Lin et al., 2003). Explanations for this invoke physical processes which lower  $f_b$  in clusters relative to the universal fraction (see e.g. Bialek et al., 2001; He et al., 2006), baryon components that fail detection by standard X-ray and/or optical techniques (see Ettori, 2003; Lin & Mohr, 2004), or a systematic underestimate of  $\Omega_m$  by WMAP (McCarthy et al., 2007).

McCarthy et al. (2007) extensively discuss possible explanations for the missing baryons. They concluded that the observed stellar mass function limits the contribution by low mass stars and brown dwarfs to a negligible fraction of the total stellar

---

<sup>1</sup>When the WMAP5 data are combined with the distance measurements from the Type Ia supernovae (SN) and the Baryon Acoustic Oscillations (BAO),  $f_b = \Omega_b/\Omega_m = 0.1654 \pm 0.0062$  (Komatsu et al., 2009).

mass; furthermore they rule out a contribution by large amounts of centrally concentrated gas, on the bases of inconsistencies with current X-ray data and the assumption of hydrostatic equilibrium. Consideration of the so called intra-cluster light (ICL) results into a discrepancy at the  $3.2\sigma$  level with respect to WMAP3 across the mass range  $6 \times 10^{13} - 10^{15} M_{\odot}$  (Gonzalez et al., 2007). As discussed by these authors, systematics may help reconciling their results with the WMAP estimate.

In this respect, the correct determination of the gas mass fraction may be crucial. In fact, studies of the individual baryon components (stars associated with galaxies and gas) have shown that the stellar ( $f_{500}^{\text{stars}} = M_{500}^{\text{stars}}/M_{500}$ ) and gas mass fractions within  $R_{500}$ <sup>2</sup> ( $f_{500}^{\text{gas}} = M_{500}^{\text{gas}}/M_{500}$ ) exhibit opposite behaviours as a function of the total system mass. In particular clusters have a higher gas mass fraction than groups (Vikhlinin et al. 2006; Arnaud et al. 2007; Sun et al. 2009), but a lower stellar mass fraction (Lin et al., 2003). This has been interpreted as a difference in the star formation efficiency between groups and clusters (David et al. 1990; Lin et al. 2003; Laganá et al. 2008)

On the other hand the mass dependence of the gas fraction and the discrepancy between the baryon mass fraction in groups/clusters and the WMAP value can be understood in terms of non-gravitational processes. In fact AGN-heating (which can drive the gas outside the potential well) or gas pre-heating (which inhibites the gas from falling towards the center of the potential) can explain the lack of gas within  $r_{500}$  in groups. Therefore groups appear as the critical systems to assess the universality of the baryon fraction, and to understand complex physical processes affecting both the gas and the stellar components.

Little work has been conducted on estimation of the baryon mass fraction at the group regime, mainly because of the lack of groups in existing catalogues and the difficulty of estimating masses for the individual components and the total. An insufficient sampling of the range in total mass spanned by groups and clusters is problematic for studying their overall properties in terms of mean and scatter of the population<sup>3</sup>. A galaxy group/cluster is the result of the assembly history of the dark matter halo, as well as of the star formation processes affecting the gas. Both processes lead to multivariate outcomes and produce a large intrinsic scatter in the distribution of the observed properties of groups and clusters. Therefore it is essential to have a large enough sample to be representative of the population, and unbiased by selection effects, to be able to investigate the mean trend precisely.

<sup>2</sup> $R_{\Delta}$  ( $\Delta=500,200,2500$ ) is the radius within which the mass density of a group/cluster is equal to  $\Delta$  times the critical density ( $\rho_c$ ) of the Universe. Correspondingly,  $M_{\Delta} = \Delta \rho_c(z) (4\pi/3)R_{\Delta}^3$  is the mass inside  $R_{\Delta}$ .

<sup>3</sup>The conclusions of Lin et al. (2003) and Gonzalez et al. (2007), for example, are based only on, respectively, 27 and 23 systems, but only 3 and 5 of them are less massive than  $10^{14} h^{-1} M_{\odot}$ .

## 2 Baryon mass fraction in groups and clusters

---

Once such a sample is available, interesting questions to address are: (1) How does the stellar mass fraction behave across the total range of masses? (2) Does the relation between the stellar mass fraction and the total system mass evolve with redshift? (3) How does the gas mass fraction change as a function of the system total mass? (4) Is the total baryonic fraction in groups/clusters of galaxies consistent with the WMAP5 value?

In this paper we select the currently largest X-ray selected sample of groups from the COSMOS 2 deg<sup>2</sup> survey which consists of 91 high-quality systems at  $0.1 \leq z \leq 1$ . Existing observations currently do not give constraints on the evolution of the baryonic components in individual systems at  $z \geq 0.1$ . Our data allow us to put constraints on the redshift evolution of the average stellar fraction with mass, which we find to be consistent with zero (§4.2). Observational constraints on the evolution of the average gas mass fraction also suggest zero evolution in the cluster regime (Allen et al., 2004). We assume that this is applicable to our groups in the absence of observations to the contrary and we note that simulations support this hypothesis (Kravtsov et al., 2005).

We complement our sample with 27 nearby clusters investigated by Lin et al. (2003) in order to achieve a span of two orders of magnitude in total mass ( $10^{13} < M < 10^{15} M_{\odot}$ ). In §4.3 the total mass of stars associated with galaxies is directly determined for each group, and we investigate the relation between the stellar mass fraction and the total mass of the system. In §4 we combine the stellar mass fraction estimates with the most recent determination of the relation between gas mass fraction and total mass based on a compilation of 41 local ( $z \leq 0.2$ ) X-ray groups and clusters, spanning the same range in mass as ours (Pratt et al., 2009), and we compute the total baryon fraction. We discuss results in §4.5. We adopt a  $\Lambda$ CDM cosmological model ( $\Omega_m = 0.258$ ,  $\Omega_{\Lambda} = 0.742$ ) with  $H_0 = 72 \text{ km s}^{-1} \text{ Mpc}^{-1}$ , consistently with WMAP5 (Dunkley et al., 2009; Komatsu et al., 2009). Unless otherwise stated all quantities are estimated at an overdensity of 500.

## 2.2 The sample

### 2.2.1 The COSMOS survey of galaxy groups

The *Cosmic Evolution Survey* (COSMOS, Scoville et al. 2007a) was designed to probe how galaxies, active galactic nuclei (AGN), and dark matter evolve together within the large-scale structure. The survey is based on multi-wavelength imaging and spectroscopy from X-ray to radio wavelengths and covers a 2 deg<sup>2</sup> area, including HST imaging of the entire field (Koekemoer et al., 2007). Large-scale structures in the COSMOS field have been characterized in terms of galaxy overdensity using photo-

metric redshifts (Scoville et al., 2007b), weak lensing convergence maps (Massey et al., 2007), diffuse X-ray emission (Finoguenov et al., 2007) and a combination of these (Guzzo et al., 2007). In particular, the entire COSMOS region was imaged through 54 overlapping XMM-*Newton* pointings (1.5 Ms, Hasinger et al. 2007). Additional *Chandra* observations (1.8 Ms, Elvis et al. 2006) mapped the central region to higher resolution.

In this study we use X-ray detection, gravitational lensing signal, optical photometric and spectroscopic data of the clusters and groups identified in the COSMOS survey. The X-ray data reduction is described in detail in Finoguenov et al. (2007) and Finoguenov et al. (in preparation). From a composite mosaic of the XMM-*Newton* and *Chandra* X-ray data, it has been possible to detect and measure the flux of extended sources (i.e., groups and clusters) down to a limit of  $10^{-15}$  erg s $^{-1}$  cm $^{-2}$ , as described in the corresponding catalogue (Finoguenov et al. in preparation). Extended source detection was based on a wavelet scale-wise reconstruction of the image, as described in Vikhlinin et al. (1998), employing angular scales from 8'' to 2.1'. Clusters and groups of galaxies were effectively selected by the spatial extent of their X-ray emission, following the approach of Rosati et al. (1998), Vikhlinin et al. (1998), and Moretti et al. (2004). The cluster detection algorithm consists of: (1) removal of the background, (2) detection of AGN, (3) removal of AGN flux from large scale, and (4) search for extended emission. As a result, a total of 219 X-ray extended sources were identified in the redshift range  $0 < z < 1.6$ ; they span the rest-frame 0.1–2.4 keV luminosity range  $10^{41} \leq L_X \leq 10^{44}$  erg s $^{-1}$ , which is typically populated by groups and poor clusters.

Quality flags tag individual systems. Flag 1 is assigned to objects whose center corresponds to the X-ray peak of the source, while flag 2 objects have their spectral extraction region redefined to include only their robust association with a unique optical system. A redshift was assigned to each candidate X-ray group/cluster, corresponding to the mean of the photometric redshift (photo- $z$ ) distribution of the red-sequence galaxies as identified in Tanaka et al. (in preparation), if present, and lying within the X-ray overdensity contour region. This redshift is checked against the available spectroscopic redshifts mostly provided by the  $z$ COSMOS spectroscopic survey (Lilly et al., 2007). The presence of a red-sequence is not required for the group/cluster detection: if no overdensity of red sequence galaxies is found in the photo- $z$  space, the spectroscopic data only are checked for the presence of a galaxy overdensity in the same area. Flag 3 is assigned to high- $z$  ( $z > 1$ ) not spectroscopically confirmed candidate groups. Flag 4 is assigned when multiple optical counterparts are present within the X-ray overdensity contour region. In this study only systems with quality

## 2 Baryon mass fraction in groups and clusters

---

flag 1 or 2 are considered.

The galaxy–group detection is irrespective of any optical characteristic, being based only on the presence of an X-ray extended source. The X-ray selection is an approximate selection by halo mass, due to the tight X-ray luminosity–mass relation (Pratt et al., 2009); in this regard our selection is thus unbiased with respect to both the optical properties of the groups in our sample and the X-ray characteristic of the systems. The purposes of the present study lead us to introduce three further selection criteria: (1) only candidate groups/clusters detected in X-rays with a significance higher than  $3\sigma$  on the flux determination are considered. Selection of the most robust candidates minimizes contamination by loose galaxy aggregations or superposition of AGN along the line of sight. (2) Only X-ray extended sources with  $L_X > 10^{42}$  erg s $^{-1}$  are considered, in order to limit contamination from starburst galaxies (Grimm et al., 2003) or field elliptical galaxies with X-ray halos (Diehl & Statler, 2007). (3) We limit the redshift range to  $0.1 \leq z \leq 1.0$ , where photo- $z$  of individual galaxies are most robust (Ilbert et al., 2009); furthermore, in this range the quality of the photo- $z$  is equivalent to that of low resolution spectroscopy.

Figure 22 reproduces the X-ray luminosity distribution as a function of redshift for the candidate X-ray groups/clusters within  $z=1$  (151 out of 219 systems). The flag 1+2 sample selected for this study contains 114 objects, of which 44 were present in Finoguenov et al. (2007). It contains only 3 systems at  $z \leq 0.2$  (Figure 22), which is the redshift range covered by analogous studies on  $f_b$  in groups/clusters (Lin et al., 2003; Gonzalez et al., 2007). On the other hand, it contains systems with particularly low X-ray luminosities (i.e., with  $10^{42} < L_X < 5 \times 10^{42}$  erg s $^{-1}$ ), though only for  $z < 0.5$ . The sample considered in this study is reduced to 91 objects after removal of 23 groups with unreliable estimates of the total stellar mass in galaxies (§ 2.3.2). Out of these 91 candidate groups/poor clusters, 51 are already spectroscopically confirmed (i.e. are associated with at least 3 galaxies with similar spectroscopic redshifts).

### 2.2.2 COSMOS X-ray-selected groups: total mass estimate

In the original catalogue (Finoguenov et al. in preparation),  $M_{200}$  is computed using an  $L_X$ – $M_{200}$  relation established via the weak lensing analysis in Leauthaud et al. (2010). Briefly, the COSMOS group sample is divided into nine bins that span the redshift range  $0.1 < z < 0.9$  and with  $10^{41.8} < L_X/E(z) < 10^{43.5}$  erg s $^{-1}$ , where the function  $E(z) \equiv \sqrt{\Omega_m(1+z)^3 + \Omega_\Lambda}$  represents the Hubble parameter evolution for a flat metric. Only systems with a clear, visually identified BCG are used for this analysis, to minimize issues due to incorrect centering. For each bin, the weak lensing signal is calculated from  $r \sim 50$  kpc to  $r \sim 3$  Mpc in logarithmically spaced radial bins.

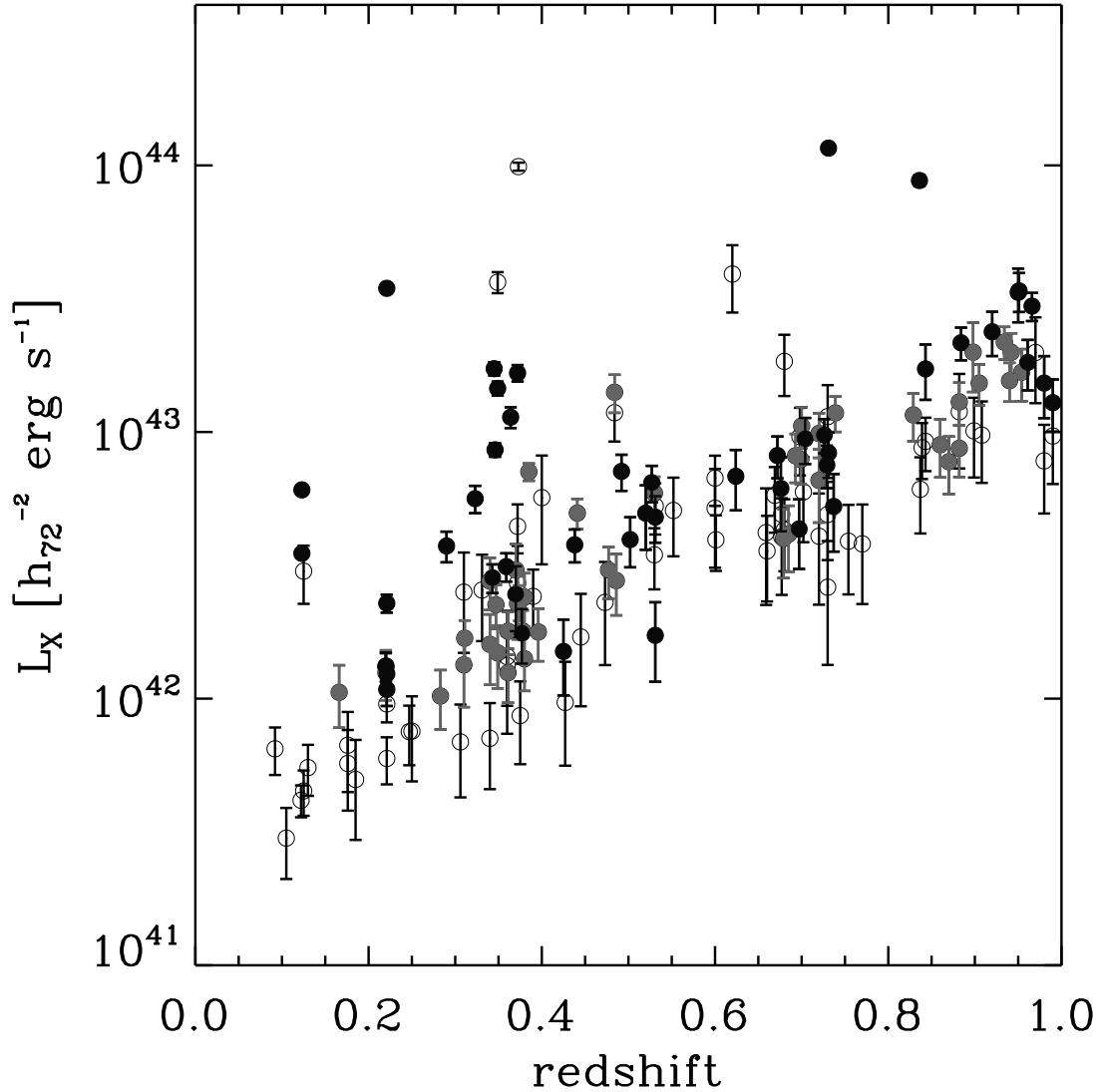


Figure 12: Rest-frame 0.1–2.4 keV luminosity vs. redshift for the 151 COSMOS candidate X-ray groups/clusters at  $0.1 < z < 1.0$ . Filled circles mark the 91 objects considered in this study: dark or light grey identifies objects with flag 1 (45) or 2 (46), respectively.

A weak lensing signal is detected all the way to 3 Mpc ensuring that the lens density is probed well beyond the virial radius. The results are fit with a parametric model which is the sum of a NFW profile (Navarro et al., 1997) and a point-source term due to the mass of the central BCG. The theoretical relation between mass and concentration from Zhao et al. (2008) has been used in the fit for the NFW component and the mean stellar mass of the central BCG’s is used in order to scale the point source term. A comparison between the relation obtained from the combination of the the COSMOS data and cluster data from Hoekstra (2007) is consistent with that obtained by Rykoff

## 2 Baryon mass fraction in groups and clusters

---

et al. (2008) based on SDSS data. We adopt the following functional form for the  $L_X$ -M relation,

$$\frac{M_{200} E(z)}{M_0} = A \left( \frac{L_X E(z)^{-1}}{L_{X,0}} \right)^\alpha \quad (5)$$

where  $M_0 = 10^{13.7} M_\odot$ ,  $L_{X,0} = 10^{42.7} \text{ erg s}^{-1}$ . Fitting only the COSMOS data yields the best fit parameters  $\log_{10}(A) = 0.106 \pm 0.053$  and  $\alpha = 0.56 \pm 0.12$  (cited errors are statistical only). Further details regarding the weak lensing analysis in COSMOS can be found in Leauthaud et al. (2010).

The baryon fraction in groups/clusters can be studied at any radius, though it is desirable to study it at the largest radius possible with respect to the virial radius of the system because of the radial dependencies of the different components. The largest radius for which reliable X-ray hydrostatic masses are available is  $R_{500}$  (e.g. Arnaud et al., 2005; Vikhlinin et al., 2006; Sun et al., 2009). Hereafter we use  $M_{500}$  instead of  $M_{200}$ , to enable a comparison at the same radius with previous studies on  $f_b$  in nearby groups/clusters. The catalogue value of  $M_{200}$  is converted into  $M_{500}$  assuming an NFW profile with a constant concentration parameter ( $c = 5$ ).

### 2.2.3 COSMOS galaxies: multiwavelength photometry and photometric redshifts

The COSMOS area has been imaged in 30 bands including broad- (SUBARU Taniguchi et al. 2007a; CFHT McCracken et al. in preparation), medium-, and narrow-bands (SUBARU; Taniguchi et al. in preparation), ranging from the far-ultraviolet (GALEX Zamojski et al. 2007) to the mid-infrared (*Spitzer* Sanders et al. 2007). This multi-wavelength dataset is collected in a master photometric catalogue. Capak et al. (in preparation) discuss in detail source detection and extraction of photometry. The COSMOS photometric catalogue is complete down to a total  $i$ -band magnitude of 26.5 AB mag. Ilbert et al. (2009) and Salvato et al. (2009) computed highly reliable photometric redshifts with unprecedented accuracy for a survey this large, owing to the extraordinarily large number of photometric bands. Redshifts were attributed to individual galaxies via a standard  $\chi^2$  fitting procedure (Arnouts et al., 2002) encoded in *Le Phare*<sup>4</sup>, written by S. Arnouts and O. Ilbert. Best-fit solutions from this photo- $z$  algorithm were trained on a composite spectroscopic sample of objects brighter than  $i_{\text{AB}} = 25$  (see table 3 in Ilbert et al., 2009), mostly made of  $\sim 4,000$  bright galaxies (i.e., with  $i_{\text{AB}} < 22.5$ ) observed as part of the  $z$ COSMOS spectroscopic survey (Lilly et al., 2007). Comparison of photometric and spectroscopic redshifts gives a typical r.m.s. scatter of the photo- $z$ 's equal to  $\sigma_{\text{photo-}z} = 0.02 \times (1 + z)$  for  $i_{\text{AB}} \leq 25$  and

<sup>4</sup>[www.lam.oamp.fr/arnouts/LE.PHARE.html](http://www.lam.oamp.fr/arnouts/LE.PHARE.html)

$z < 1.25$  (Ilbert et al., 2009). In the presence of X-ray emitting objects (AGNs), photometric redshifts were independently estimated by Salvato et al. (2009).

As a by-product of the photo- $z$  determination, spectroscopic types were attributed to individual galaxies on the basis of their best-fit broad-band spectral energy distributions (SEDs). This information is used to estimate the stellar mass of a galaxy, which is obtained from the conversion of the Ks-band luminosity (Ilbert et al., 2009) using an evolving galaxy-type dependent stellar mass-to-Ks-band luminosity ratio  $M/L_{Ks}$  (Arnouts et al., 2007). This relation has been established using a Salpeter initial mass function (Salpeter, 1955). Stellar masses of individual galaxies are contained in the COSMOS photometric catalogue; the fractional error on the stellar mass of a galaxy is typically equal to 34% , and is dominated by the mean scatter on  $M/L_{Ks}$  (Arnouts et al., 2007).

This uncertainty pertains to the aforementioned method of estimating stellar masses. Individual galaxy stellar masses may differ by a factor 2–3, depending on the method used to estimate the mass (e.g Longhetti & Saracco 2009; Küpcü Yoldaş et al. 2007). This uncertainty is the product of several factors; it mostly reflects the range of assumptions in differing models as for the star-formation history (e.g., single burst vs. multiple bursts vs. continuum star-formation activity) and the attenuation of stellar light by dust (e.g., starburst-like vs. normal star-forming disc-like). In addition, it results from different implementations of complex physics, such as the asymptotic-giant-branch phase of stellar evolution and metal enrichment). This scatter does not reflect the uncertainty of the present method, which is 34% for individual galaxies as detailed above. This latter value is the uncertainty we attribute to individual galaxy stellar masses in the present study.

#### 2.2.4 Nearby clusters

The COSMOS sample is mostly composed of groups. Therefore we complement it with a sample of 27 nearby X-ray selected clusters with sufficiently deep 2MASS photometry (Lin et al. 2003, LMS03) to estimate accurate stellar masses. The total and stellar masses were derived by LMS03 in a manner consistent with ours. In particular, the total cluster mass is estimated from an  $M_{500}-T_X$  relation. The stellar masses are estimated from the total K band luminosity of each cluster, assuming an average stellar mass-to-light ratio which takes into account the varying spiral galaxy fraction as a function of the cluster temperature.

LMS03 provide estimates of the total gas fraction obtained from either X-ray data or from a scaling relation; we use instead the most recent scaling relations of Pratt et al. (2009), based on hydrostatic mass estimates, in order to reduce systematic effects.

We apply this both to our sample and the one of LMS03.

### 2.3 Data Analysis

#### 2.3.1 Galaxy stellar mass function: completeness and extrapolation

The low-mass end of the galaxy stellar mass function of the individual COSMOS groups/poor clusters is probed to different extents by observations, since these systems span a rather large redshift range ( $0.1 \leq z \leq 1$ ). In order to achieve a common footing, the completeness in galaxy absolute magnitude (stellar mass) of the sample must be understood.

First, we divide the sample into two redshift bins (0.1–0.5 and 0.5–1.0) containing a similar number of objects, since the cosmic stellar mass density is observed to drop by a factor of 2 from  $z \sim 0$  to 1 in the field (Wilkins et al. 2008 and references therein). The completeness mass is estimated at  $z=0.5$  and  $z=1.0$  from a fit of its behaviour as a function of redshift, obtained using a sampling of 0.1 in redshift as follows (Bolzonella et al. in preparation). Firstly we derive the stellar mass ( $M_{\text{lim}}$ ) that each object would have if its apparent magnitude was equal to the sample limit magnitude (i.e.  $i_{AB}=25$ ), viz. ,

$$\log M_{\text{lim}} = \log M + 0.4 \times (i_{AB} - 25.0), \quad (6)$$

where  $M$  is the stellar mass of a galaxy with apparent magnitude  $i_{AB}$ . Secondly we derive the 95% percentile of the distribution in  $M_{\text{lim}}$  for galaxies in the lower 20% percentile in magnitude (i.e.  $i_{AB} \geq 23.6$ ) in each bin of 0.1 in redshift. Finally a fit to the corresponding envelope as a function of redshift is performed for  $0.1 \leq z \leq 1.0$ ; the ensuing values represent the stellar mass completeness as a function of redshift for our sample. Figure 13 illustrates the behaviour of the stellar mass completeness as a function of redshift.

For instance, the stellar mass completeness at  $z=1$  ( $M_{\text{compl}} = 10^{10.4} M_{\odot}$ ) is about an order of magnitude lower than the so-called “transition” stellar mass at  $z \leq 1$  (e.g. Bundy et al., 2005; Pannella et al., 2006). This confirms that a rich mixture of morphologies and, thus, star-formation histories (Sandage, 1986) is present among the member galaxies of the COSMOS X-ray selected groups/poor clusters.

We compute the total stellar mass associated with galaxies of a given system as follows. We first add the stellar masses of galaxies more massive than the completeness mass (at  $z=0.5$  or 1) for which membership to a given group/poor cluster is determined (as described in §2.3.2.1). Taking into account the mass of the individual galaxies, rather than their statistical distribution (as in Lin et al. 2003), becomes increasingly

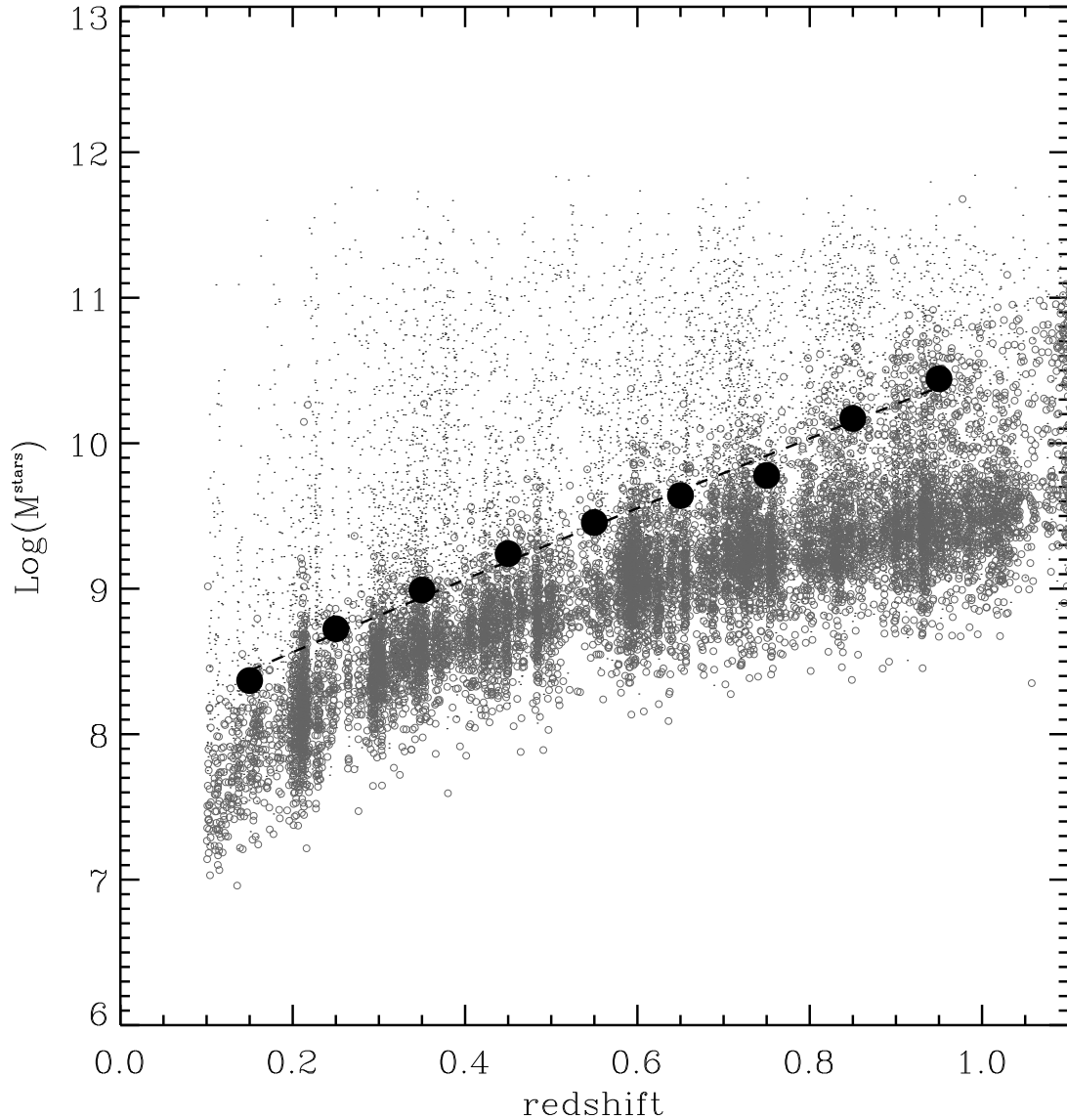


Figure 13: The completeness stellar mass for our sample is computed from the fit (black dashed line) to the 95% percentile of the distribution in  $M_{\text{lim}}$  (see text) for galaxies in the 20% lower percentile in magnitude (grey circles) as a function of redshift. The black dots represent the stellar masses for all galaxies with  $i_{AB} \leq 25$ . To reduce the plot size, we plot only one point in ten.

important for groups, where the BCG is a large fraction of the total stellar mass.

The contribution from less massive galaxies is estimated in a statistical manner from the composite stellar mass function (Giodini et al. in preparation), which can be robustly obtained only within two broad redshift bins ( $0.1 \leq z \leq 0.5$  and  $0.5 < z \leq 1.0$ ). The stacked stellar mass function for systems falling in each redshift bin is fitted with

## 2 Baryon mass fraction in groups and clusters

---

a single Schechter function (Schechter, 1976); the correction factor for stellar masses lower than the completeness mass, down to  $\sim 10^8 M_\odot$  (typical mass of a dwarf galaxy), is given by:

$$1 - \frac{\int_{M_{\text{compl}}}^{10^{13}} f(M) \cdot M \, dM}{\int_{10^8}^{10^{13}} f(M) \cdot dM}, \quad (7)$$

where  $M_{\text{compl}}$  is the completeness mass for the given redshift range. The fractional contribution to the total stellar mass budget of galaxies with  $10^8 M_\odot \leq M \leq M_{\text{compl}}$  corresponds to  $\sim 9\%$  ( $\sim 1\%$ ) at redshifts 0.5–1.0 (0.1–0.5). These values are almost negligible, as in Lin et al. (2003), which confirms that the total stellar mass associated with galaxies can be achieved almost directly from the data for our sample of X-ray-selected groups/poor clusters at  $0.1 \leq z \leq 1$ .

### 2.3.2 Total stellar mass (in galaxies)

#### 2.3.2.1 Statistical membership

As a first step, we estimate a projected total stellar mass, which is the sum of the stellar masses of all potential member galaxies down to the completeness mass of either redshift bin to which a group belongs (i.e. 0.1–0.5 or 0.5–1.0). Candidate members are defined as all the galaxies within a projected distance equal to  $R_{500}$  from the X-ray centroid of a group/poor cluster and within  $0.02 \times (1+z)$  from its redshift (given in the X-ray catalogue). Then we perform a foreground/background correction by measuring the total stellar mass of galaxies contained in 20 circular areas which have the same radius as  $R_{500}$  and have photometric redshifts consistent with that of a given system within the errors. These areas do not overlap either with the group or with other groups at the same redshift and are chosen to represent the coeval field environment. Field galaxies are selected in redshift and stellar mass following the same criteria as for the selection of potential member galaxies previously described. The mean and the standard deviation of the distribution of the total stellar masses computed in the 20 regions are taken as the value of the stellar mass associated with the foreground/background and its uncertainty, respectively. Finally, the foreground/background value is subtracted from the initial estimate of the total stellar mass of the system.

If the error on the foreground/background value is larger than half of the estimated total stellar mass content in galaxies of a given system, this system is removed from the sample. Obviously a system is excluded also if the foreground/background correction exceeds the estimated total stellar mass content in galaxies. The variance on the total stellar mass budget in galaxies for a system is given by the sum in quadrature of the background uncertainty and the error on the total stellar mass of the galaxies of the

system.

Furthermore we checked the influence of masked areas on the reliability of the computed total stellar masses of individual groups. A region of the COSMOS area is masked when the image quality is poor owing to different reasons (e.g. field boundary, saturated stars, satellite tracks and image defects). For galaxies with elliptical-like SEDs reliable photo- $z$ 's can be determined also in masked areas; therefore early-type galaxies falling in masked areas are considered. On average, the contribution of these objects to the stellar mass budget of a group is not expected to be negligible. In fact, in 30 out of 37 cases where early-type galaxies falling in masked areas are retrieved, the new stellar mass fraction (computed in §2.4.1) is consistent with that of other groups with the same  $M_{500}$ , whatever the redshift. Conversely, late-type galaxies falling in masked areas are not considered and the impact of this choice is tested *a posteriori*. For 23 out of 114 groups the number of statistically established member galaxies is less than 6 and the total stellar mass is systematically lower than the mean for groups of similar total masses, irrespective of  $M_{500}$ <sup>5</sup>. These 23 objects span the entire total mass range and their exclusion does not affect our results on the stellar mass fraction; at the same time, the scatter in the stellar mass fraction decreases by 30%<sup>6</sup>. Only the resulting sample of 91 galaxy systems with at least 6 members, spanning two orders of magnitude in X-ray luminosity, is considered in the following analysis; hereafter it is designated the COSMOS X-ray selected group sample.

### 2.3.2.2 Deprojection

The total stellar mass in galaxies so far estimated refers to a cylindrical section of the system projected onto the plane perpendicular to the line of sight. We therefore need to deproject the total stellar mass from two to three dimensions. The average galaxy distribution is described by a projected NFW profile in two dimensions (Bartelmann, 1996; Navarro et al., 1997):

$$\Sigma(x) = \frac{2\rho_s r_s}{x^2 - 1} f(x) , \quad (8)$$

---

<sup>5</sup>This tells that 5 members only is insufficient to determine the stellar mass budget of a group. In fact, when the total stellar mass or luminosity of a system is computed from a population of discrete sources, the scatter in the ensuing value turns out to be non linear when the number of discrete sources becomes small (e.g. of order ten or less), as demonstrated by Gilfanov et al. (2004) in an analogous application.

<sup>6</sup>Nevertheless these objects are potentially an interesting sub-population characterized by an extremely slow build-up of stellar mass. Further optical follow up will help to better assess their properties.

## 2 Baryon mass fraction in groups and clusters

---

where

$$f(x) = \begin{cases} 1 - \frac{2}{\sqrt{x^2-1}} \arctan \sqrt{\frac{x-1}{x+1}} & (x>1) \\ 1 - \frac{2}{\sqrt{1-x^2}} \operatorname{arctanh} \sqrt{\frac{1-x}{1+x}} & (x<1) \\ 0 & (x=1) \end{cases} \quad (9)$$

and as a generalized NFW profile in three dimensions

$$\rho(x) = \frac{\rho_s}{x(1+x)^2}. \quad (10)$$

In both equations the radial coordinate  $x$  is the radius in units of a scale radius  $r_s$ ,  $x \equiv r/r_s$ . The scale radius corresponds to the ratio between  $R_{200}$  and the concentration parameter  $c$  for the system. An average profile is produced using all 91 systems in our final sample, with a central density normalized to the number of groups. This high signal-to-noise, average two-dimensional galaxy distribution is best-fitted by a two-dimensional NFW profile where  $r_s = 0.27 R_{200}$ . The average radial profile is shown in Figure 14 together with its best fit (with a reduced  $\chi^2$  value equal to 1.2). We remark that our aim is not to compute the concentration parameter of the galaxy distribution for individual systems, otherwise we should take into account the scatter in the evolution of the concentration parameter as a function of redshift. Instead we want to compute an average correction for projection of the mass profile of a system as calculated in §2.3.2.1.

Using the best-fit values, we compute correction factors by integrating the average profile out to  $R_{500}$ :

$$dpf = \frac{\int_0^{R_{500}} \rho(r) \cdot 4\pi r^2 dr}{\int_0^{R_{500}} \Sigma(r) \cdot 2\pi r dr}. \quad (11)$$

The deprojected total stellar mass of a system is then given by

$$M_{500}^{\text{stars}} = dpf \times M_{\text{proj},500}^{\text{stars}}, \quad (12)$$

where  $dpf = 0.86$  is the correction factor.

## 2.4 Results

### 2.4.1 Stellar mass budget (galaxy component)

Figure 16a shows the behaviour of the total (deprojected) stellar mass in galaxies within  $R_{500}$ ,  $M_{500}^{\text{stars}}$ , as a function of the total mass  $M_{500}$  for the 91 COSMOS X-ray selected groups. The distribution in Figure 16a exhibits a rather well defined trend,

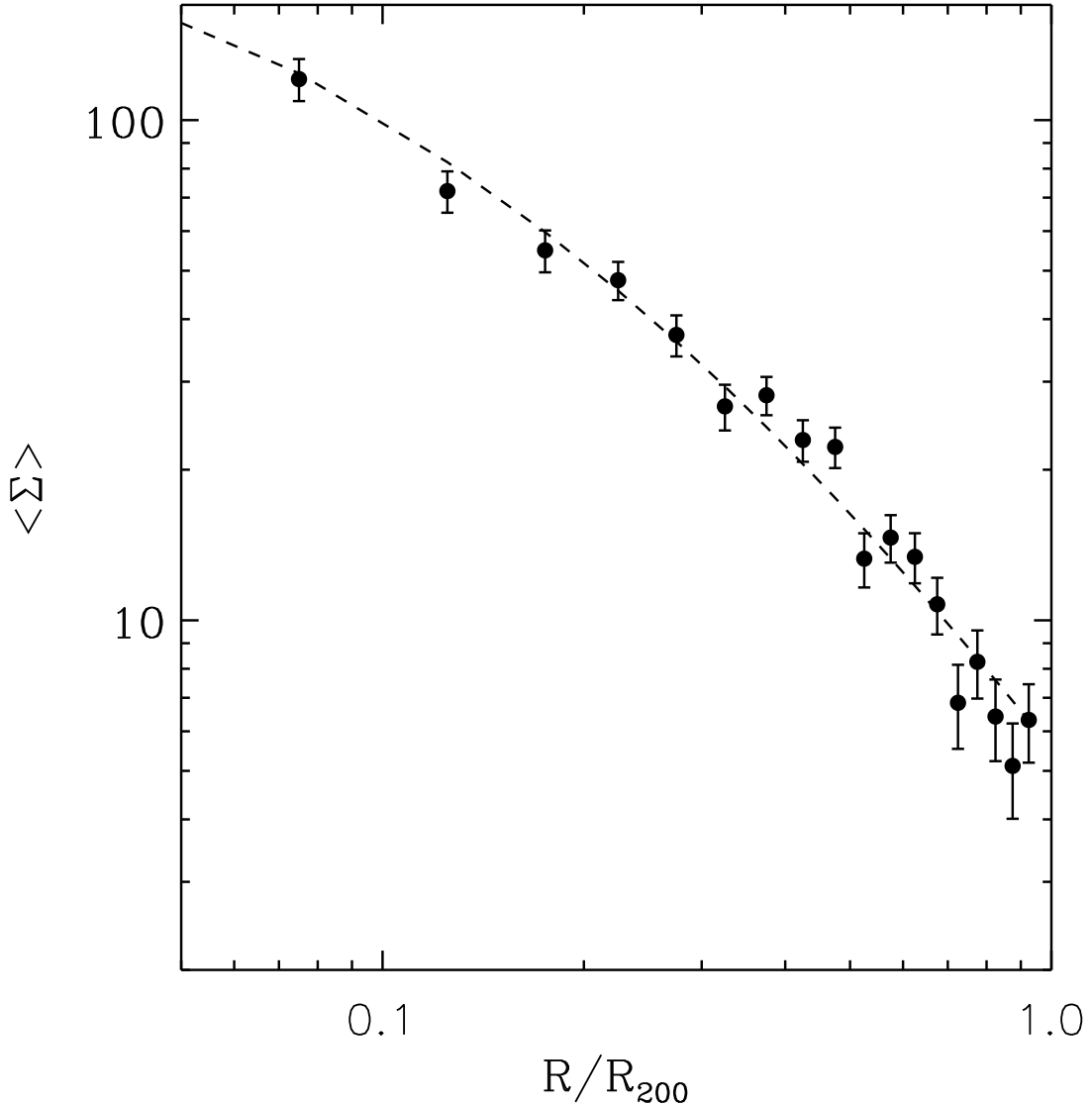


Figure 14: Radial profile of the average number galaxy density for the 91 COSMOS groups/poor clusters. The dashed line shows the best fit NFW profile ( $c \sim 4$ ). The unit of the surface density is number per area in unit of  $\pi R_{200}^2$  and normalized to the total number of systems.

although a large scatter is present, especially at low masses, where values can range by a factor of 10 at a fixed total mass. Part of this large scatter may have a physical origin: different merging histories produce different total mass-to-light ratios for fixed total assembled mass (cf. Sales et al., 2007).

We fit the relation between total stellar mass in galaxies and total mass for all 91 systems and for the 45 flag=1 groups only. Since the distribution in Figure 16a exhibits an intrinsic scatter larger than the errors on the individual points, the fit is performed

## 2 Baryon mass fraction in groups and clusters

---

using the weighted least square with intrinsic scatter (WLSS) method discussed in Pratt et al. (2006). This algorithm takes into account uncertainties on both stellar mass and total mass and the presence of intrinsic scatter in the data. There is a robust correlation between  $M_{500}^{\text{stars}}$  and  $M_{500}$  in the COSMOS X-ray selected groups:

$$M_{500}^{\text{stars}} = (0.30 \pm 0.02) \times \left( \frac{M_{500}}{5 \times 10^{13} h_{72}^{-1}} \right)^{\alpha}, \quad (13)$$

where  $\alpha=0.81\pm0.11$  for the entire sample and  $\alpha=0.72\pm0.13$  for the flag=1 subsample, and the (logarithmic) intrinsic scatter is equal to 35% in both cases<sup>7</sup>.

Fitting the stellar-to-total mass ratio vs. total mass of the system for the full sample of COSMOS X-ray selected groups only we find

$$f_{500}^{\text{stars}} = 5.0_{-0.1}^{+0.1} \times 10^{-2} \left( \frac{M_{500}}{5 \times 10^{13} M_{\odot}} \right)^{-0.26 \pm 0.09}. \quad (14)$$

A fit to the Flag=1 sample gives equivalent results. Remarkably the relation between the mass fraction of stars in galaxies and the total mass of the system for the COSMOS X-ray selected groups is consistent within the errors with the one found in nearby clusters by LMS03 and Laganá et al. (2008). We now extend the range of total masses using the results from local clusters selected by LMS03, converting their measurements to our cosmology. Since these authors do not give the uncertainties associated with their total mass estimates, we assign a fixed fractional total mass uncertainty equivalent to the mean of that for the COSMOS groups ( $\sim 30\%$ ). The best fit of the combined sample is

$$f_{500}^{\text{stars}} = 5.0_{-0.1}^{+0.1} \times 10^{-2} \left( \frac{M_{500}}{5 \times 10^{13} M_{\odot}} \right)^{-0.37 \pm 0.04}, \quad (15)$$

with a typical logarithmic intrinsic scatter of  $\sim 50\%$ . The data and best fit relations are shown in Figure 16b.

To better elucidate trends with total mass, we divided the data set into five logarithmic bins of equal size in total mass, and computed the mean and standard deviation of the values of the mass fraction of stars in galaxies in each bin using the biweight estimators of Beers et al. (1990); they are relatively large, which gives a measure of the heterogeneity of the population. The large points with error bars show the trend

---

<sup>7</sup>This result is robust against the presence of a pair of groups which are detected at the same redshift, but with a separation of the order of  $R_{500}$ . The two objects of this pair lie above the best-fit relation reproduced in Figure 16a, perhaps as an effect of a bias in their estimated total stellar masses in galaxies. However, new fits performed after excluding these two groups give the same results as the previous ones.

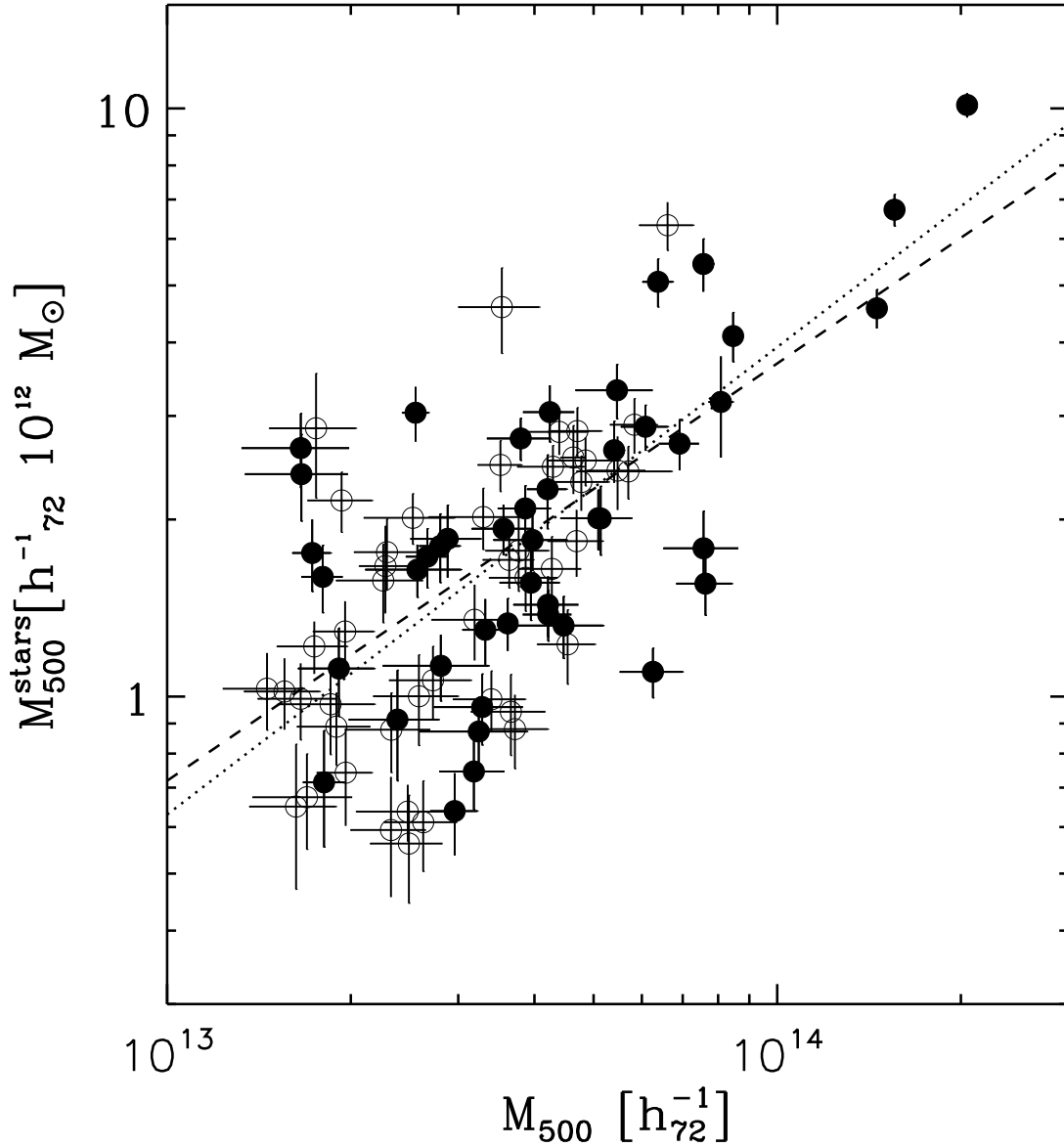


Figure 15: Total stellar mass in galaxies vs. total mass for the 91 COSMOS X-ray selected groups/poor clusters. Filled (empty) grey circles identify objects with flag=1 (2). The dashed (dotted) line represents the best fit relation derived for flag=1 (all) groups (see equation 13) derived taking into account uncertainties in both quantities and the intrinsic scatter of the relation.

of these binned data with total mass: there is good agreement with the best fitting regression line to the unbinned points, as expected.

## 2 Baryon mass fraction in groups and clusters

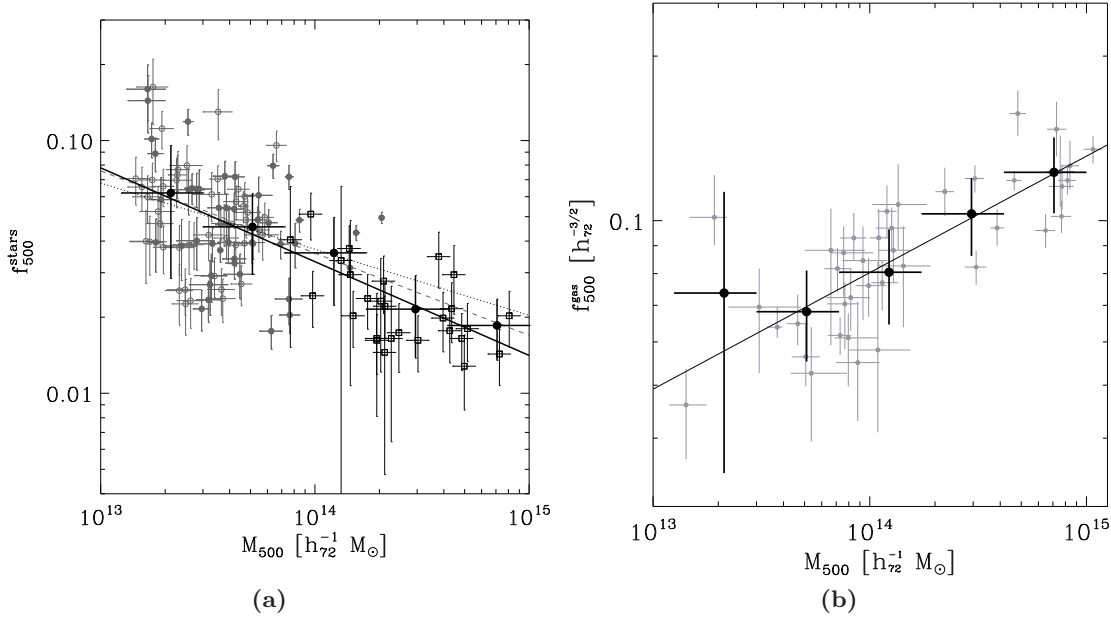


Figure 16: *(a)*: stellar-to-total mass ratio vs. total mass for the combined sample of 91 COSMOS X-ray selected groups (same symbols as in Figure 16a) plus 27 nearby clusters of LMS03 (empty squares). The dashed line represents the best-fit relation derived for flag=1 groups of the COSMOS sample and the dotted line represents the fit to all COSMOS groups. The solid line shows the best fit relation for all COSMOS groups plus local clusters. All fits are derived taking into account uncertainties in both quantities and the intrinsic scatter in the relation. The ensuing fit parameters are given in Table 4. The large points with error bars show the biweight mean and standard deviation of these data binned in 5 logarithmic bins in total mass. *b*: gas fraction as a function of the system mass from a combined sample of 41 clusters and groups (Vikhlinin et al. 2006, V06; Arnaud et al. 2007, APP07; Sun et al. 2009, S08). The solid line is the best fit relation  $f_{500}^{\text{gas}} \propto M_{500}^{0.2}$ . The large points with error bars show the mean and standard deviation of these data binned in 5 bins of total mass.

Table 1. The best fit parameters for the relation between stellar mass fraction and total mass (Eq. 14 and Eq. 15) for three samples considered. Data were fitted with a power law  $f_{500}^{\text{stars}} = N(M_{500}/5 \times 10^{13} M_{\odot})^{\alpha}$ .

Sample	Log(N) <sup>a</sup>	$\alpha$
COSMOS flag=1	-1.35±0.01	-0.33±0.12
COSMOS flag=1+2	-1.35±0.01	-0.26±0.09
COSMOS+LM03	-1.37±0.01	-0.37±0.04

### 2.4.2 Evolutionary considerations

Finally we inspect the presence of evolution of the relation between  $f_{500}^{\text{stars}}$  and  $M_{500}$  by considering only systems at  $z \leq 0.5$  (we cannot fit the relation for the high redshift

Table 2. Measured values for  $f_{500}^{\text{gas}}$  and  $f_{500}^{\text{stars}}$  as in Figure 28. Uncertainties correspond to the standard deviation of the mean (see text for details).

$M_{500}/[h_{72}^{-1}M_{\odot}]$	$f_{500}^{\text{stars}}$	$f_{500}^{\text{gas}}$	$f_{500}^{\text{stars+gas}}$
2.1e+13	0.062±0.005	0.074±0.028	0.136±0.028
5.1e+13	0.045±0.002	0.068±0.005	0.113±0.005
1.2e+14	0.036±0.004	0.080±0.003	0.116±0.005
3.0e+14	0.021±0.002	0.103±0.008	0.124±0.009
7.1e+14	0.019±0.002	0.123±0.007	0.141±0.007

systems since they do not cover a sufficient range in total mass). The ensuing fit is fully consistent with that obtained for the entire sample within the uncertainties.

We can put a constraint on the possible evolution of the relation by evaluating the change in the mean of  $f_{star}$  for massive systems ( $M_{500} > 5 \times 10^{14}M_{\odot}$ ) in two redshift bins ( $z \leq 0.5$  and  $z > 0.5$ ). The average  $f_{star}$  changes from  $0.031 \pm 0.013$  at  $z \leq 0.5$  to  $0.039 \pm 0.019$  at  $z > 0.5$ , a less than one sigma difference in mean values. Even taking the maximum distances between the two values given the uncertainties, the stellar mass fraction does not change by more than 35%.

A second way to investigate a possible evolution of the stellar mass fraction in galaxies is to plot the ratio of the stellar fraction to the mean relation as a function of redshift ( $r_f(z) = f_{star}(z)/\langle f_{star} \rangle$ ). Using the same five bins in total mass as above, no trend in  $r_f(z)$  is evident. However a fit of  $r_f(z)$  gives a robust upper limit on the evolution over the maximum redshift range (0–1) of 40%. Taking the median redshift of each redshift bin (0.22, 0.72), the upper limit on the evolution of the stellar fraction is less than 20%. This number is consistent with the upper limit on the evolution of the relation between total star fraction and  $M_{500}$  given by Balogh et al. (2008). Therefore we conclude that our data do not support the existence of a significant evolution in the zero-point and slope of the  $f_{500}^{\text{stars}}-M_{500}$  relation between redshifts 0 and 1.

### 2.4.3 The total baryon mass fraction

#### 2.4.3.1 The gas mass fraction

In order to determine the total baryon mass fraction in individual systems, we need to estimate the amount of baryons in the form of hot gas which make the intra-cluster medium (ICM). Unfortunately, this cannot be achieved from most of the existing X-ray observations of the total sample because their signal-to-noise is insufficient for the purpose. Therefore, we have to resort to an estimate of the mean trend of the gas

## 2 Baryon mass fraction in groups and clusters

---

mass fraction as a function of  $M_{500}$  established from an independent sample of well observed groups and clusters at  $z \leq 0.2$ , selected from the samples of Vikhlinin et al. 2006 (V06), Arnaud et al. 2007 (APP07) and Sun et al. 2009 (S08). These authors computed gas mass fractions at  $R_{500}$  from hydrostatic mass estimates for 10 (V06), 10 (APP07) and 21 (S08, including the best quality tiers 1 and 2 systems) clusters and groups, respectively. The combined sample contains 41 systems and spans the total mass range  $1.5 \times 10^{13} - 1.1 \times 10^{15} M_{\odot}$ . After conversion to a common cosmology, a fit of the combined data set using the WLSS regression yields:

$$f_{500}^{\text{gas}}(h/0.7)^{3/2} = (9.3_{-0.2}^{+0.2}) \times 10^{-2} \left( \frac{M_{500}}{2 \times 10^{14} M_{\odot}} \right)^{0.21 \pm 0.03}. \quad (16)$$

with a scatter of 17 per cent about the best fitting regression line. The data and resulting fit are shown in Figure. 16b. As discussed in the introduction we assume that this relation is not evolving, in the absence of observations to the contrary. To better elucidate trends with total mass, we divided the data set into the same logarithmic bins in total mass as for the stellar mass fraction, and computed the mean and standard deviation of the distribution of the gas mass fraction values in each bin. The large points with error bars show the trend of these binned data with total mass. The observed relation suggests that lower mass systems have proportionally less gas than high mass systems. Further discussion is available in Pratt et al. (2009).

### 2.4.3.2 The baryon mass fraction (in galaxies and ICM)

We now combine the results on the stellar and gas mass fractions derived in the previous two sections to investigate the behaviour of the baryonic mass fraction as a function of total mass. At this stage no contribution is considered from the ICL as defined in §2.4.4.3. In each logarithmic mass bin we sum the mean contribution from stellar and ICM mass components. The values of  $f_{500}^{\text{stars}}$  and  $f_{500}^{\text{gas}}$  in each bin are shown in Table 2. As we wish to determine the behaviour of the average systems in a given mass bin, for each component the uncertainty is calculated from the standard deviation of the mean (the standard deviation divided by  $\sqrt{N-1}$ , where  $N$  is the number of data points in the bin). The uncertainty on the total baryon mass content is then estimated from the quadratic sum of the individual uncertainties for the stellar and ICM contributions. Figure 28 (lower panel) reproduces the average behaviour of the sum of the two baryonic components estimated in the previous sections (i.e. ICM gas and stars associated with galaxies) as a function of total mass for galaxy systems with  $2 \times 10^{13} \leq M_{500} \leq 8.1 \times 10^{14} M_{\odot}$ . The ensuing baryon mass fraction is an increasing

function of the system mass:

$$f_{500}^{\text{stars+gas}} = (0.123 \pm 0.003) \times \left( \frac{M_{500}}{2 \times 10^{14} M_{\odot}} \right)^{0.09 \pm 0.03}, \quad (17)$$

This expression is obtained after excluding the lowest mass point which is affected by an extremely large uncertainty since the corresponding gas fraction is estimated from only two groups.

## 2.4.4 Comparison with WMAP

### 2.4.4.1 Raw values

As Figure 28 shows, there is a gap between the values of  $f_{500}^{\text{stars+gas}}$  estimated from WMAP5 and those obtained here; this discrepancy, before any correction, is significant at more than  $5\sigma$  for systems less massive than  $\sim 10^{14} M_{\odot}$  (see Table 3), where the uncertainties are calculated as described in §2.4.3.2.

### 2.4.4.2 Values corrected for gas depletion

We now correct the value of the baryon fraction for gas depletion. As discussed in Frenk et al. (1999), simulations without feedback suggest that the ICM has a slightly more inflated distribution than the dark matter (see also observations by Pratt & Arnaud 2002), resulting in a decrease in the gas fraction of 10% at  $R_{500}$ . In the absence of indications to the contrary we do not assume a mass dependence for the gas depletion. For average massive clusters ( $\langle M_{500} \rangle = 7 \times 10^{14} M_{\odot}$ ) the value of gas depletion-corrected  $f_{500}^{\text{stars+gas+depl}}$  is consistent within  $1.4\sigma$  with the WMAP5 estimate. However the gas depletion corrected value in the group regime ( $\langle M_{500} \rangle = 5 \times 10^{13} M_{\odot}$ ) is still  $4.5\sigma$  discrepant from that of WMAP5<sup>8</sup>.

### 2.4.4.3 Values corrected for gas depletion and ICL

The existence of a diffuse stellar component in galaxy groups/clusters is now a well established observational result, but the way the ICL is defined and measured is not unique (see Zibetti 2008 for a recent review). The quality of our observations is insufficient to measure the contribution of diffuse, very low surface brightness light ( $> 25.8$  K-mag arcsec<sup>-2</sup>) within  $r_{500}$  directly for individual systems in the sample. To quantify the amount of stellar mass which is associated with diffuse light that

<sup>8</sup>We note that this discrepancy represents a lower limit if a further 10% reduction of the gas mass is applied due to the clumpiness of the ICM as in Lin et al. (2003). However this correction is not applied in most of the studies of gas component in clusters.

## 2 Baryon mass fraction in groups and clusters

Table 3. Discrepancy of  $f_b$  from the WMAP5 value in sigma units

$M_{500}/[h_{72}^{-1}M_{\odot}]$	$\Delta_{f_b}/[\sigma_{f_b}]$	$\Delta_{f_b}/[\sigma_{f_b}]^a$	$\Delta_{f_b}/[\sigma_{f_b}]^b$
2.1e+13	>1.2	>0.8	>0.3
5.1e+13	5.3	4.5	3.3
1.2e+14	5.1	4.2	3.2
3.0e+14	3.7	2.6	2.1
7.1e+14	2.6	1.4	1.0

<sup>a</sup>After correction for gas depletion.

<sup>b</sup>After correction for gas depletion and ICL.

escapes detection during the standard photometry extraction with SExtractor (Capak et al., 2007), we are guided by previous observational results. In particular we consider Zibetti et al. (2005), Krick & Bernstein (2007) and Gonzalez et al. (2005). Zibetti et al. (2005) used stacking analysis of 683 systems at  $z=0.2-0.3$  ranging in total mass from a few times  $10^{13}$  to  $5 \times 10^{14} M_{\odot}$  (the average total mass is  $7 \times 10^{13} M_{\odot}$ ), selected from a  $1500 \text{ deg}^2$  of SDSS-DR1, reaching the unprecedented surface brightness limit of  $\sim 32 \text{ mag arcsec}^{-2}$  (R-band in the  $z=0.25$  observed frame). They show that on average the ICL contributes  $\sim 11\%$  of the stellar light within 500 kpc. In a complementary study Krick & Bernstein (2007) used a sample of massive clusters with a range of morphology, redshift and densities to find that the ICL contributes with 6%–22% to the total cluster light in  $r$ -band within one quarter of the virial radius, finding no appreciable correlation with cluster mass. Given these results, we assume that the contribution of the ICL to the total mass of a system is equal to its observed contribution to the total light and ranges between 11 and 22%. This range is consistent with the theoretical results by Murante et al. (2007) and Purcell et al. (2008), in their attempt of modelling the ICL by numerical simulations. Furthermore given the complete lack of observational constraints, we assume that the ICL mass fraction is not evolving with redshift for  $0 < z < 1$ ; this is supported by the simulation of Dubinski et al. (2003) as shown in Feldmeier et al. (2004). We discuss the impact of our choice on the results in §2.4.5. The final gas depletion corrected values including the ICL contribution of  $f_{500}^{\text{stars+gas+depl+ICL}}$  are lower than the WMAP5 estimate across the entire explored mass range;  $f_{500}^{\text{stars+gas+depl+ICL}}$  is in agreement with the WMAP5 result within  $1\sigma$  in the massive cluster regime, but still discrepant at a significance level of at least  $3.3\sigma$  for groups (see Figure 28).

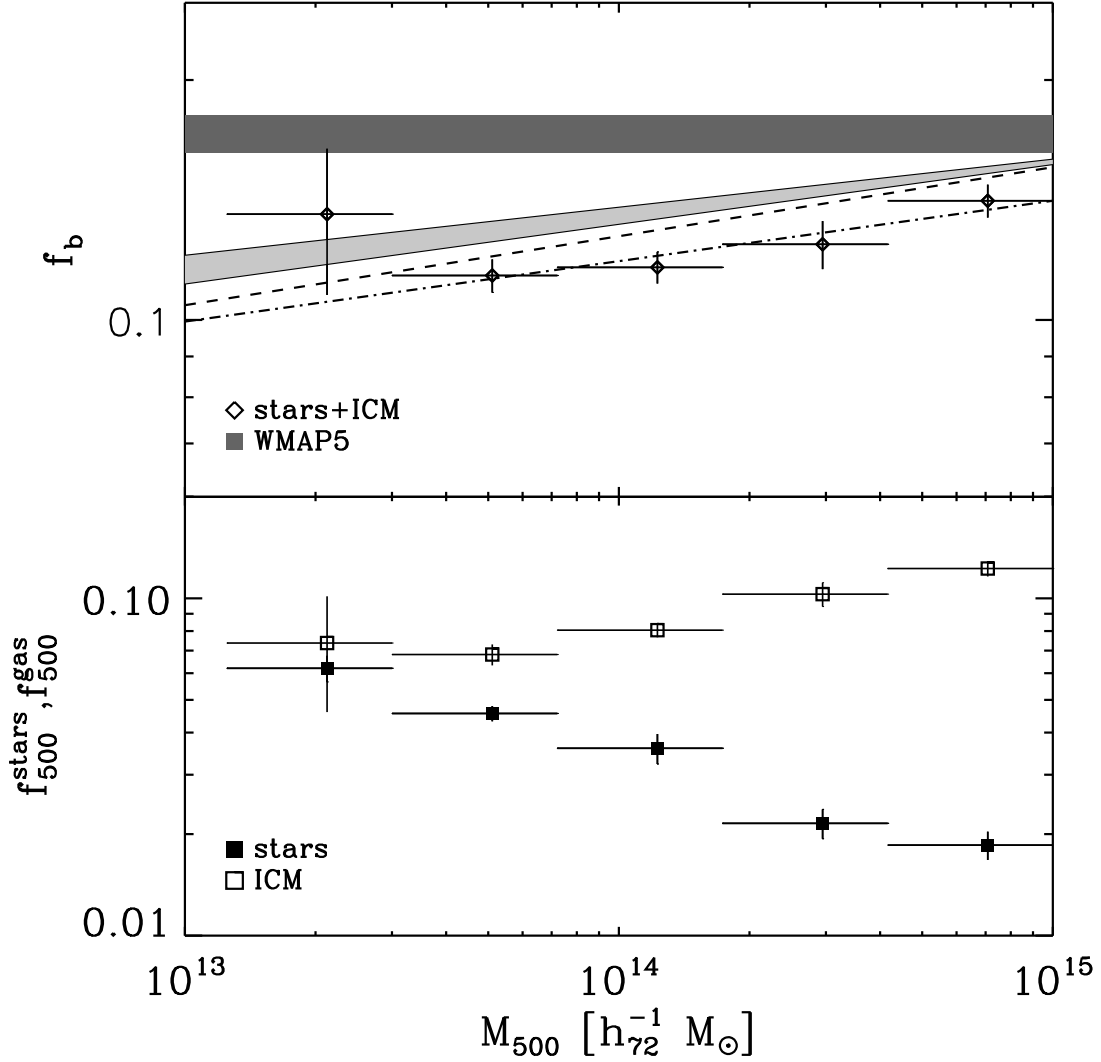


Figure 17: Lower panel: average stellar to dark mass ratio (filled points) for the COSMOS+LM03 sample and average gas fraction (empty points). Uncertainties are computed from the standard deviation of the mean in all cases. Upper panel: total baryonic fraction obtained summing the points in the lower panel compared with the universal value by WMAP5 (dark grey stripe). The dashed-dotted line represents the fit to the measured points. The dashed line represents the fit to the points where the gas fraction has been corrected for a 10% gas depletion. The light grey stripe is the fit to the relation taking in account both gas depletion and a constant (11–22%) ICL contribution to the stellar mass.

### 2.4.5 Impact of systematic effects

The basic observational result of the present study is that the baryon mass fraction, corrected for gas depletion and ICL contribution, is consistent with WMAP5 estimate within  $1\sigma$  for clusters with  $\langle M \rangle = 7 \times 10^{14} M_{\odot}$  but is significantly ( $3.3\sigma$ ) lower for groups with  $\langle M \rangle = 5 \times 10^{13} M_{\odot}$ . At the cluster scale our result on the baryon fraction is consis-

## 2 Baryon mass fraction in groups and clusters

---

tent with that of Lin et al. (2003), indicating that different approaches do not show systematic differences in the determination of the gas fraction scaling with the cluster mass. Furthermore we note that the scaling relation determined by Pratt et al. (2009) is based on three different samples of groups and clusters: this should reduce the potential bias produced by sample selection. In Pratt et al. (2009) the best fit relation to the combined data from hydrostatic estimates reproduces the REXCESS sample distribution where the gas masses have been estimated using the M–T relation of Arnaud et al. (2005). This suggests that potential systematic effects on our estimates of the gas mass fractions at low redshifts are negligible.

In the absence of direct estimates of the gas fraction at  $z > 0.2$ , we have to rely upon the results of existing simulations, which predict the gas fraction within  $r_{500}$  to increase on average by  $\sim 5\%$  (adiabatic simulations) or 10–20% (simulations with cooling and star formation) between  $z=0$  and  $z=1$  for groups and poor clusters (Kravtsov et al., 2005). Applying a correction to this effect at the median redshift of the COSMOS group sample (by 5–10% at  $z=0.5$ ), the discrepancy in the baryon mass fraction between groups of  $\langle M \rangle = 5 \times 10^{13} M_{\odot}$  and WMAP5 is reduced to 3.0–2.6  $\sigma$ . Therefore we conclude that systematic underestimates of the gas fraction alleviate but do not solve the discrepancy at the group scale.

Since inside groups the stellar mass fraction is comparable to the gas mass fraction, we analyze the impact of the ICL fraction and the adopted stellar mass–to–light ratio (M/L) of the galaxy population. We have adopted a mass independent correction to the total stellar mass fraction for ICL, equal to 11–22%. If a strong anti–correlation between the ICL mass fraction and the total mass of the system exists, and the true ICL mass fraction is equal to  $\sim 50\%$  at the group scale, an agreement between our total baryonic mass fraction and the WMAP5 estimate is reached. Such a figure has been claimed by Gonzalez et al. (2007) for a sample of 23 BCG–dominated clusters and groups. However the ICL–to–BCG light ratio (ICL/BCG) is strongly dependent on the decomposition of the total surface brightness profile of the two components and the photometric depth (Gonzalez et al. 2005; Zibetti 2008). We note that Gonzalez et al. (2005) give ICL/BCG  $> 5$  by applying a simultaneous decomposition of the surface brightness distribution of BCG+ICL in two De Vaucouleurs components: the outer one is considered as the genuine ICL and the inner one as the BCG. Conversely, Zibetti et al. (2005) obtain ICL/BCG  $< 0.5$  by fitting only the inner profile with a De Vaucouleurs model (which represents the BCG) and considering all the residual light as ICL. Nevertheless, Zibetti (2008) applied a two–De Vaucouleurs decomposition to the Zibetti et al. (2005) data obtaining ICL/BCG  $\sim 2$ , and concluded that the ICL+BCG–to–total light ratio is a much more robust measurement, which is likely equal to 0.3

(in light) for systems of average mass  $7 \times 10^{13} M_{\odot}$ . The high value of ICL/BCG found by Gonzalez et al. (2007) may be the result of a sample bias, as suggested by the same authors. On the other hand the lack of trends reported by Zibetti et al. (2005) could be intrinsically biased by the adoption of a fixed metric aperture of 500 kpc, which correspond to smaller fraction of R200 for more massive clusters. Given the steeper profile of the ICL with respect to galaxies, the ICL fraction of more massive clusters could be overestimated and a correction for this effect could reconcile these results with the negative trend found by Gonzalez et al. (2007), but not with the extreme values of ICL+BCG-to-total light ratio. Generally, it is evident that better determinations of the trends of the ICL with cluster mass and richness are needed.

The COSMOS groups sample contains a whole range of systems, which exhibit a BCG-to-galaxy stellar mass ratio from 0.2 to 0.9. For these groups the estimated ICL+BCG-to-total light ratio for the average group is 0.36, broadly consistent with the generally accepted average value of 0.3 (Gonzalez et al. 2007; Zibetti 2008). This suggests that we are not missing an important contribution of the stellar mass in our analysis, in spite of our definition of ICL.

Another systematic effect may be introduced by the computation of the stellar mass-to-light ratio for the ensemble of the member galaxies and the ICL. In our case we use M/L values that correspond to the individual star formation histories of individual member galaxies (Arnouts et al., 2007) and we do not make assumption on the M/L of the ICL. Hence the major source of systematics on the stellar mass-to-light ratio of our galaxies is given by the adopted initial mass function (IMF). For instance, a change from a standard Salpeter to a Chabrier IMF reduces the M/L by 30% (Longhetti & Saracco, 2009). This translates into a decrease by 30% of the stellar mass associated with galaxies which makes the bulk of the total stellar mass in our systems. There is no compelling reason to abandon the Salpeter IMF (Renzini, 2005), but it is a possibility explored in the literature. Lin et al. (2003) obtained the stellar mass-to-light ratio for the ensemble of group/cluster member galaxies by folding in a morphological type dependent M/L with the temperature dependence of the spiral fraction; Gonzalez et al. (2007) assumed that the ICL and all member galaxies share the same stellar M/L, as the one that characterise an early type galaxy. The latter case assumes that the intergalactic stars are homogeneous with the BCG stellar population. However, it has been suggested that the ICL may (also) origin from the stripping of non-BCG galaxies inside the group/cluster (Purcell et al. 2008; Pierini et al. 2008), which are on average bluer than the BCG, especially in groups (Zabludoff & Mulchaey 1998; Weinmann et al. 2006; Poggianti et al. 2006). For example, if the ICL mass-to-light ratio used in Gonzalez et al. (2007) is overestimated by a factor 2, it translates in the systematic

## 2 Baryon mass fraction in groups and clusters

---

overestimation of the baryon mass fraction by 10%.

This systematic effect has the same amplitude, but opposite sign, of the potential offset applied to the gas fraction–mass relation according to Gonzalez et al. (2007). Therefore we conclude that a  $3\sigma$  discrepancy between the baryon mass fraction of groups and the WMAP value holds against major systematic effects on the stellar populations either diffuse or associated with galaxies.

An overestimate of the total M/L is not enough to explain the values of the stellar mass fraction for the lowest mass systems in Gonzalez et al. (2007) which largely exceed the constraint on the total baryon fraction set by WMAP5 (as also noted in Balogh et al. 2008). A way out is a systematic and large underestimate of the total masses of these systems, as also suggested by Balogh et al. (2008)<sup>9</sup>.

We conclude that a robust estimate of the total mass is crucial for systems with the lowest mass (in our sample  $\langle M_{500} \rangle \sim 2 \times 10^{13} M_{\odot}$ ). Our estimates are based on the  $L_X$ – $M_{200}$  relation established via the weak lensing analysis in Leauthaud et al. (2010), and exhibit a typical uncertainty of 30%. The use of different total mass estimators could offer a test of the presence of systematics, but unfortunately this is still hard to achieve for statistical large samples of groups at different redshifts.

### 2.5 Discussion

We have investigated if the discrepancy between estimates of the total baryon mass fraction obtained from observations of the CMB and of galaxy groups persists when a large, unbiased sample of well-characterized groups is considered. The COSMOS 2 deg<sup>2</sup> survey meets this requirement, yielding 91 candidate X-ray groups/poor clusters at redshift  $0.1 \leq z \leq 1$ . In order to extend the span in total mass to two orders of magnitude ( $2 \times 10^{13} < M_{500} < 1.2 \times 10^{15} M_{\odot}$ ), we consider 27 nearby clusters investigated by Lin et al. (2003). Comparable robust measurements of total mass and total stellar mass (in galaxies) exist for individual objects of both subsamples, as shown in the previous sections. In addition, the same scaling relation is used to estimate the gas mass fraction in both subsamples. This enables us to build a joint sample of 118 X-ray selected groups and clusters at  $z \leq 1$  for which the importance of systematics is reduced (see §2.2). For this sample, the behaviour of the total stellar mass fraction as a function of the total mass can be investigated for a large range in total mass and, for the first time, in redshift (at least for groups). The results of our analysis and their impact on the widely accepted paradigm of the hierarchical growth of structure in the

---

<sup>9</sup>These objects certainly impact the strongly inverse total mass dependence of the total stellar mass fraction found by Gonzalez et al. (2007).

universe are discussed hereafter.

### 2.5.1 The stellar mass fraction

We have shown (Figure 16b) that the stellar-to-total mass ratio in COSMOS groups and in 27 local clusters is anticorrelated with the total mass of the system. This relation is given by  $f_{500}^{\text{stars}} \propto M_{500}^{-0.37 \pm 0.04}$ , which holds also after introducing the mass independent correction for the ICL (see §2.4.4). The global trend between  $f_{500}^{\text{stars}}$  and  $M_{500}$  is consistent with that observed in clusters at  $z < 0.3$  both by LMS03 and Laganá et al. (2008) using much smaller samples. We extend their results to the low mass regime by one decade and to higher redshift.

The difference in the number of stars formed per unit of halo mass between groups and clusters has been interpreted in terms of a varying efficiency of the star formation with the total mass of the system (e.g. Lin et al., 2003). A variation in the star-formation efficiency for systems with virial temperatures  $\geq 10^7$  K is a result of simulations by Springel & Hernquist (2003); it is interpreted in terms of cooling flows being less efficient in shutting off star formation in groups. An alternative possibility is that clusters are formed not only by merging of groups and smaller clusters but also that they accrete a large fraction of their galaxies (with a low stellar mass fraction, of the order of 0.01) from the field (White & Frenk 1991; Marinoni & Hudson 2002). However after a mass independent correction for the ICL contribution (introduced in §2.4.4), the relation  $f_{500}^{\text{stars}} \propto M_{500}^{-0.37 \pm 0.04}$  is in agreement with the constraint on the slope set by the hierarchical model of structure formation under the assumption that at least half of the stars in groups were formed by  $z = 1$  (Balogh et al., 2008)<sup>10</sup>. This is supported by the apparent absence of evolution for this relation in our sample within the redshift range 0.1–1. This shows how observational studies such as the present one can improve the constraints on models and foster our understanding of the underlying physical processes.

### 2.5.2 The total baryon mass fraction

Combining the computed stellar mass fraction with the estimated gas mass fraction derived from the mean local relation in Pratt et al. (2009), we find that the gas plus stellar (galaxies) baryon mass fraction increases by  $\sim 25\%$  (from  $\sim 0.11$  to  $\sim 0.14$ ) when the total mass increases by a factor of one hundred. After a constant 10% correction for gas depletion and a further correction for a constant 11–22% ICL contribution, the value of  $f_{500}^{\text{stars+gas+depl+ICL}}$  for an average cluster is consistent within  $1\sigma$  with the

<sup>10</sup>We note that a steeper relation is obtained when the strongly inverse mass dependent ICL fraction of Gonzalez et al. (2007) is used (see Balogh et al. (2008) for the discussion).

## 2 Baryon mass fraction in groups and clusters

---

cosmic value measured by WMAP, while the  $f_{500}^{\text{stars+gas+depl+ICL}}$  found for an average group differs from it at more than  $3\sigma$ . Given the heterogeneity of the sample (see e.g. Figure 16b), for some objects the gap between  $f_{500}^{\text{stars+gas+depl+ICL}}$  and the WMAP5 value could be negligible or, conversely, statistically more significant for objects in the same bin of total mass, but at the two extremes of the distribution in  $f_{\text{stars}}^{500}$ . Unfortunately we do not have a measure of the gas mass fraction for individual objects, therefore we focus on the behaviour of the average object. We did likewise for the ICL by assuming a fixed fractional contribution of 11–22% across the entire mass range. Possible systematic effects introduced by our definition and estimate of the ICL contribution are discussed in §2.4.5. Here we stress that they do not lead to an anomalously low BCG+ICL contribution to the total mass of the system. Thus the discrepancy at the groups regime is not erased by uncertainties on the stellar mass fraction. In the absence of evidence for a systematic and relevant underestimation of the gas mass fraction in our systems (see §2.4.5), we interpret the discrepancy as a lack of gas, by 33%, at the group regime. This may be produced by feedback (stellar and/or AGN), as suggested by high-resolution cosmological simulations including cooling, star formation, supernova feedback, and AGN radio-mode feedback in galaxy clusters and groups (Puchwein et al. 2008, Bower et al. 2008, Short & Thomas 2008). Since supernova feedback appears to be insufficient to explain the  $L_X$ – $T$  relation (Puchwein et al., 2008), feedback by AGN seems necessary. According to this interpretation, gas can be removed from within  $R_{500}$  mainly as a consequence of the mechanical heating produced by a central AGN. The action of the AGN is larger in groups than in clusters simply because the potential well is shallower in the former systems. In a forthcoming work we will quantify the feedback by AGN radio-mode for the COSMOS groups. Another proposed mechanism capable of accounting for the "missing" gas is "filamentary heating" (Voit & Bryan, 2001). Low entropy gas is consumed in star formation before the group formation, which eventually raises the entropy of the gas which becomes the ICM. The resulting higher entropy level inhibits the gas from falling towards the center of the potential well, which can explain the lack of gas in the central region of groups (Sun et al., 2009).

### 2.6 Conclusions

The baryon mass fraction is a parameter which can be constrained by the primordial light elements abundance set by the nucleosynthesis at early epochs. It can be independently measured from observations of the CMB (e.g. WMAP) or of galaxy groups/clusters. Different studies of the baryon mass fraction in nearby galaxy sys-

tems have reported values lower than the one from WMAP, the discrepancy being larger for groups than clusters. We investigate if this discrepancy persists when a sample of local clusters is supplemented by a large, unbiased sample of groups at  $0.1 \leq z \leq 1.0$ . Hereafter we list our conclusions.

1. The stellar mass fraction associated with galaxies is anticorrelated with the mass of the system:  $f_{500}^{\text{stars}} \propto M_{500}^{-0.37 \pm 0.04}$ . This is consistent with previous results on local clusters. The validity of this result is now extended by one decade in total mass and to redshift 1.
2. The previous relation holds after correcting the stellar mass fraction for a mass independent 11–22% contribution from the ICL as suggested by both observations and simulations. The slope of the  $f_{500}^{\text{stars}}-M_{500}$  relation is consistent with the constraint set by the hierarchical paradigm of structure formation (Balogh et al., 2008). No significant evolution in the relation between  $f_{500}^{\text{stars}}$  and  $M_{500}$  is observed. This supports the scenario in which massive clusters form mostly by merging of less massive groups and clusters, and observed groups in the redshift range 0–1 have formed the bulk of their stellar mass by  $z \sim 1.0$ .
3. Combining measured values of the stellar mass fraction with values of the gas mass fraction estimated from an average relation obtained for a local sample,  $f_{500}^{\text{stars+gas}}$  increases by 25% from groups to clusters. After the introduction of appropriate corrections for gas depletion and ICL contribution, the total baryonic mass fraction at the groups regime still differs from the WMAP5 value at  $3.3\sigma$ . We interpret the origin of this discrepancy as a lack of gas (by 33%), which can be produced either by feedback (supernovae and/or radio-mode AGN heating) or by "filamentary heating".

Our results provide useful constraints on simulations of the aforementioned processes. In particular the availability of a large unbiased sample of groups offers direct and stringent constraints on models rather than relying on extrapolation of the behaviour of the stellar fraction as a function of mass in the entire family of systems with  $10^{13} < M_{500} < 10^{14} M_{\odot}$ . Future observations will increase both the statistics and the redshift sampling rate, so that a test and extension of our conclusions will be possible.

## Acknowledgments

The authors thank the anonymous referee for her/his valuable comments, which led to a significant improvement of the paper. We acknowledge the contributions of the entire COSMOS collaboration; more informations on the COSMOS survey are available

## 2 Baryon mass fraction in groups and clusters

---

at <http://www.astr.caltech.edu/~cosmos>. This research was supported by the DFG Cluster of Excellence "Origin and Structure of the Universe". D.P. acknowledges support by the German *Deutsches Zentrum für Luft- und Raumfahrt*, *DLR* project number 50 OR 0405.

# Bibliography

- Allen, S. W., Schmidt, R. W., Ebeling, H., Fabian, A. C., & van Speybroeck, L. 2004, MNRAS, 353, 457
- Arnaud, M., Pointecouteau, E., & Pratt, G. W. 2005, A&A, 441, 893
- Arnaud, M., Pointecouteau, E., & Pratt, G. W. 2007, A&A, 474, L37
- Arnouts, S., et al. 2002, MNRAS, 329, 355
- Arnouts, S., et al. 2007, A&A, 476, 137
- Balogh, M. L., McCarthy, I. G., Bower, R. G., & Eke, V. R. 2008, MNRAS, 385, 1003
- Bartelmann, M. 1996, A&A, 313, 697
- Beers, T. C., Flynn, K., & Gebhardt, K. 1990, AJ, 100, 32
- Bialek, J. J., Evrard, A. E., & Mohr, J. J. 2001, ApJ, 555, 597
- Biviano, A., & Salucci, P. 2006, A&A, 452, 75
- Bower, R. G., McCarthy, I. G., & Benson, A. J. 2008, MNRAS, 390, 1399
- Bundy, K., Ellis, R. S., & Conselice, C. J. 2005, ApJ, 625, 621
- Capak, P., et al. 2007, ApJS, 172, 99
- David, L. P., Arnaud, K. A., Forman, W., & Jones, C. 1990, ApJ, 356, 32
- Diehl, S., & Statler, T. S. 2007, ApJ, 668, 150
- Dubinski, J., Koranyi, D., & Geller, M. 2003, Astrophysical Supercomputing using Particle Simulations, 208, 237

## Bibliography

---

- Dunkley, J., et al. 2009, *ApJS*, 180, 306
- Elvis, M., & C-COSMOS Team 2006, *Bulletin of the American Astronomical Society*, 38, 1006
- Ettori, S. 2003, *MNRAS*, 344, L13
- Evrard, A. E. 1997, *MNRAS*, 292, 289
- Feldmeier, J. J., Mihos, J. C., Morrison, H. L., Harding, P., Kaib, N., & Dubinski, J. 2004, *ApJ*, 609, 617
- Finoguenov, A., et al. 2007, *ApJS*, 172, 182
- Frenk, C. S., et al. 1999, *ApJ*, 525, 554
- Gilfanov, M., Grimm, H.-J., & Sunyaev, R. 2004, *MNRAS*, 351, 1365
- Gonzalez, A. H., Zabludoff, A. I., & Zaritsky, D. 2005, *ApJ*, 618, 195
- Gonzalez, A. H., Zaritsky, D., & Zabludoff, A. I. 2007, *ApJ*, 666, 147
- Grimm, H.-J., Gilfanov, M., & Sunyaev, R. 2003, *MNRAS*, 339, 793
- Guzzo, L., et al. 2007, *ApJS*, 172, 254
- Hasinger, G., et al. 2007, *ApJS*, 172, 29
- He, P., Feng, L.-L., Fang, L.-Z. 2006, *ApJ*, 623, 601
- Hoekstra, H. 2007, *MNRAS*, 379, 317
- Ilbert, O., et al. 2009, *ApJ*, 690, 1236
- Koekemoer, A. M., et al. 2007, *ApJS*, 172, 196
- Komatsu, E., et al. 2009, *ApJS*, 180, 330
- Kravtsov, A. V., Nagai, D., & Vikhlinin, A. A. 2005, *ApJ*, 625, 588
- Krick, J. E., & Bernstein, R. A. 2007, *AJ*, 134, 466
- Küpcü Yoldaş, A., et al. 2007, *A&A*, 463, 893
- Laganá, T. F., Lima Neto, G. B., Andrade-Santos, F., & Cypriano, E. S. 2008, *A&A*, 485, 633
- Leauthaud, A., et al. 2010, *ApJ*, 709, 97

- Lilly, S. J., et al., 2007, *ApJS*, 172, 70
- Lin, Y.-T., Mohr, J. J., & Stanford, S. A. 2003, *ApJ*, 591, 749
- Lin, Y.-T., & Mohr, J. J. 2004, *ApJ*, 617, 879
- Longhetti, M., & Saracco, P. 2009, *MNRAS*, 174
- Marinoni, C., & Hudson, M. J. 2002, *ApJ*, 569, 101
- Massey, R., et al. 2007, *Nature*, 445, 286
- McCarthy, I. G., Bower, R. G., & Balogh, M. L. 2007, *MNRAS*, 377, 1457
- Moretti, A., et al. 2004, *A&A*, 428, 21
- Murante, G., Giovalli, M., Gerhard, O., Arnaboldi, M., Borgani, S., & Dolag, K. 2007, *MNRAS*, 377, 2
- Navarro, J. F., Frenk, C. S., & White, S. D. M. 1997, *ApJ*, 490, 493 (NFW)
- Pannella, M., et al. 2006, *ApJ*, 639, L1
- Pierini, D., Zibetti, S., Braglia, F., Böhringer, H., Finoguenov, A., Lynam, P. D., & Zhang, Y.-Y. 2008, *A&A*, 483, 727
- Poggianti, B. M., et al. 2006, *ApJ*, 642, 188
- Pratt, G. W., & Arnaud, M. 2002, *A&A*, 394, 375
- Pratt, G. W., Arnaud, M., & Pointecouteau, E. 2006, *A&A*, 446, 429
- Pratt, G. W., Croston, J. H., Arnaud, M., & Böhringer, H. 2009, *A&A*, 498, 361
- Puchwein, E., Sijacki, D., & Springel, V. 2008, *ApJ*, 687, L53
- Purcell, C. W., Bullock, J. S., & Zentner, A. R. 2008, *MNRAS*, 391, 550
- Rosati, P., della Ceca, R., Norman, C., & Giacconi, R. 1998, *ApJ*, 492, L21
- Renzini, A. 2005, *The Initial Mass Function 50 Years Later*, 327, 221
- Rykoff, E. S., et al. 2008, *MNRAS*, 387, L28
- Sanders, D. B., et al. 2007, *ApJS*, 172, 86
- Sales, L. V., Navarro, J. F., Lambas, D. G., White, S. D. M., & Croton, D. J. 2007, *MNRAS*, 382, 1901

## Bibliography

---

- Salpeter, E. E. 1955, *ApJ*, 121, 161
- Salvato, M., et al. 2009, *ApJ*, 690, 1250
- Sandage, A. 1986, *A&A*, 161, 89
- Schechter, P. 1976, *ApJ*, 203, 297
- Scoville, N., et al. 2007, *ApJS*, 172, 1
- Scoville, N., et al. 2007, *ApJS*, 172, 150
- Short, C. J., & Thomas, P. A. 2008, arXiv:0811.3166
- Springel, V., & Hernquist, L. 2003, *Astrophysical Supercomputing using Particle Simulations*, 208, 273
- Sun, M., Voit, G. M., Donahue, M., Jones, C., Forman, W., & Vikhlinin, A. 2009, *ApJ*, 693, 1142
- Taniguchi, Y., et al. 2007, *ApJS*, 172, 9
- Vikhlinin, A., McNamara, B. R., Forman, W., Jones, C., Quintana, H., & Hornstrup, A. 1998, *ApJ*, 502, 558
- Vikhlinin, A., Kravtsov, A., Forman, W., Jones, C., Markevitch, M., Murray, S. S., & Van Speybroeck, L. 2006, *ApJ*, 640, 691
- Voit, G. M., & Bryan, G. L. 2001, *Nature*, 414, 425
- Weinmann, S. M., van den Bosch, F. C., Yang, X., & Mo, H. J. 2006, *MNRAS*, 366, 2
- White, S. D. M., & Frenk, C. S. 1991, *ApJ*, 379, 52
- White, S. D. M., Navarro, J. F., Evrard, A. E., & Frenk, C. S. 1993, *Nature*, 366, 429
- Wilkins, S. M., Trentham, N., & Hopkins, A. M. 2008, *MNRAS*, 385, 687
- Zabludoff, A. I., & Mulchaey, J. S. 1998, *ApJ*, 496, 39
- Zamojski, M. A., et al. 2007, *ApJS*, 172, 468
- Zhao, D. H., Jing, Y. P., Mo, H. J., & Boerner, G. 2008, arXiv:0811.0828
- Zibetti, S. 2008, in *Dark Galaxies and Lost Baryons*, IAU Symposium, Vol. 244, p. 176–185
- Zibetti, S., White, S. D. M., Schneider, D. P., & Brinkmann, J. 2005, *MNRAS*, 358, 949

# Radio galaxy feedback in X-ray selected groups from COSMOS: the effect on the ICM

*S. Giodini, V. Smolcic, A. Finoguenov, H. Boehringer, L. Birzan, G. Zamorani, A. Oklopčic, D. Pierini, G.W. Pratt, E. Schinnerer, R. Massey, A.M. Koekemoer, M. Salvato, D.B. Sanders, J. S. Kartaltepe, D. Thompson*

*The Astrophysical Journal, in press*

## Abstract

We quantify the importance of the mechanical energy released by radio-galaxies inside galaxy groups. We use scaling relations to estimate the mechanical energy released by 16 radio-AGN located inside X-ray detected galaxy groups in the COSMOS field. By comparing this energy output to the host groups' gravitational binding energy, we find that radio galaxies produce sufficient energy to unbind a significant fraction of the intra-group medium. This unbinding effect is negligible in massive galaxy clusters with deeper potential wells. Our results correctly reproduce the breaking of self-similarity observed in the scaling relation between entropy and temperature for galaxy groups.

## 3.1 Introduction

Galaxy groups are important laboratories in which to investigate the importance of non–gravitational processes in structure formation. These processes are potentially more important in galaxy groups than in massive clusters because of their lower gravitational binding energy. This is suggested by the significant deviation of the observed X–ray luminosity and entropy versus temperature ( $L_X$ –T and  $S$ –T) scaling relations in groups compared to the relation expected in a purely gravitational scenario (see also Pratt & Arnaud 2003; Markevitch 1998; Arnaud & Evrard 1999; Ponman et al. 2003; Sun et al. 2009; Pratt et al. 2009). Radiative cooling can be invoked to explain this deviation, but then the predicted fraction of stars in clusters of a given mass is incorrect (Voit, 2005; Balogh et al., 2008). To simultaneously explain the properties of the intra–cluster/group medium (ICM) and account for the observed properties of galaxies, it is necessary to take into account a major contribution to the cluster/group energetics from non–gravitational heating.

The two main sources of non–gravitational heating are star–formation and active galactic nuclei (AGN). Cosmological simulations (e.g. Kay 2004; Bower et al. 2006; Sijacki & Springel 2006) show that both processes are required to reproduce the properties of the ICM. In particular, recent simulations by Bower et al. (2008) successfully reproduce both the galaxy and ICM properties (see Short & Thomas 2009) when they include a ”radio–mode” AGN feedback phase: in this phase the movement of bubbles inflated by the AGN jets transfers energy into the gas within the cluster (mechanical heating). The observable objects providing this type of feedback inside groups and clusters would be radio galaxies (Croton et al., 2006). The main difference between the Bower et al. (2008) model and others, including radio–mode AGN, (Bower et al. 2006; Sijacki & Springel 2006; Puchwein et al. 2008;) is that it allows the radio mode feedback to expel gas from the X-ray emitting regions of the system.

The importance of such AGN-feedback in groups could explain the observational result by Lin et al. (2003), McCarthy et al. (2007) and Giodini et al. (2009), that the total baryon fraction in groups is lower than the cosmic value estimated from cosmic microwave background (CMB) observations (see Giodini et al. 2009 for more details). The discrepancy decreases in systems of higher total mass, such that it is  $<1\sigma$  for massive clusters.

In this Paper we propose a simple, direct method to test the hypothesis that radio galaxies in groups can indeed inject enough mechanical energy to unbind the intra–cluster gas. The Paper is structured as follows. In Section 2 we select a sample of 16 groups from the COSMOS 2 deg<sup>2</sup> survey discussed in Giodini et al. (2009), each hosting

a radio galaxy within the virial radius (Schinnerer et al. 2007; Smolčić et al. 2008), plus a control sample of massive clusters from Birzan et al. (2004). In Sections 4.3 and 4.4 we then compare the groups’ binding energy to the mechanical energy output by the radio sources, derived from their total radio luminosity through scaling relations. Applying this method, we show that the mechanical removal of gas from the group region is indeed energetically feasible for systems below  $\sim 3 \times 10^{14} M_{\odot}$ . In Section 4.5 we discuss how this scenario compares to the deviation in the scaling relation between entropy and temperature at the groups scale.

We adopt a  $\Lambda$ CDM cosmology with  $h=0.72$ ,  $\Omega_m=0.25$ ,  $\Omega_{\Lambda}=0.75$ .

## 3.2 The samples

### 3.2.1 Radio galaxies in X–ray detected groups

We use the catalog of 91 X–ray selected groups from the COSMOS survey (Scoville et al. 2007a; Finoguenov et al. in preparation), selected as described in Giodini et al. (2009). Extended source detection was performed using a multiscale wavelet reconstruction of a mosaic of XMM and Chandra data. For each group, member galaxies are identified within  $R_{500}^1$  of the group center, utilizing the high quality photometric redshifts available ( $\sigma(\Delta z)/(1+z)=0.02$  at  $i_{AB}^2 < 25$ , Ilbert et al. 2009).

We use a sub-sample of the VLA–COSMOS catalog (Schinnerer et al. 2007; Smolčić et al. 2008) to identify radio galaxies lying inside the X–ray selected groups. Of the 60 radio galaxies<sup>3</sup> identified within the VLA–COSMOS Large Project (Schinnerer et al. 2007; 1.49 GHz), about 80% have been associated with a secure optical counterpart (Smolčić et al., 2008) with  $i_{AB} \leq 26$ , and accurate photometry (thus also with accurate photometric redshifts; Ilbert et al. 2009; Salvato et al. 2009).

We have cross-correlated this sample of radio galaxies with the X–ray selected galaxy groups in 3D space using a search radius of  $1 \times R_{200}$  (Finoguenov et al. in preparation) around the groups’ centers and within  $0.02 \times (1+z)$  from the group’s redshift. This resulted in a sample of 16 systems matched in position and redshift. In Appendix A we show the contours of the radio 20 cm and X–ray emission superimposed to the

---

<sup>1</sup>  $R_{\Delta}$  ( $\Delta=500,200$ ) is the radius within which the mass density of a group/cluster is equal to  $\Delta$  times the critical density ( $\rho_c$ ) of the Universe. Correspondingly,  $M_{\Delta} = \Delta \rho_c(z) (4\pi/3) R_{\Delta}^3$  is the mass inside  $R_{\Delta}$ .  $M_{200}$  is computed using an  $L_X$ – $M_{200}$  relation established via the weak lensing analysis in Leauthaud et al. 2010. The catalogue value of  $M_{200}$  is converted into  $M_{500}$  assuming an NFW profile with a concentration parameter computed from the mass-dependent relation of Macciò et al. (2007).

<sup>2</sup> AB magnitude in the SUBARU i band.

<sup>3</sup> The term “radio galaxy” is used here to describe an extended radio source with clear jet/lobe structure.

### 3 Radio–galaxy feedback in X–ray selected groups

---

SUBARU  $zp$  band image for each of the groups. In 9 out of 16 cases the radio galaxy is located in the core of the group (defined as  $R < 0.15R_{200}$ ). The 20 cm radio luminosity densities<sup>4</sup> of these galaxies range from  $\sim 5.5 \times 10^{22} - 4.8 \times 10^{25} \text{ W Hz}^{-1}$ , with a median luminosity of  $8.9 \times 10^{24} \text{ W Hz}^{-1}$  ( $\nu F_\nu \sim 7.3 \times 10^{38} - 6.4 \times 10^{41} \text{ erg s}^{-1}$ , with a median luminosity of  $1.18 \times 10^{41} \text{ erg s}^{-1}$ ). This median luminosity is at the high end of the radio luminosity distribution of the full radio AGN sample (c.f. Fig. 17 in Smolčić et al. 2008, and Fig. 5 in Smolčić et al. 2009), consistent with previous findings that powerful radio galaxies inhabit group-scale environments (e.g. Baum et al. 1992). The redshift distribution of the 16 groups is fairly uniform between 0.1 and 1, with the exception of 6 sources concentrated at  $z \sim 0.3$  (where a large structure extends throughout the whole COSMOS field). The groups have X–ray luminosities ranging from  $1 \times 10^{42}$  to  $8.7 \times 10^{43} \text{ erg s}^{-1}$  and span a mass range of  $2 \times 10^{13} < M_{200} < 2 \times 10^{14} M_\odot$  with a median mass of  $7.14 \times 10^{13} M_\odot$ .

#### 3.2.2 The comparison sample of massive clusters

The COSMOS X–ray sample is mostly composed of groups. We complement it with 12 well known radio galaxies inside massive clusters, extracted from the sample of Birzan et al. (2004). We use those clusters from the Birzan’s sample which overlap with the HIFLUGCS survey (Reiprich & Boehringer, 2002) so that we can use the X–ray parameters determined from the HIFLUGCS clusters. In addition we require that the radio source within those clusters is associated with a secure NIR counterpart in the 2MASS catalogue (Skrutskie et al., 2006). These requirements eliminate 4 of the clusters in the original Birzan et al. sample. Each of these clusters contain X–ray cavities associated with radio bubbles likely connected with AGN activity of the central galaxy. The radio galaxies have been identified within the NRAO VLA Sky Survey (NVSS) at 1.49 GHz (Condon et al., 1998), except in the case of the Centaurus Cluster where data come from the 1.41 GHz Parkes Radio Sources Catalogue (Wright & Otrupcek, 1990). The 20 cm radio luminosities of the radio galaxies range between  $2 \times 10^{39}$  and  $2 \times 10^{43} \text{ erg s}^{-1}$ , with a median luminosity of  $1.4 \times 10^{42} \text{ erg s}^{-1}$ , more than 10 times higher than the median radio luminosity of the radio galaxies in the COSMOS sample.

The X–ray parameters for these clusters are provided by the X–ray analysis in the HIFLUGCS survey, and converted for the standard cosmology used in this paper. The sample consists of very local clusters, ranging in their total mass between  $1 \times 10^{14} < M_{200} < 1.2 \times 10^{15} M_\odot$  with a median mass of  $4.25 \times 10^{14} M_\odot$ , almost 10 times

---

<sup>4</sup>Computed using the total flux densities ( $F_\nu$ ). K–correction is also applied assuming a spectral index of  $\alpha = 0.7$  ( $F_\nu \propto \nu^{-\alpha}$ ).

higher than the median total mass of the systems in the COSMOS sample

## 3.3 Analysis of the COSMOS group sample

### 3.3.1 Mechanical energy input by radio galaxies in groups

We estimate the mechanical energy input by a radio galaxy into the ICM over the group lifetime from the mechanical luminosity of the radio source multiplied by the fraction of time a massive galaxy spends in the radio-AGN phase. The mechanical luminosity for the radio galaxies in our sample is estimated from the scaling relation presented in Bîrzan et al. (2008). These authors studied a sample of galaxy clusters showing signatures of cavities and bubbles in the X-ray surface brightness 2D distribution, with a powerful radio source as a central galaxy. The cavity power of the radio source, estimated from the  $pdV$  work of the jet/lobe on the surrounding ICM, is found to be correlated (albeit with a large scatter) with the monochromatic radio power at 1.49 GHz of the central galaxies ( $P_{1.49\text{ GHz}}$ ) as

$$P_{cav} \propto P_{1.49\text{ GHz}}^{0.35 \pm 0.07} \quad (18)$$

(see Eq. 16 in Bîrzan et al. 2008).  $P_{1.49\text{ GHz}}$  is computed from the radio-emission of the entire source. This estimate is a lower limit to the mechanical luminosity of the AGN outbursts, since it does not take into account the energy dissipated (e.g. in shocks).  $P_{cav}$  is related to the  $pdV$  work through

$$P_{cav} = \frac{4PV}{\tau} \quad (19)$$

(Churazov et al. 2002; Bîrzan et al. 2008), where  $\tau$  is the duration of each single AGN outburst and 4 is the factor used for relativistic plasma. Smolčić et al. (2009) investigated the fraction of radio AGN as a function of cosmic time and stellar mass of the galaxy. This fraction can be related, through a probability argument detailed in Smolčić et al. (2009), with the time a galaxy of a given stellar mass and at a given redshift spends as a radio galaxy ( $\tau_{\text{radio}}$ ). Using this result we can estimate the average duration of radio sources as a function of redshift and stellar mass of the host galaxy (see Fig. 12 in Smolčić et al. 2009)<sup>5</sup>. This gives a plausible time-scale during which

---

<sup>5</sup>To derive the values of  $\tau_{\text{radio}}$  Smolčić et al. (2009), it is assumed that the radio parent population (red massive galaxies) is formed at  $z = 3$  (Renzini, 2006) and survives until  $z = 0$ . Since the COSMOS radio galaxies are not at  $z = 0$ , the time-scales computed in Smolčić et al. (2009) coincide with ours if multiplied by  $\frac{t(z=z_{gal})-t(z=3.0)}{10^9 \text{ yr}}$ , where  $t$  is the age of the universe at redshift  $z$  and  $z_{gal}$  is

### 3 Radio–galaxy feedback in X–ray selected groups

---

the radio AGN can have injected mechanical energy into its environment. For the 16 COSMOS X–ray selected groups,  $\tau_{radio}$  ranges between 0.003 and 4.18 Gyr, with a median value of 3.1 Gyr. The mechanical energy contribution can then be estimated as

$$E_{\text{mech}} = P_{\text{cav}} \times \tau_{\text{radio}}. \quad (20)$$

The values of  $E_{\text{mech}}$  for our sources are shown in Table 1 and span a range between  $\sim 2 \times 10^{57} - 3 \times 10^{61}$  erg  $\text{h}_{72}^{-2}$ . The uncertainties in the radio mechanical energy input are dominated by the scatter in the scaling relation used to convert the monochromatic power into mechanical luminosity, which amounts to 0.85 dex, and by the uncertainties on  $\tau_{\text{radio}}$ . We use  $\tau_{\text{radio}}$  as derived from an average estimate over a sample of radio galaxies in the COSMOS field as a whole, irrespective of their environment. One might expect the density of the environment surrounding the jets to have a significant impact on the jet lifetime. However, the fraction of radio galaxies that resides within the COSMOS groups is comparable with the fraction of red massive galaxies within groups in the control sample used in Smolčić et al. (2009) (respectively 18% and 16% within  $R_{200}$ ); this assures that the statistical argument used to compute the time–scales holds also in this case. Furthermore we can estimate an average time–scale based on only extended radio galaxies in the whole COSMOS group sample as follows. Of the 141 COSMOS groups at  $z < 1$  and with  $L_X > 10^{42}$  erg  $\text{s}^{-1}$ , 32 contain a multi–component radio galaxy. Therefore the average duration of the radio galaxy activity during this time interval is  $(32/141) \times (t(z=1) - t(z=0))$ . This is  $\sim 1.7$  Gyr, a time–scale comparable with the average life–time estimated with the method by Smolčić et al. (2009) ( $\sim 1.6$  Gyr<sup>6</sup>).

#### 3.3.2 Binding energy of the intra–group medium

We consider the shape of the dark matter halos to be characterized by NFW (Navarro et al., 1996) radial profiles

$$\rho(x) = \frac{\rho_{\text{crit}} \delta_c}{x(x+1)^2} \quad (21)$$

where  $x = r/r_s$ ,  $r_s$  is the characteristic radius, and  $\rho_c$  is the critical density of closure of the universe.  $\delta_c$  is defined as

$$\delta_c = \frac{200 c^3}{3 \ln(1+c) - c/(1+c)} \quad (22)$$

---

the redshift of the radio galaxy.

<sup>6</sup>computed as  $\frac{\text{max}(\tau_{\text{radio}}) - \text{min}(\tau_{\text{radio}})}{2}$

### 3.3 Analysis of the COSMOS group sample

Table 4. For each of the 16 COSMOS groups, the columns indicate 1) X-ray catalogue ID number 2) R.A. 3) Dec. 4) redshift 5) Power at 1.4 GHz 6) Mechanical Power 7) Binding energy  $\pm 1\sigma$  confidence limit 8)  $E_{mech} \pm 1\sigma$  confidence limit 9)  $\tau_{radio}$  10) distance from the center

XID	R.A. [J2000]	DEC. [J2000]	$z$	$P_{1.49\text{ GHz}}$ [ $10^{24}$ W/Hz]	$P_{cav}$ [ $10^{36}$ W]	$E_{binding}$ [ $10^{60}$ erg]	$E_{mech}$ [ $10^{60}$ erg]	$\tau_{radio}$ [Gyr]	$R/R_{200}$
107	149.60965	2.14799	0.28	1.11	7.353	$5.916^{2.342}_{1.937}$	$0.514^{3.087}_{0.441}$	0.221	0.3783
262	149.60007	2.82118	0.34	19.0	19.85	$127.9^{38.80}_{26.49}$	$24.15^{144.9}_{20.70}$	3.858	0.0011
253	149.75626	2.79472	0.49	6.71	13.78	$40.16^{12.26}_{9.721}$	$10.14^{60.85}_{8.693}$	2.332	0.0042
246	149.76132	2.92909	0.34	0.90	6.828	$289.8^{76.73}_{67.46}$	$7.003^{42.02}_{6.003}$	3.252	0.6181
311	149.93796	2.60627	0.34	6.38	13.54	$17.27^{4.792}_{3.907}$	$0.183^{1.101}_{0.157}$	0.042	0.2195
264	149.99847	2.76914	0.16	0.32	4.775	$6.940^{3.179}_{2.247}$	$0.004^{0.027}_{0.003}$	0.003	0.0007
281	150.08617	2.53141	0.88	8.90	15.21	$84.94^{27.05}_{22.45}$	$1.241^{7.450}_{1.064}$	0.258	0.8614
191	150.11434	2.35651	0.22	1.71	8.554	$8.380^{2.959}_{2.150}$	$6.122^{36.73}_{5.248}$	2.269	0.0757
237	150.11774	2.68425	0.34	27.7	22.65	$105.1^{31.65}_{23.49}$	$19.56^{117.4}_{16.77}$	2.738	0.0027
29	150.17996	1.76887	0.34	30.0	23.29	$58.49^{16.80}_{12.77}$	$31.63^{189.8}_{27.11}$	4.306	0.0016
64	150.19829	1.98628	0.43	12.4	17.11	$21.10^{7.358}_{4.941}$	$18.06^{108.4}_{15.48}$	3.348	0.0030
35	150.20661	1.82327	0.52	10.2	16.00	$30.87^{11.07}_{8.342}$	$15.32^{91.95}_{13.13}$	3.037	0.0008
6	150.28821	1.55571	0.36	1.13	7.401	$77.91^{20.23}_{17.35}$	$0.070^{0.425}_{0.060}$	0.030	0.2279
149	150.41566	2.43020	0.12	0.05	2.564	$50.31^{14.98}_{10.32}$	$0.002^{0.014}_{0.002}$	0.003	0.1957
40	150.41386	1.84759	0.96	48.5	27.54	$108.1^{34.85}_{24.40}$	$1.786^{10.71}_{1.530}$	0.205	0.4888
120	150.50502	2.22506	0.83	16.4	18.88	$425.0^{112.5}_{90.06}$	$24.92^{149.5}_{21.36}$	4.185	0.0267

and  $c$  is the concentration of the halo. The scale radius and the concentration are linked by the relation  $r_s = R_{500}/c_{500}$ , where  $c_{500}$  is the dark matter concentration inside  $R_{500}$ . We estimate the binding energy out to  $R_{500}$  because the kinetic energy of the infall velocity field along filaments becomes important beyond this radius (Evrard et al., 1996) and our simple model may not then be applicable. Furthermore, we can evaluate reliable gas masses from the X-ray observations only within  $R_{500}$ . For simplicity, we assume that the gas follows the same distribution as the dark matter. We define as binding energy the total potential energy needed to push the ICM gas inside  $R_{500}$  beyond  $R_{200}$ . The binding energy is computed as

$$\begin{aligned}
 E_{binding} &= \int_0^{M_{g,500}} [\phi(r) - \phi(R_{200})] dM_g \\
 &= 4\pi \int_0^{R_{500}} \phi(r) \rho_g(r) r^2 dr
 \end{aligned} \tag{23}$$

### 3 Radio–galaxy feedback in X–ray selected groups

---

We neglect the additive constant given by the term  $\phi(R_{200})$ , as it is small with respect to the other terms of the equation. We use the definition of gas mass within  $R_{500}$  as

$$M_g = M_g(R_{500}) = 4\pi \int_0^{R_{500}} \rho_g(r) r^2 dr. \quad (24)$$

The potential of a spherical NFW model is (Hayashi et al., 2007)

$$\phi(r) = A \times \frac{\ln(1+x)}{x} \quad (25)$$

where  $A$  is

$$A = -\frac{G M_{200}}{r_s (\ln(1+c) - c/(1+c))} \quad (26)$$

Thus, substituting the terms into Equation 23, we compute the binding energy of the ICM gas in a NFW dark matter halo as follows:

$$E_{\text{binding}} = f_{\text{gas}} 4\pi \rho_{\text{crit}} \delta_c A r_s^3 \int_0^{c_{500}} \frac{\ln(1+x)}{(1+x)^2} dx \quad (27)$$

where  $f_{\text{gas}}$  is the gas fraction. The concentration parameter for the COSMOS groups has been computed from the mass-dependent relation of Macciò et al. (2007). The errors bars on the binding energy are estimated using a Monte Carlo method to numerically propagate the errors on  $M_{200}$  and  $R_{200}$ , the scatter in the  $c$ - $M_{200}$  and in the  $f_{\text{gas}}$ - $M_{500}$  relation.

We cannot estimate the gas masses from most of the existing X-ray observations of the COSMOS X–ray selected groups because of insufficient signal-to-noise. We therefore estimate the gas fraction in the groups from the mean trend of the gas mass fraction as a function of  $M_{500}$ . This trend was established from an independent compilation of high quality observations of local ( $z < 0.2$ ) groups and clusters in the same mass range as the sample under consideration here (Pratt et al., 2009). The observed relation ( $f_{\text{gas}} \propto M_{500}^{0.21}$ ) suggests that lower mass systems have proportionally less gas than high mass systems.

## 3.4 Analysis of the galaxy cluster sample

### 3.4.1 Mechanical energy input by radio galaxies in massive clusters

In order to compare the energy input from radio galaxies in groups and clusters, we include in our analysis a sample of well known radio galaxies in massive clusters, extracted from the sample of (Bîrzan et al. 2004; see Section 3.2.2). We use their tabulated value of  $pdV$  to compute the mechanical energy input over the average time

the galaxy has spent as a radio galaxy. Birzan et al. provide a value for the energy input for both filled and radio ghost cavities. In order to obtain a measure of the average input, we sum the  $pdV$  for all the cavities in a cluster and multiply it by the number of events (i.e. how often the radio jet was turned on). The latter is given by the ratio between  $\tau_{radio}$  and the duration of a single radio event (assuming that all the active AGN phases have the same duration).

We choose the oldest cavity’s age as an indication of the duration of the radio event. Birzan et al. (2004) calculate the age of each cavity in three ways: 1. the time required for the cavity to rise at the sound velocity; 2. the time required for the bubble to rise buoyantly at the terminal velocity; 3. the time required to refill the displaced volume. We adopt the average of the three age estimates; this is generally similar to the age computed for a buoyantly rising bubble. We take the error on the cavity’s age to be the difference between the shortest and longest life–time estimated via the three different methods.

As  $\tau_{radio}$  for our sample is derived following Smolčić et al. (2009), it depends on the redshift and the stellar mass of the radio galaxy. We computed the stellar masses for the central radio galaxy in the massive cluster sample using the K–band photometry provided by the 2MASS survey (Skrutskie et al., 2006). This method is robust, since radio galaxies contain mostly type 2 (obscured) AGN, whose emission does not significantly contaminate the optical–NIR part of the galaxy spectrum. We assume a  $M/L_K$  ratio for a stellar population with an age of  $\sim 10$  Gyr (corresponding to the age of the stars in a galaxy at  $z \sim 0$ ), obtained by Drory et al. (2004) ( $M/L_K = 1.4$  with a Salpeter IMF). The quoted error on the  $M/L_K$  in Drory et al. (2004) is 25–30%: a change in stellar mass of this magnitude does not affect significantly the time–scales we estimate. The stellar masses are then converted to a Chabrier IMF by subtracting an offset of 0.2 dex.

#### 3.4.2 Binding energy of the intra–cluster medium

We compute the binding energy for the Birzan et al. clusters in the same way as for the COSMOS groups, using the value of  $M_{200}$  and  $R_{200}$  provided by the X–ray analysis in the HIFLUGCS survey (Reiprich & Boehringer 2002). We assume a constant concentration parameter of 5. Errors on  $E_{binding}$  are propagated numerically via a Monte Carlo method, in the same way as the COSMOS groups (see Section 3.3.2). As well as computing the binding energy of clusters individually, we also test the cluster result using the scaling relations adopted for the COSMOS groups, both for computing  $M_{200}$  (Leauthaud et al., 2010) and for estimating their mechanical energy output (Birzan et al., 2008). The change in our calculations does not qualitatively affect our results.

### 3 Radio–galaxy feedback in X–ray selected groups

---

The values of  $E_{\text{binding}}$  change by less than a factor 2 on average, while values of  $E_{\text{mech}}$  are perturbed randomly within the error bars.

## 3.5 Results

### 3.5.1 The balance of radio–input and binding energy

Figure 22 shows the binding energy of the gas versus the energy output from radio galaxies. In the group regime, the two energies span a comparable range of values ( $10^{58}$ – $10^{61}$  ergs), while for clusters the binding energy exceeds the total mechanical output of radio–galaxies by a factor approximately of  $\sim 10^2$ – $10^3$ . In particular, for seven groups the two energies are consistent at  $1\sigma$  level, and for all other groups except two the equality holds at  $3\sigma$ , meaning that radio–galaxies potentially provide sufficient energy to unbind the gas in a large fraction of these groups. It is interesting to note that, in all the groups with  $E_{\text{mech}} \sim E_{\text{binding}}$ , the radio galaxy lies within  $0.15 \times R_{200}$  from the center of the group. This suggests that a radio galaxy in a group is most likely to input sufficient energy into the ICM to unbind a part of the gas if it lies at the core of the group. Moreover, radio sources outside the group core reside in lower density environments, and our calculations of those binding energies may be overestimates. The different energy balance in groups and clusters demonstrates the importance of AGN heating in groups, and shows that the mechanical removal of gas from groups is energetically possible. This has important consequences for the understanding of the baryonic budget in these systems (see Giodini et al. 2009).

### 3.5.2 Can radio galaxies offset radiative cooling in galaxy groups?

We now compare the mechanical energy input by radio–galaxies with the energy required to offset the cooling in the group center ( $E_{\text{cool}}$ ). As detailed in Fabian et al. (1994), Peterson et al. (2003) and McNamara & Nulsen (2007), the cooling time in cluster/group centers can be lower than the Hubble time, implying that large reservoirs of cold gas could accumulate in these regions. However, evidence that the gas does not cool below approximately one third of the virial temperature (Kaastra et al., 2004) indicates the presence of a heat source providing enough energy to offset the cooling. Several studies (e.g. Peterson et al. 2003, Peterson & Fabian 2006, McNamara & Nulsen 2007) suggest AGN feedback as a viable heating source. To test this hypothesis, we check whether the cooling energy is lower than the mechanical energy of the rising bubbles. We estimate  $E_{\text{cool}}$ , assuming that the time during which the gas has been cooling is equal to the lifetime of the group, which we assume to be 5 Gyr

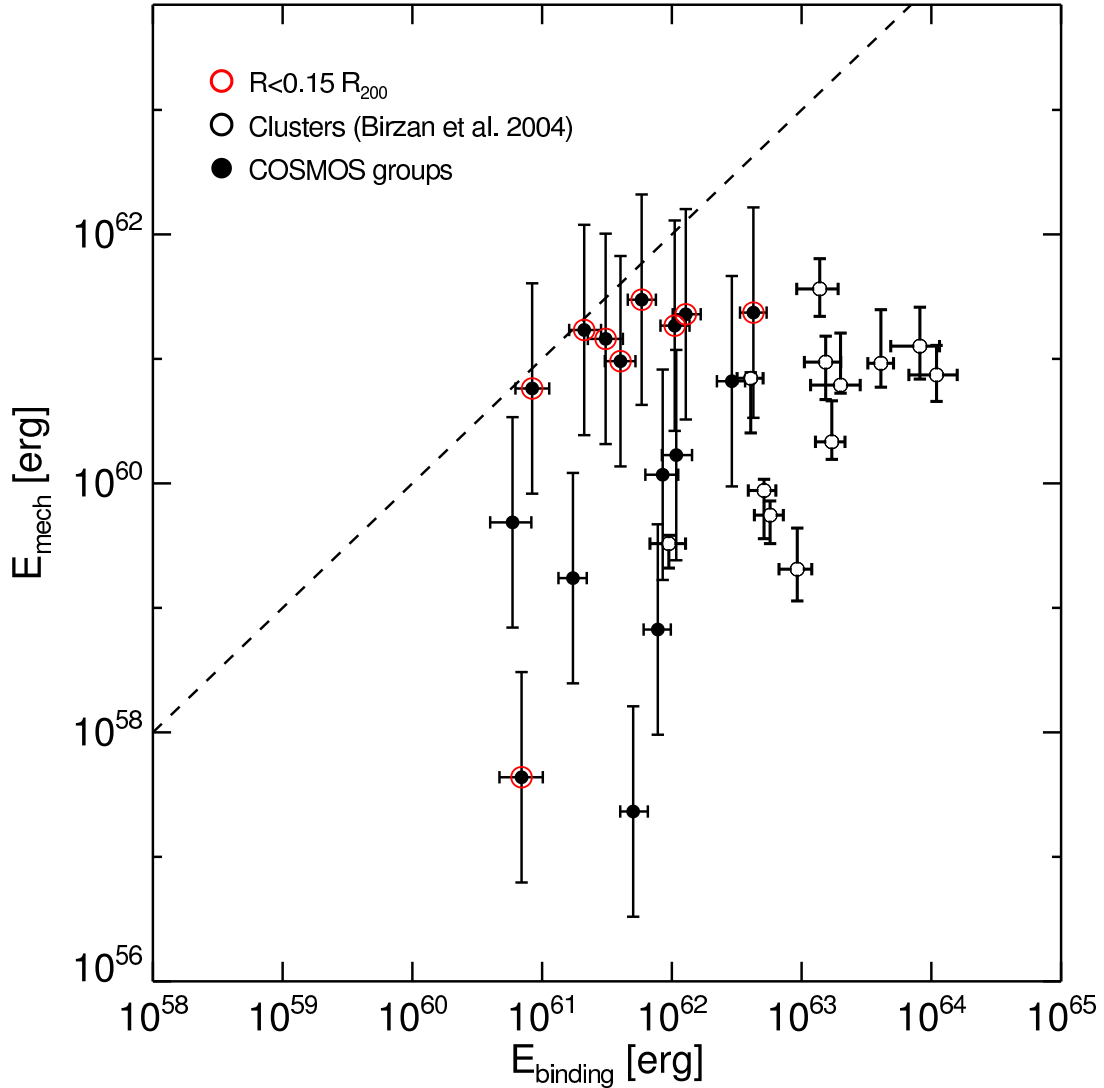


Figure 18: Binding energy of the cluster/group gas versus the output mechanical energy from radio-galaxies. Solid points show the 16 X-ray selected groups in the COSMOS field that host a radio galaxy within their virial radius. Large concentric circles indicate groups that host a radio galaxy within the core ( $R \leq 0.15 \times R_{200}$ ). Open points show the sample of massive local clusters drawn from Birzan et al. 2004. The dashed line shows equality. The binding energy in clusters exceeds the total mechanical output by a factor of  $\sim 10^2$ – $10^3$ . In all cases except one where a radio galaxy lies in the centre of a group, the mechanical energy output from the radio galaxy is of the same order as the binding energy for the COSMOS groups analyzed here.

(Voigt & Fabian, 2004). The cooling energy can then be estimated as:

$$E_{\text{cool}} = L_{\text{cool}} \times t_v = f_{\text{cool}} L_{\text{bol}} \times t_v \quad (28)$$

### 3 Radio–galaxy feedback in X–ray selected groups

---

where  $t_v$  is the lifetime of the group, and  $f_{\text{cool}}$  is the fraction of bolometric luminosity assumed to be emitted inside the cooling radius (where the cooling time of the gas is lower than the Hubble time). In general this contribution is found to be  $\gtrsim 10\%$  of the total cluster X–ray luminosity (McNamara & Nulsen, 2007). Also, the scatter in the  $L_X$ – $T$  scaling relation due to the contribution of cool core clusters can be up to a factor of 2 (Chen et al. 2007; Pratt et al. 2009). Given these considerations, we assume that 25% of the total bolometric X–ray luminosity is emitted inside the cooling radius (Peres et al., 1998). Since the relative contribution of the cool core to the total X–ray luminosity is higher in groups than in massive clusters, this value is a good estimate of the average contribution of the cooling core to the total luminosity of a group.

In Figure 19 we compare  $E_{\text{mech}}$  and  $E_{\text{cool}}$  in our groups. The mechanical energy injected by all but one of the core radio–galaxies is higher than the radiative losses, and exceeds  $E_{\text{cool}}$  by an order of magnitude in several cases. We can thus conclude that radiative losses do not greatly affect the net energy output of radio–galaxies in the cores of groups. On the other hand, the mechanical output by non-central radio galaxies is typically of the same order as  $E_{\text{cool}}$ . Moreover, these sources reside mostly outside the cooling radius ( $\sim 0.15 R_{200}$ ), where the cooling time is higher than the Hubble time. In this location, the gas does not lose as much energy through radiative cooling as in the core of the group, so these galaxies do not provide the required feedback at the right location.

#### 3.5.3 Impact of systematic effects

The above calculations rest on several assumptions and should be regarded as rough estimates. One critical simplification is the calculation of the lifetime of a radio–galaxy: the statistical argument used in Smolčić et al. (2009) relies on knowledge about the parent population that hosts the radio–galaxies. In the absence of evidence to the contrary, we assume that there is no significant difference between the radio–galaxy elliptical hosts in groups and in low density environments (Feretti & Giovannini, 2007). We note that even if  $\tau_{\text{radio}}$  were incorrect by a factor of 4, the mechanical output in clusters would still be significantly lower than the binding energy, but would remain consistent with the binding energy for many of the groups (see Figure 22).

Other biases may arise from the scaling relation of Birzan et al., which we use to compute the mechanical energy: the large scatter in the  $P_{1.49\text{GHz}}$ – $P_{\text{cav}}$  relationship (0.85 dex) means that care must be taken when using the inferred value as the mean mechanical energy, since most of our calculations rest on the assumption that over the cluster/group lifetime each burst has on average the same power. Indeed, Nipoti &

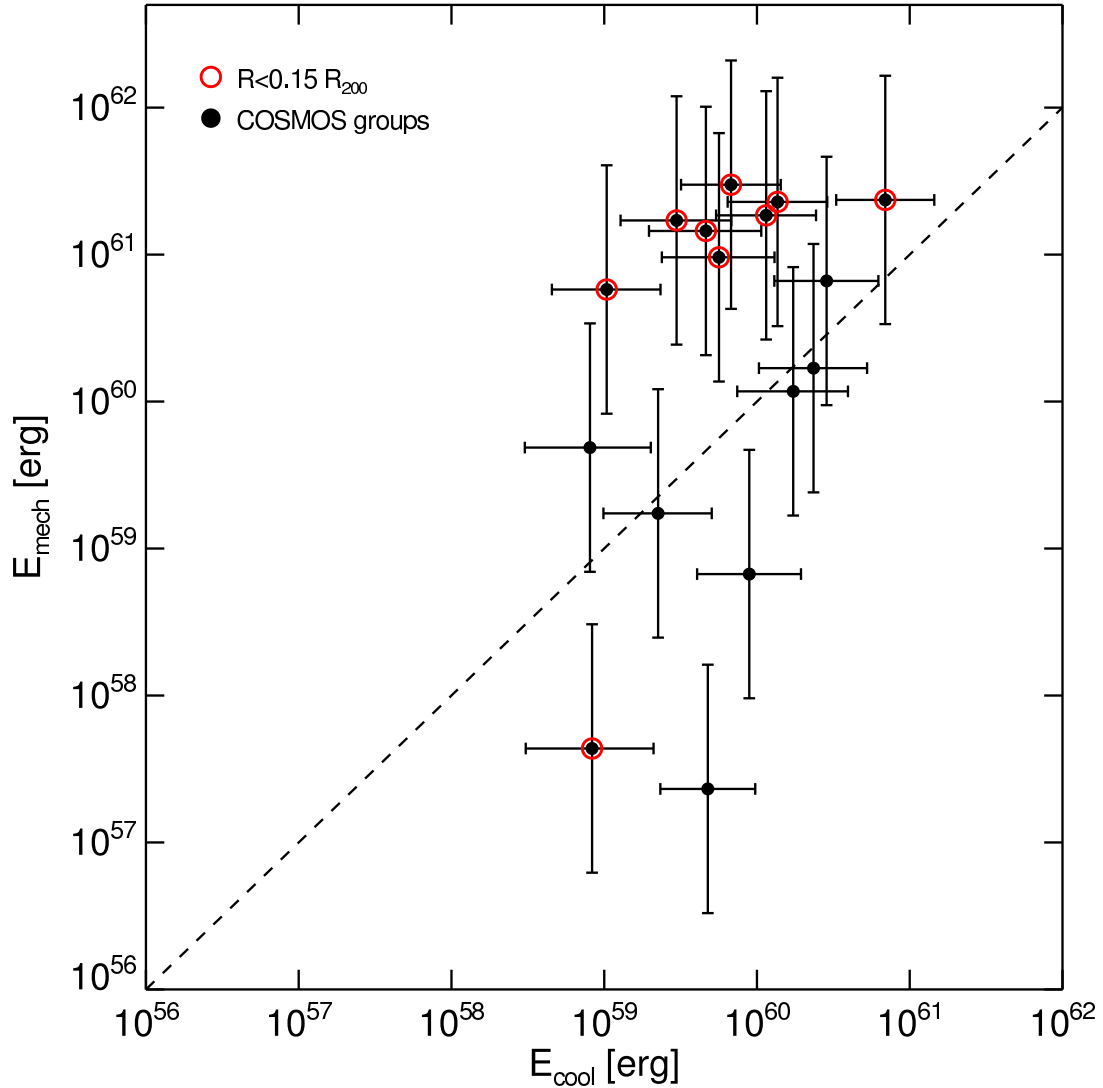


Figure 19: The output mechanical energy from radio-galaxies ( $E_{\text{mech}}$ ) versus energy radiated inside the cooling radius ( $E_{\text{cool}}$ ; i.e. energy required to offset the cooling in the group center) for 16 X-ray selected groups from the COSMOS survey. The dashed line shows the equality line. Red circles mark the radio-galaxies inside  $0.15 \times R_{200}$ . Uncertainties on  $E_{\text{cool}}$  are computed allowing an error of a factor 2 on  $f_{\text{cool}}$ .

Binney (2005) suggested that the distribution of the outbursts over the cluster/group lifetime is log-normal rather than gaussian; therefore in any system there would be a good chance of observing smaller than average jet powers. Instead, much of the power would be generated by rare, more powerful outburst, such as that observed in MS 0735+7421 by Gitti et al. (2007). These arguments rest on the assumption that the observed scatter in  $P_{1.49\text{GHz}}-P_{\text{cav}}$  in the observed ensemble of clusters is a

### 3 Radio–galaxy feedback in X–ray selected groups

---

good description of the time variability of the AGN power in individual objects. In general the ensemble scatter is an upper limit to the scatter in the time variability. If we assume this scatter to represent also for the time variability, we are statistically underestimating the mechanical energy output over the group lifetime by a factor that we compute as follows. The scatter in the Birzan et al. relationship (0.85 dex) corresponds to a probability  $\gtrsim 80\%$  of observing a value smaller than the mean from a single observation (cf. Nipoti & Binney 2005). Thus, if we assume that the observed value of  $P_{1.49\text{GHz}}$  scatters around the median of the distribution, the ratio between the median and the mean for a lognormal distribution (which depends only on the scatter  $\sigma$ ) tells us the scaling factor for the 'true' mean mechanical energy:

$$\frac{\text{mean}}{\text{median}} = \frac{e^{\sigma^2}}{2} = 6.8. \quad (29)$$

Therefore the typical observed mechanical power may be underestimated by a factor  $\leq 7$  with respect to the mean. This value, though not negligible, goes in the direction of further increasing the mechanical output, confirming the effect we found.

Furthermore, if the bubble were over–pressured when compared to the surrounding ICM (Heinz et al., 1998), the expanding bubble would carry a shock and the mechanical power may be underestimated, as well as reported by Birzan et al. (2004). This effect would also boost the mechanical energy to higher values, further strengthening our results.

We have also used preliminary results from VLA 324 MHz data (Smolcic et al. in preparation) to double-check our estimates of the mechanical energy output from radio–galaxies. Only 12 of the 16 radio–galaxies are detected in the 324 MHz band and, in all these cases,  $E_{\text{mech}}$  computed using these data (using Eq.15 in Birzan et al. 2008) is consistent within the error bars with the value computed at 1.49 GHz. As a further check, the total radio luminosity can be computed with higher precision from break frequencies for 7 of the 16 sources, using the the Myers & Spangler (1985) approximation. The value of  $E_{\text{mech}}$  obtained with this improved method is consistent within the error bars with that obtained using monochromatic data.

### 3.6 Discussion: the entropy in X–ray groups

The injection of energy by radio galaxy activity into the ICM modifies the thermodynamical state of the gas, raising the entropy ( $S$ ) by a significant amount compared to

### 3.6 Discussion: the entropy in X-ray groups

that generated by gravitational collapse. We define the entropy as

$$S \propto \frac{kT}{n_e^{2/3}} \quad (30)$$

where  $T$  is the gas temperature in keV and  $n_e$  is the gas electron density (Voit, 2005). An excess entropy of 50–100 keV cm<sup>-2</sup> is indeed observed at the group regime, causing a deviation from the  $S$ – $T$  relation (Ponman et al., 2003). The excess entropy is measured in the central regions (at 0.1  $R_{200}$ ). In the following we make an order of magnitude calculation of the excess entropy generated by the energy injected, then compare it with that observed in groups and predicted from the theory. We recompute the expected  $S$ – $T$  relation taking into account this excess energy, and compare it with the observational constraints of Ponman et al. (2003).

The change in entropy caused by injection of energy under constant pressure is

$$\Delta S = \frac{2}{5} \frac{\Delta E}{n_e} \frac{\gamma_T^{5/3} - 1}{\gamma_T - 1} \quad (31)$$

(Lloyd-Davies et al., 2000), where  $\Delta E$  is the injected energy per particle,  $\gamma_T$  is the ratio between the initial and final temperature (a value between 1.1 and 2.0, Lloyd-Davies et al. 2000), and  $n_e$  is the initial electron density ( $n_e=10^{-2}$  assuming the energy is deposited in the cluster core, e.g. Sanderson & Ponman 2003). We compute  $\Delta E$  from the mechanical energy input of radio galaxies as follows:

$$\Delta E = E_{\text{mech}} \times \frac{m_p \mu}{M_{\text{gas}}} \quad (32)$$

with  $M_{\text{gas}} = f_{\text{gas}} M_{200}$ , where  $f_{\text{gas}}$  is estimated from the relation between gas fraction and total mass in Pratt et al. (2009). This calculation does not depend on the details of the energy injection process. We obtain values of excess entropy between 10 and 60 keV cm<sup>-2</sup>. This is a rough calculation but predicts values similar to those in Voit & Donahue (2005). These authors show that an additional energy input episodic on 10<sup>8</sup> yrs timescale is needed to explain the excess entropy found observationally in the core of clusters (Ponman et al., 2003; Donahue et al., 2005). The additional energy produces an entropy pedestal: Voit (2005) calculates 10 keV cm<sup>-2</sup> to be the minimum entropy boost needed to explain observations, and he predicts it to be larger for groups.

The mechanical energy injected by radio galaxies into the 16 COSMOS X-ray selected groups is roughly independent on the group mass (see Figure 22). This is not unexpected, since the black-hole masses (which are a zeroth order indicator of the

### 3 Radio–galaxy feedback in X–ray selected groups

---

mechanical energy output; Merloni & Heinz 2007) range only between  $10^8$ – $10^9 M_\odot$  in radio galaxies (see Figure 7 in Smolčić et al. 2009). At the cluster regime may not be true that the mechanical energy is independent on cluster mass. Indeed Chen et al. (2007) infer, from the strength of clusters’ cooling cores, that a mechanical input higher than anything observed in groups is necessary to balance the cooling of the gas in the strong cool core clusters. However, it has been shown by the same authors that much ( $\sim 90\%$ ) of that energy input would be radiated away to balance the cooling, and therefore would not participate to the mechanical removal of the gas.

From these considerations, we can predict how the scaling relation between entropy and temperature is affected by the injection of a constant excess energy by radio galaxies. As shown in Finoguenov et al. (2008), the energy deposition into the ICM ( $\Delta E$ ) is proportional to the change in entropy  $\frac{\Delta S}{S}$  for a given typical  $n_e$ . We use  $n_e=10^{-2}$  as the typical value of the density within  $0.1 R_{200}$ , where the majority of the energy is deposited (deposition radius; Sanderson & Ponman 2003). Using the scaling of  $M_{\text{gas}} \propto T^2$  and  $E_{\text{mech}} = \text{const}$ , then

$$\frac{\Delta S}{S} \propto \frac{E_{\text{mech}}}{M_{\text{gas}}} \propto \frac{C}{T^2}. \quad (33)$$

where  $C$  is a constant and  $M_{\text{gas}}$  is the mass of the gas within the deposition radius. We can then infer the functional dependence of  $S$  on the virial temperature of the ICM as

$$S = S_0 + \Delta S = S_0 \times \left(1 + \frac{\Delta S}{S_0}\right) \propto \left(T_0 + \frac{C}{T_0}\right), \quad (34)$$

where  $S_0$  and  $T_0$  are respectively the entropy and the temperature of the gas before the injection of energy from a radio galaxy. The value of  $C$  is computed using Equation 3 in Finoguenov et al. (2008) and has a median value of 2.56 if the energy is deposited inside the cooling radius. We assume the cooling radius to be  $0.10 R_{200}$  (e.g. Ponman et al. 2003) and show the inferred functional form of  $S(T)$  in Figure 20. Remarkably, the shape of the resulting scaling relation (solid line) deviates from the self-similar one (dashed line) around  $\sim 4$  keV, in agreement with the observed scaling relation measured at  $0.1 R_{200}$  by Ponman et al. (2003) (black crosses; these points are binned means). The deviation of the  $\sim 1$  keV point indicates that a lower excess entropy is needed to explain very cold groups. This can be achieved requiring that the mechanical energy is deposited at a larger radius in these groups. Indeed if the deposition radius increases also  $M_{\text{gas}}$  within this radius increases. Therefore using Equation 33 we would obtain a lower values of  $\frac{\Delta S}{S_0}$  (and thus entropy) for these groups, matching eventually the observational point of Ponman et al. (2003) at  $\sim 1$  keV; if this

is the case, it would confirm that the effect of feedback is more global in groups than in clusters (De Young, 2010, cf.). Therefore, the injection of an excess energy that is independent of groups' mass, thus temperature, (as we observe from radio galaxies in the COSMOS groups) correctly predicts the deviation of the observed  $S$ - $T$  relation from the purely gravitational relation at the group scale.

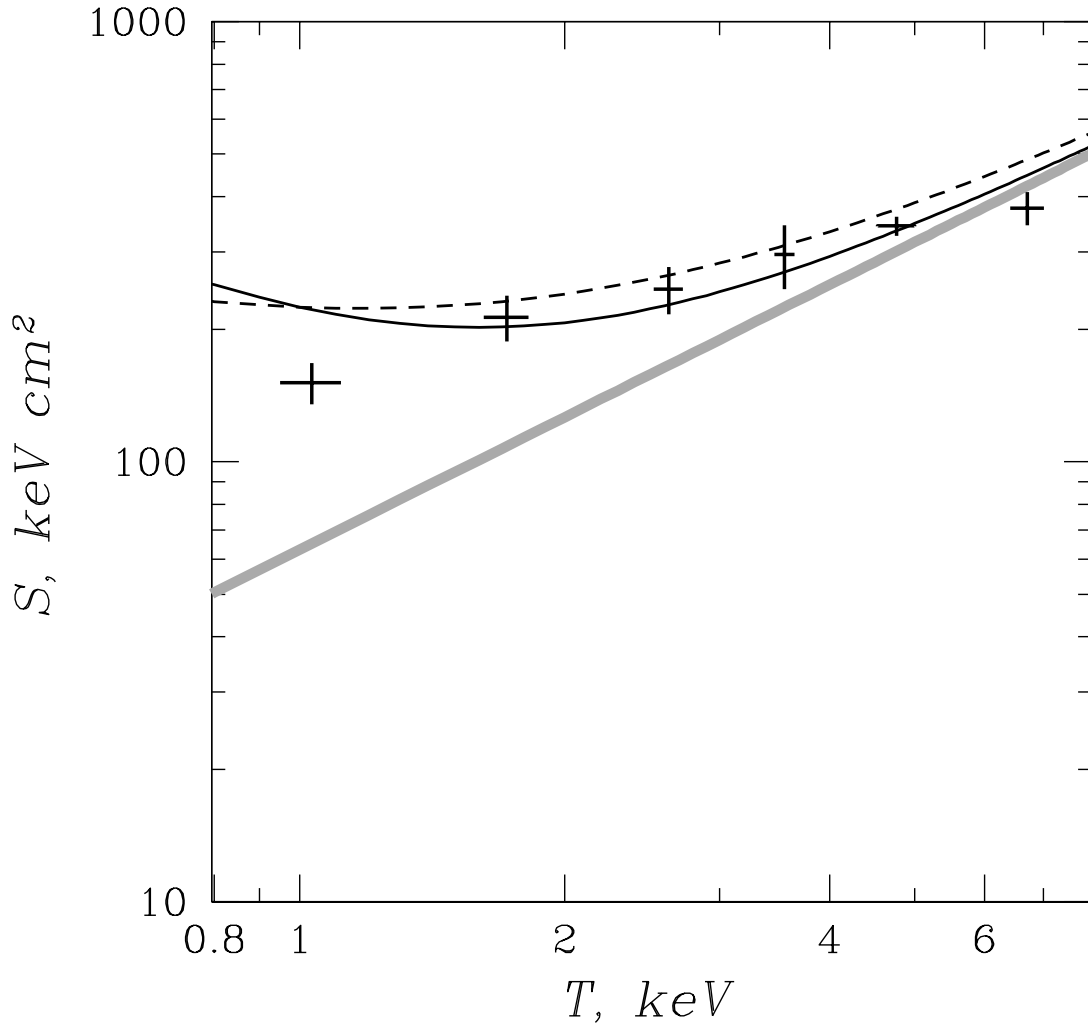


Figure 20: Scaling relation between entropy ( $S$ ), measured at  $0.1 R_{200}$ , and temperature ( $T$ ). The solid black line is the inferred relation accounting for a constant energy excess injected by radio galaxies (see text for details). The grey line is the expected self-similar relation. The points show the binned means from the observations by Ponman et al. (2003). The dashed line is the same as the solid line but considering the self-similar scaling  $M_{gas} \propto T^{1.5}$

## 3.7 Conclusions

In this Paper we have quantified the importance of the mechanical energy input by radio galaxies inside galaxy groups. In particular we report a striking difference between clusters and groups of galaxies: while the binding energy of the ICM in clusters exceeds the mechanical output by radio AGN, the two quantities are of the same order of magnitude in groups that host a radio galaxy within  $0.15 R_{200}$ . This suggests that, while clusters can be mostly considered to be closed systems, the mechanical removal of gas is energetically possible from groups. This has implications that help explain recent findings on the baryonic fraction in groups of galaxies. Giodini et al. (2009) reported a  $\sim 30\%$  lack of gas in groups compared with the cosmological baryon mass fraction evaluated from the 5 years *Wilkinson Microwave Anisotropy Probe* (Dunkley et al., 2009). It has been suggested that this gas has been removed by AGN feedback.

This is consistent with cosmological models in which feedback from radio galaxies is invoked to successfully explain galaxy group/cluster properties. Based on a well selected sample of galaxy groups and clusters that host radio galaxies, we have observationally shown for the first time that this scenario is energetically feasible. We have further shown that a constant injection of excess energy by radio galaxy naturally reproduces the self-similar breaking observed in the scaling relation between the entropy and temperature of groups.

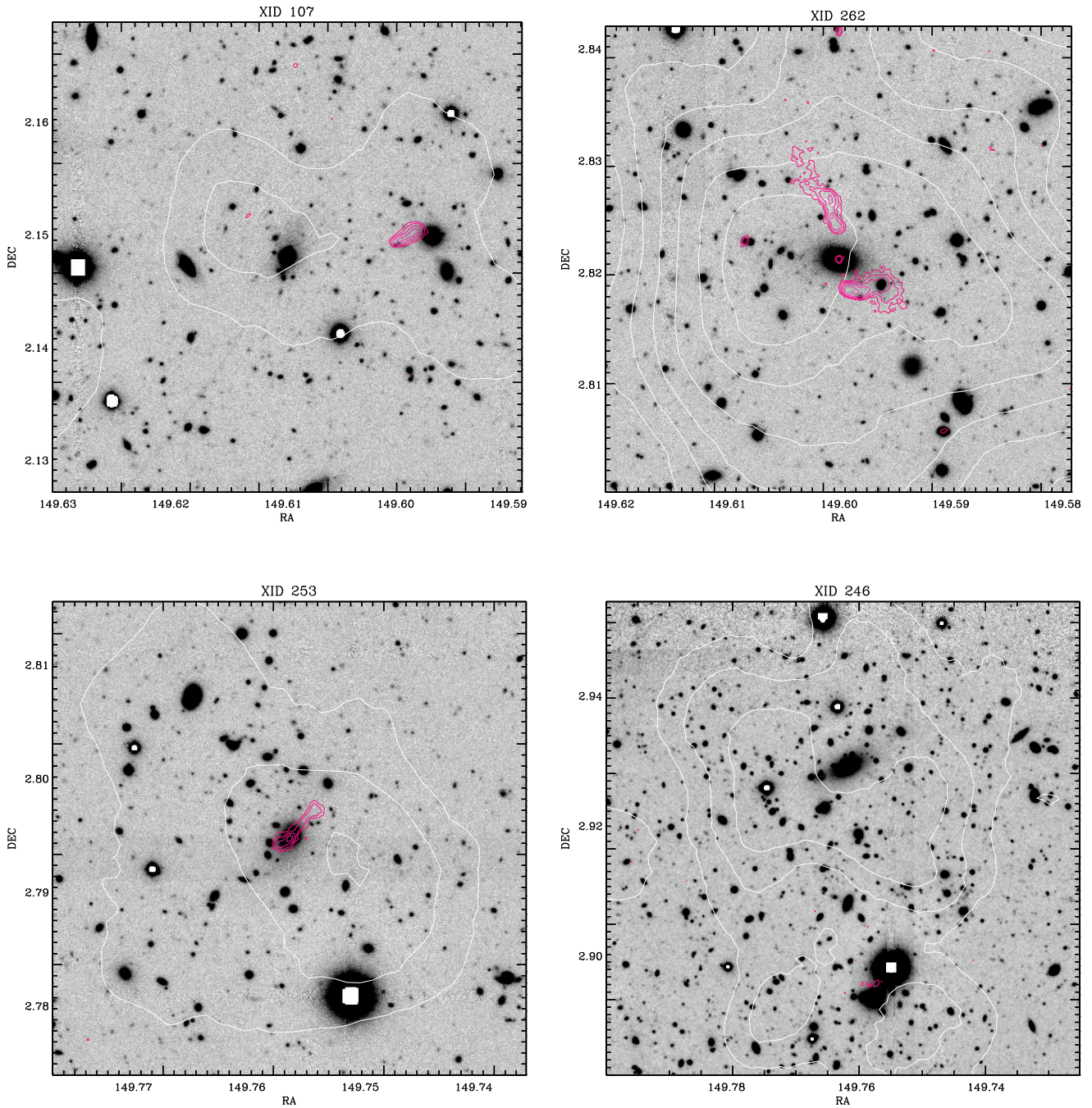
## Acknowledgements

SG acknowledges support by the DFG Cluster of Excellence ‘Origin and Structure of the Universe’. SG thanks A. Merloni for helpful comments. VS acknowledges support from the Owens Valley Radio Observatory, which is supported by the National Science Foundation through grant AST-0838260. VS and AO thank Unity through Knowledge Fund ([www.ukf.hr](http://www.ukf.hr)) for collaboration support through the “Homeland Visit” grant. AO thanks California Institute of Technology for generous support through NASA grants 1292462 and 1344606. We acknowledge the contributions of the entire COSMOS collaboration; more informations on the COSMOS survey are available at <http://www.astr.caltech.edu/~cosmos>.

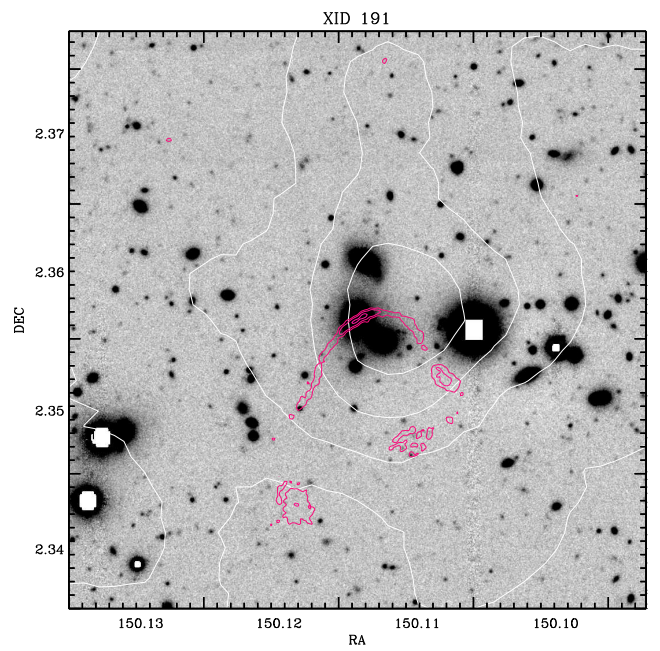
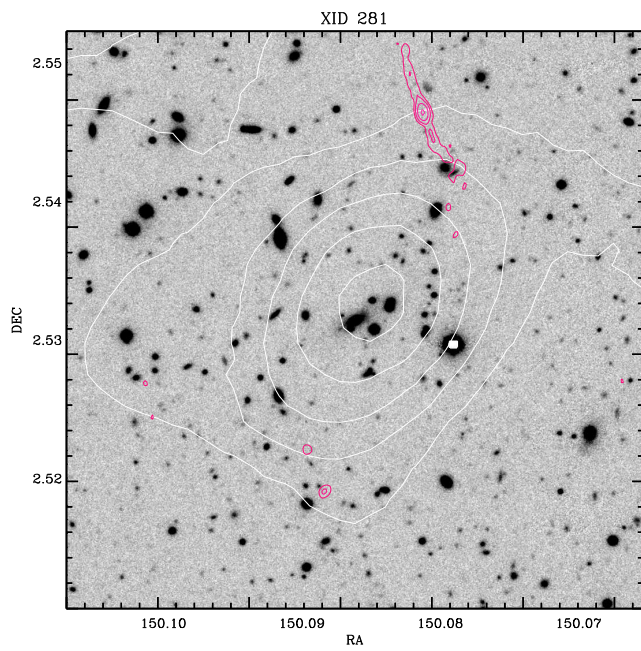
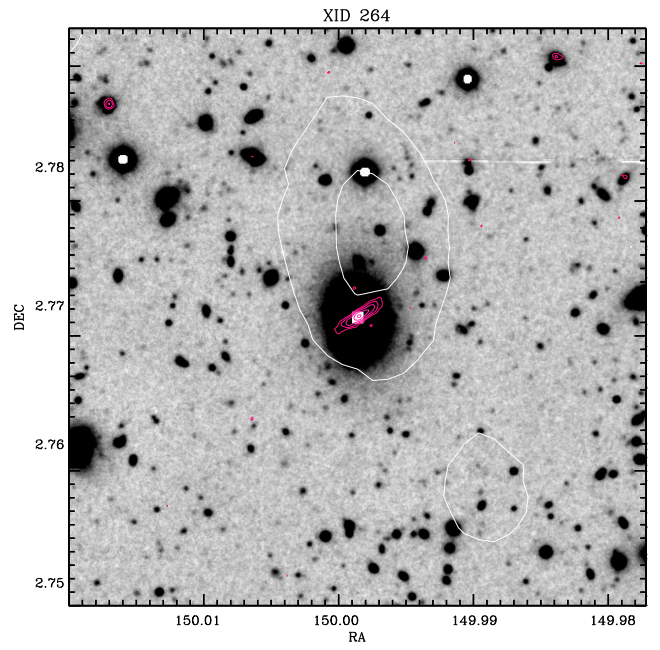
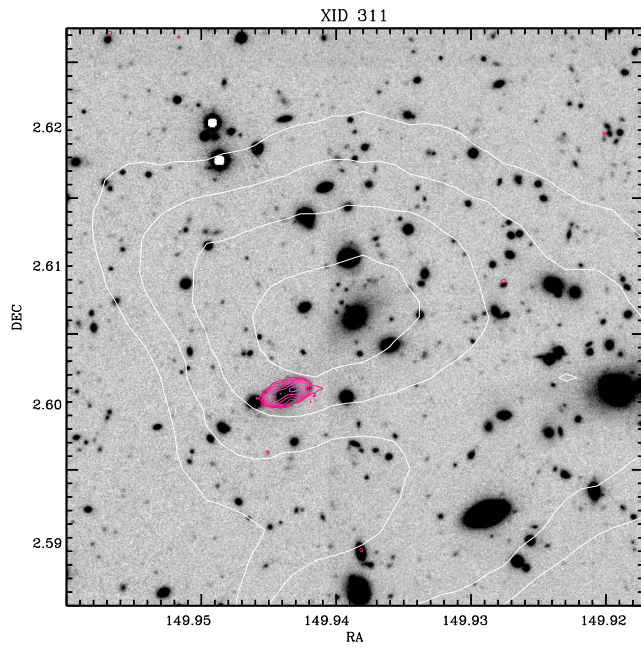
## 3.8 Radio Images

### 3 Radio–galaxy feedback in X–ray selected groups

Figure 21: Figure 26 presents the contours maps of the radio 20 cm emission (magenta lines) superimposed to the SUBARU  $zp$  band image for each of the groups listed in Table 4. Images are  $3 \times 3$  arcmin and centered on the group center, except XID246 which is  $4 \times 4$  arcmin wide and offset from the center group because of its location on the edge of the SUBARU field coverage. The white line shows the contours of X–ray flux significance. The contours correspond to  $[3, 6, 9, 12, 15, 18, 21, 24] \sigma$  X–ray flux significance.

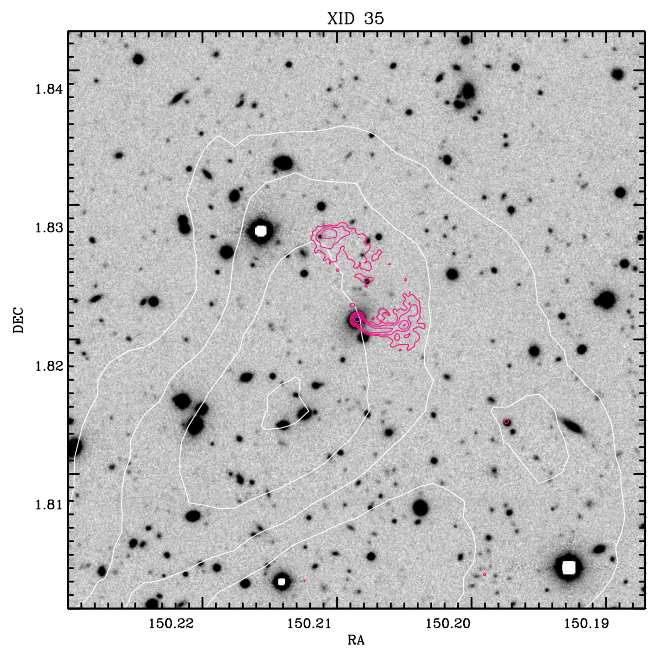
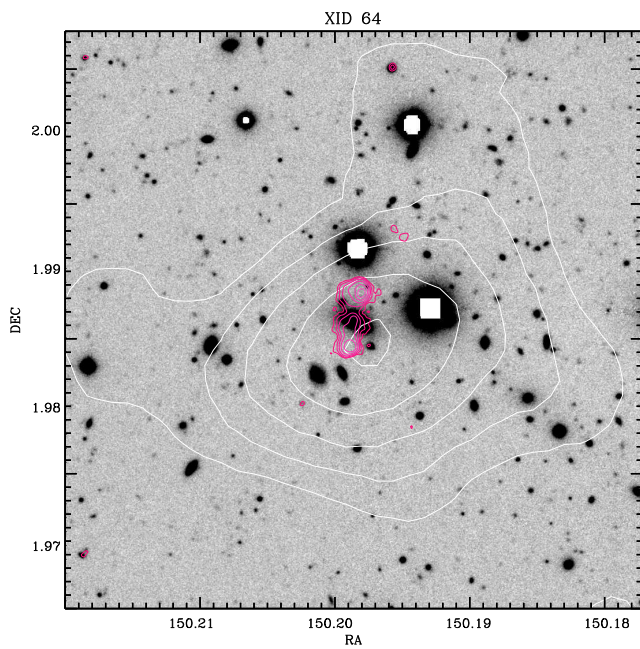
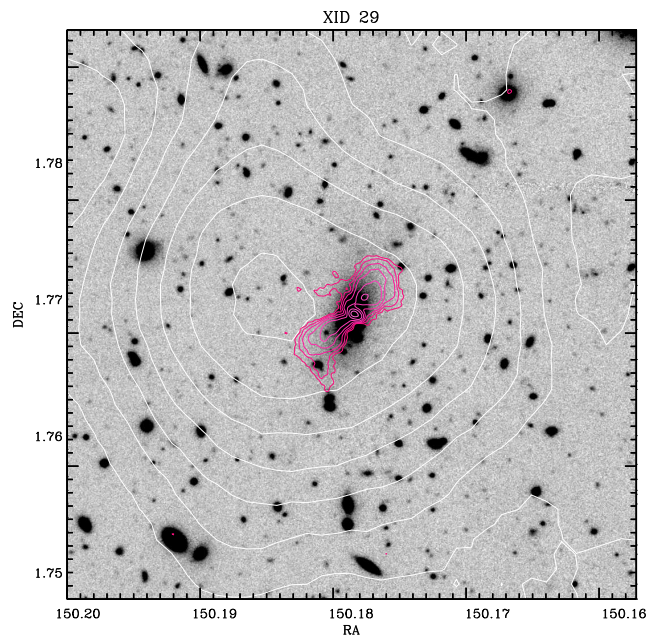
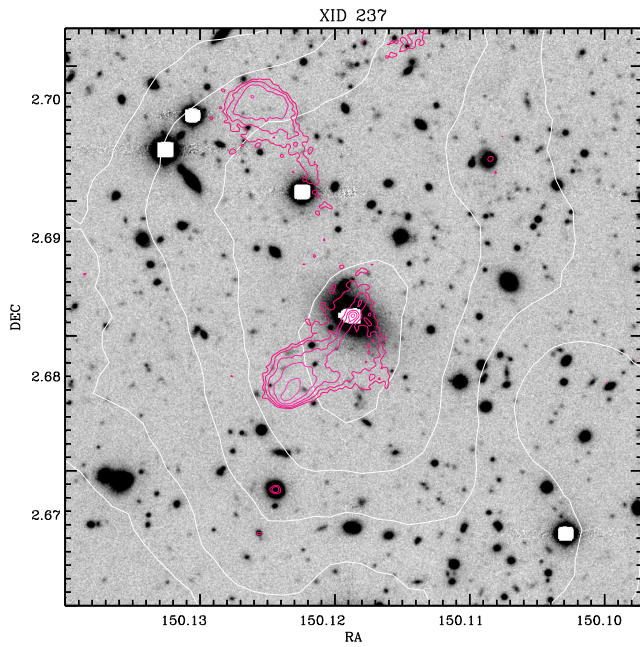


### 3.8 Radio Images

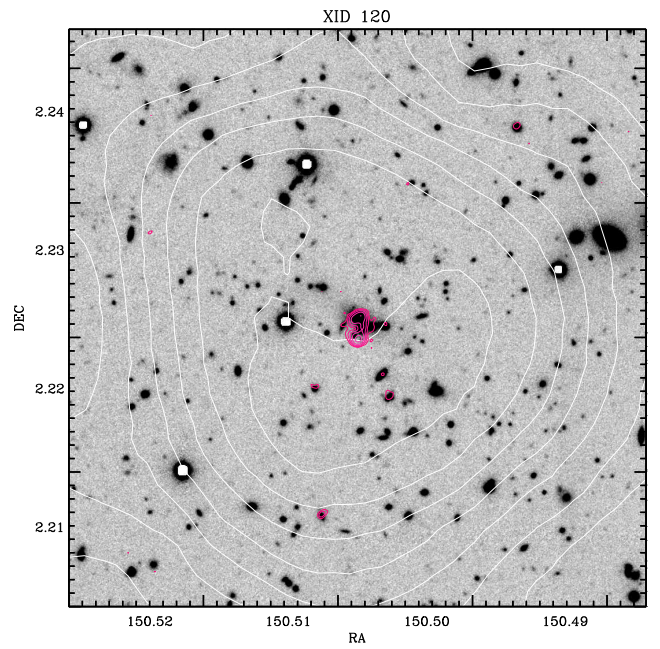
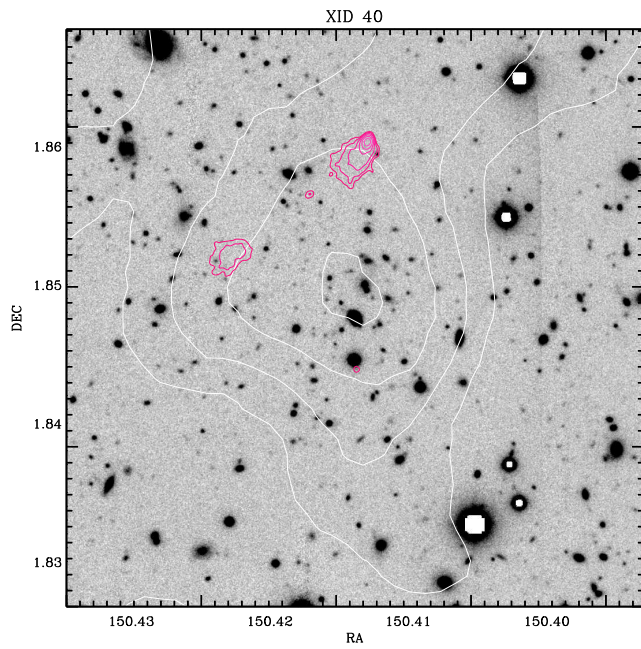
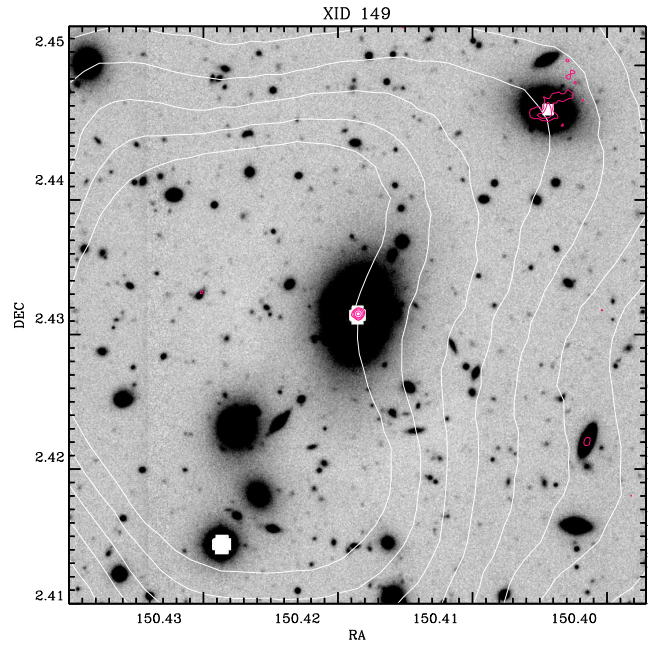
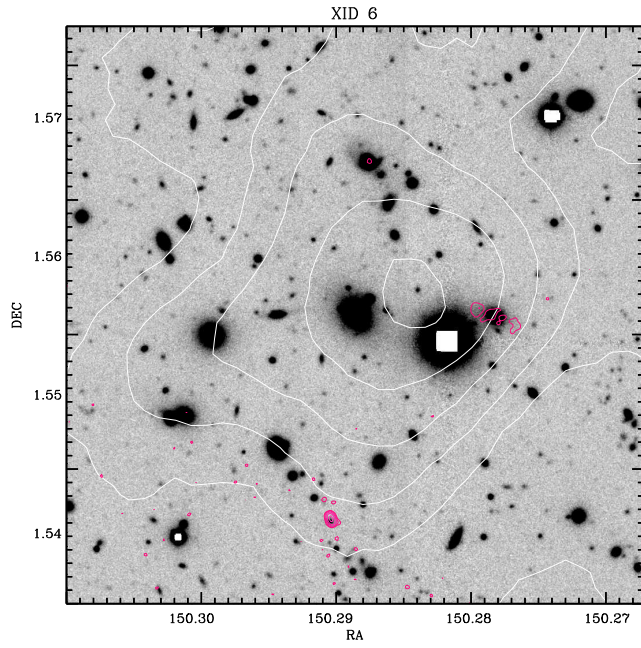


### 3 Radio-galaxy feedback in X-ray selected groups

---



### 3.8 Radio Images





# Bibliography

- Arnaud, M., & Evrard, A. E. 1999, MNRAS, 305, 631
- Balogh, M. L., McCarthy, I. G., Bower, R. G., & Eke, V. R. 2008, MNRAS, 385, 1003
- Baum, S. A., Heckman, T. M., & van Breugel, W. 1992, ApJ, 389, 208
- Bîrzan, L., Rafferty, D. A., McNamara, B. R., Wise, M. W., & Nulsen, P. E. J. 2004, ApJ, 607, 800
- Bîrzan, L., McNamara, B. R., Nulsen, P. E. J., Carilli, C. L., & Wise, M. W. 2008, ApJ, 686, 859
- Bower, R. G., Benson, A. J., Malbon, R., Helly, J. C., Frenk, C. S., Baugh, C. M., Cole, S., & Lacey, C. G. 2006, MNRAS, 370, 645
- Bower, R. G., McCarthy, I. G., & Benson, A. J. 2008, MNRAS, 390, 1399
- Chen, Y., Reiprich, T. H., Böhringer, H., Ikebe, Y., & Zhang, Y.-Y. 2007, A&A, 466, 805
- Churazov, E., Sunyaev, R., Forman, W., & Böhringer, H. 2002, MNRAS, 332, 729 S., Sunyaev, R., Forman, W., Jones, C., Boehringer, H. 2005, MNRAS, 363, L91
- Condon, J. J., Cotton, W. D., Greisen, E. W., Yin, Q. F., Perley, R. A., Taylor, G. B., & Broderick, J. J. 1998, AJ, 115, 1693
- Croton, D. J., et al. 2006, MNRAS, 365, 11
- De Young, D. S. 2010, arXiv:1001.1178
- Donahue, M., Voit, G. M., O'Dea, C. P., Baum, S. A., & Sparks, W. B. 2005, ApJ, 630, L13

## Bibliography

---

- Drory, N., Bender, R., Feulner, G., Hopp, U., Maraston, C., Snigula, J., & Hill, G. J. 2004, *ApJ*, 608, 742
- Dunkley, J., et al. 2009, *ApJS*, 180, 306
- Evrard, A. E., Metzler, C. A., & Navarro, J. F. 1996, *ApJ*, 469, 494
- Fabian, A. C., Arnaud, K. A., Bautz, M. W., & Tawara, Y. 1994, *ApJ*, 436, L63  
arXiv:astro-ph/0703494v1
- Finoguenov, A., Ruszkowski, M., Jones, C., Brügggen, M., Vikhlinin, A., & Mandel, E. 2008, *ApJ*, 686, 911
- Giodini, S., et al. 2009, *ApJ*, 703, 982
- Gitti, M., McNamara, B. R., Nulsen, P. E. J., & Wise, M. W. 2007, *ApJ*, 660, 1118
- Hayashi, E., Navarro, J. F., & Springel, V. 2007, *MNRAS*, 377, 50
- Heinz, S., Reynolds, C. S., & Begelman, M. C. 1998, *ApJ*, 501, 126
- Ilbert, O., et al. 2009, *ApJ*, 690, 1236
- Kaastra, J. S., et al. 2004, *A&A*, 413, 415
- Kay, S. T. 2004, *MNRAS*, 347, L13
- Lin, Y.-T., Mohr, J. J., & Stanford, S. A. 2003, *ApJ*, 591, 749
- Lloyd-Davies, E. J., Ponman, T. J., & Cannon, D. B. 2000, *MNRAS*, 315, 689
- Leauthaud, A., et al. 2010, *ApJ*, 709, 97
- Macciò, A. V., Dutton, A. A., van den Bosch, F. C., Moore, B., Potter, D., & Stadel, J. 2007, *MNRAS*, 378, 55
- Markevitch, M. 1998, *ApJ*, 504, 27
- Myers, S. T., & Spangler, S. R. 1985, *ApJ*, 291, 52
- McCarthy, I. G., Bower, R. G., & Balogh, M. L. 2007, *MNRAS*, 377, 1457
- McNamara, B. R., & Nulsen, P. E. J. 2007, *ARA&A*, 45, 117
- Merloni, A., & Heinz, S. 2007, *MNRAS*, 381, 589
- Navarro, J. F., Frenk, C. S., & White, S. D. M. 1996, *ApJ*, 462, 563

- Nipoti, C., & Binney, J. 2005, MNRAS, 361, 428
- Peres, C. B., Fabian, A. C., Edge, A. C., Allen, S. W., Johnstone, R. M., & White, D. A. 1998, MNRAS, 298, 416
- Peterson, J. R., Kahn, S. M., Paerels, F. B. S., Kaastra, J. S., Tamura, T., Bleeker, J. A. M., Ferrigno, C., & Jernigan, J. G. 2003, ApJ, 590, 207
- Peterson, J. R., & Fabian, A. C. 2006, Phys. Rep., 427, 1
- Ponman, T. J., Sanderson, A. J. R., & Finoguenov, A. 2003, MNRAS, 343, 331
- Pratt, G. W., & Arnaud, M. 2003, A&A, 408, 1
- Pratt, G. W., Croston, J. H., Arnaud, M., & Böhringer, H. 2009, A&A, 498, 361
- Pratt, G. W., et al. 2009, arXiv:0909.3776
- Puchwein, E., Sijacki, D., & Springel, V. 2008, ApJ, 687, L53
- Reiprich, T. H., Böhringer, H. 2002, ApJ, 567, 716
- Renzini, A. 2006, ARA&A, 44, 141
- Sanderson, A. J. R., & Ponman, T. J. 2003, MNRAS, 345, 1241
- Salvato, M., et al. 2009, ApJ, 690, 1250
- Scoville, N., et al. 2007, ApJS, 172, 1
- Schinnerer, E., et al. 2007, ApJS, 172, 46
- Sijacki, D., & Springel, V. 2006, MNRAS, 366, 397
- Short, C. J., & Thomas, P. A. 2009, ApJ, 704, 915
- Skrutskie, M. F., et al. 2006, AJ, 131, 1163
- Smolčić, V., et al. 2008, ApJS, 177, 14
- Smolcic, V., et al. 2009, arXiv:0901.3372
- Sun, M., Voit, G. M., Donahue, M., Jones, C., Forman, W., & Vikhlinin, A. 2009, ApJ, 693, 1142
- Voigt, L. M., & Fabian, A. C. 2004, MNRAS, 347, 1130
- Voit, L. M. 2005, Reviews of Modern Physics, 77, 207

## Bibliography

---

Voit, G. M., & Donahue, M. 2005, ApJ, 634, 955

Wright, A., & Otrupcek, R. 1990, PKS Catalog (1990), 0

# The Galaxy Stellar Mass Function of COSMOS X-ray detected groups: evolution and dependence on the environment

*S. Giodini, H. Boehringer, D. Pierini, A. Finoguenov*

*To be submitted*

## **Abstract**

We present the analysis of the composite galaxy stellar mass function (GSMF) for 118 X-ray detected galaxy groups at  $0.2 < z < 1$  in the COSMOS field. Combining the photometric and X-ray information in the COSMOS survey we consider galaxies in three different environments: field, low mass groups ( $M_{200} < 5 \times 10^{13} M_{\odot}$ ), high mass groups ( $M_{200} > 5 \times 10^{13} M_{\odot}$ ). In addition we divide the galaxy sample in active and passive, according to their spectro-photometric type. We find a dip at intermediate masses ( $M \sim 10^{10} M_{\odot}$ ) in the GSMF for field and low mass groups at  $z < 1$  for both active and passive galaxies. The amplitude of the dip for passive galaxies depends on the environment, at least  $z < 0.6$ . Indeed at low redshift there is a marked difference between low/high mass groups' and field' GSMF, namely groups exhibit a much less

pronounced dip when compared to the field. We interpret this difference with the presence of an excess of passive galaxies at intermediate mass ( $M \sim 10^{10} M_{\odot}$ ) in groups, likely as a product of environmental effects. At high redshift the difference between the passive GSMF for the groups and the field (at  $M > 10^{10.1} M_{\odot}$ ) decreases. This suggests that the passive galaxies at  $M > 10^{11} M_{\odot}$  are already in place in any environment, in line with the downsizing scenario. On the other hand it also indicates that the environmentally driven growth of the passive population at intermediate mass has not yet taken place at  $z=1$ .

### 4.1 Introduction

The galaxy stellar mass function (GSMF) is a very important diagnostic to perform a census of galaxy properties, and provides a powerful mean of comparison between the population of galaxies in different environment.

Historically, the luminosity function has been the first diagnostic used to study the distribution of galaxy properties, since magnitude is a more direct observable than mass. However, the development of stellar population synthesis models and deep multi-wavelength surveys have greatly improved our ability to estimate the stellar mass content in galaxies, and to study the distribution in stellar mass, a parameter which is more directly linked to the total mass of a galaxy.

The galaxy stellar mass function is important for both cosmology and galaxy evolution to better understand the connection between galaxy distribution and the underlying dark matter distribution, and its link to the environment. In particular, the shape of the GSMF and its evolution gives very important insights on the processes that contribute to the growth in stellar mass of galaxies with time, thus giving unique information on the process driving the formation and evolution of galaxies in different environments. Also, to study the dependence of the GSMF on the environment is a way to trace the locus and timescale of the stellar mass assembly.

The GSMF has been extensively studied in deep fields, for galaxies of different colors and morphological types (e.g. Pérez-González et al. 2008) and in different environments (e.g. Balogh et al. 2001), and its shape has been generally described with a Schechter function (Schechter 1976). When fitted to the data, the shape of this function changes both as a function of the galaxy type (active/passive) and of the environment (Balogh et al. 2001; Bolzonella et al. 2009). Moreover recent studies based on deep surveys have shown clear evidence for a low-mass upturn of the local GSMF (e.g. Baldry et al. 2008; Drory et al. 2009 hereafter D09) which is adequately described by a second Schechter function, with a steep negative slope and a lower characteristic

mass. This feature is not unexpected: a steeply rising mass function for the faint population is a generic prediction of galaxy formation in the framework of hierarchical clustering (e.g. White & Rees 1978). Furthermore a faint end upturn suggests that the efficiency of feedback has levelled off at low galaxy luminosities.

However the nature of the shape of the GSMF is still a matter of debate. It has been interpreted with a bimodal behavior of red and blue galaxies (e.g. Balogh et al. 2001; Bolzonella et al. 2009), according to which the red galaxies are responsible for the hump and the blue ones for the upturn described by the double Schechter function. Another possible interpretation entails the different role of central and satellite galaxies in the different environments (Faltenbacher et al., 2010). In the light of these findings it is extremely important to study the GSMF in different environments and as a function of redshift. In this paper we investigate the GSMF of the X-ray selected groups in the COSMOS 2 degs<sup>2</sup> field and compare it to that of clusters and the field. The COSMOS survey provides a unique database of photometric and spectroscopic data, together with deep X-ray data from XMM and Chandra, and the largest catalog of X-ray detected groups up to now. We take advantage of X-ray data to provide a definition of environments based on the depth of the dark matter potential well, dividing between low mass and high mass groups. Furthermore, X-ray information provides evidence for a gravitationally bound nature of the identified groups and a better total mass proxy, giving a more solid basis for subsequent conclusions.

This study is structured as follows: in section 4.2 we describe the sample of X-ray detected groups (4.2.1) and the sample of group member galaxies (in 4.2.2). In section 4.3 we first check test data against the result from deep fields, and then we build the GSMFs as a function of redshift and mass of the galaxy systems. Results are presented in section 4.4. Finally in section 4.5 we present a discussion on the environmental dependence and evolution of the GSMF.

## 4.2 The sample

### 4.2.1 Galaxy groups in the COSMOS field

The catalog of COSMOS X-ray selected groups (status January 2010) contains  $\sim 300$  extended sources detected from a wavelet scale-wise reconstruction of the image as described in Finoguenov et al. (2007) and in Finoguenov et al. (in preparation; see also Giodini et al. 2009). The center of each system corresponds to the X-ray peak of the source or, when the latter is contaminated by AGN emission, to the center of the galaxy distribution within the extent of the X-ray source. With respect to the catalog used in Giodini et al. (2009), the present catalog takes advantage of the newly

## 4 The GSMF of COSMOS groups

---

compiled 20,000 spectra by the zCOSMOS program (Lilly et al., 2007), which enables us to spectroscopically confirm most of the X-ray selected systems. We use 118 systems from this catalog. We require that the systems are detected as extended X-ray sources at more than  $3\sigma$  significance in the flux detection. We constrain the sample at  $L_{X,0.1-2.4\text{keV}} > 10^{42}$  erg sec $^{-1}$  to limit contamination from starburst galaxies. Furthermore we limit ourselves to  $z < 1.0$ , to ensure high quality photometric redshifts, and to  $z > 0.2$  to sample enough volume per redshift interval.

92 systems out of 118 are confirmed by at least 3 galaxies at the same spectroscopic redshift within  $R_{200}$ . Spectra are provided by the zCOSMOS spectroscopic program (Lilly et al., 2007), the SDSS spectroscopic survey, or by targeted observations obtained with the Keck or Magellan telescope. The redshift of each group is derived from the peak of the spectroscopic redshift distribution within  $R_{200}$  or, in case less than three galaxies at the same redshift are present within  $R_{200}$ , from the mean of the photometric redshifts of the corresponding galaxy over-density.

The total masses of the groups are derived from the  $L_X$ - $M_{200}$  relation determined in Leauthaud et al. (2010) via the weak lensing analysis. The resulting sample of X-ray detected groups ranges between  $6.2 \times 10^{12}$  and  $2.7 \times 10^{14}$   $M_\odot$  in total mass with a median of  $3.8 \times 10^{13}$   $M_\odot$ .

The aim of this work is to investigate the galaxy stellar mass function in groups at different redshifts. Therefore we divide the groups sample into 4 redshift bins between  $z=0.2-1.0$ , spanning 0.2 in redshift each (0.2-0.4, 0.4-0.6, 0.6-0.8, 0.8-1.0). Furthermore, to study the behaviour of the galaxy stellar mass function as a function of the system's total mass, besides redshift, in the redshift range 0.2-0.4 and 0.8-1.0 we divide the systems in two bins of  $M_{200}$ . We define low mass groups those with  $M_{200} < 5 \times 10^{13}$   $M_\odot$  and high mass groups those with higher values of  $M_{200}$ . Table 4.2.1 lists the number of sources in each subsample, the volume probed by each redshift bin, and the groups median mass in each subsample. Figure 22 shows the distribution of  $M_{200}$  as a function of the redshift for the groups sample and the division in subsamples.

### 4.2.2 Galaxies in the COSMOS groups

We use the COSMOS catalogue with photometric redshifts derived from 30 broad and medium bands described in Ilbert et al. (2009) and Capak et al. (2007) (version 1.8). As a by-product of the photo- $z$  determination, spectroscopic types were attributed to individual galaxies on the basis of their best-fit broad-band spectral energy distributions (SEDs). This information is used to estimate the stellar mass of a galaxy, which is obtained from the conversion of the Ks-band luminosity (Ilbert et al., 2009) using

Table 5: Sample size

Redshift	Volume [ $10^6 \text{ Mpc}^3$ ]	$\text{Log}(M_{200,\text{med}}) [M_{\odot}]$	$N_{\text{groups}}$
LOW MASS GROUPS			
$0.2 < z < 0.4$	0.56	$2.1 \times 10^{13}$	35
$0.4 < z < 0.6$	1.23	$3.5 \times 10^{13}$	19
$0.6 < z < 0.8$	1.92	$4.1 \times 10^{13}$	28
$0.8 < z < 1.0$	2.53	$4.2 \times 10^{13}$	10
HIGH MASS GROUPS			
$0.2 < z < 0.4$	0.56	$8.8 \times 10^{13}$	9
$0.8 < z < 1.0$	2.53	$10.1 \times 10^{13}$	17

an evolving galaxy-type dependent stellar mass-to-Ks-band luminosity ratio  $M/L_{Ks}$  (Arnouts et al., 2007). This relation has been established using a Salpeter initial mass function (Salpeter, 1955). Stellar masses of individual galaxies are contained in the COSMOS photometric catalogue; the fractional error on the stellar mass of a galaxy is typically equal to 34% , and is dominated by the mean scatter on  $M/L_{Ks}$  (Arnouts et al., 2007).

We limit the galaxy selection to those brighter than  $i_{AB}^+ = 25$ , in order to ensure the accuracy of the photometric redshift to be within  $0.03 \times (1+z)$ , as shown in Figure 9 in Ilbert et al. (2009). At this magnitude limit the detection completeness is  $> 90\%$  (Capak et al. 2007). Additionally we require the galaxies to be brighter than 24 AB magnitudes in K band, to ensure the reliability of the stellar mass. We assign galaxies to the X-ray selected groups as follows. For each group we consider as member galaxies those within a radial distance of  $R_{500}$  from the group’s center and within two times the error of the groups’ photometric redshift. In order to compare the galaxies’ stellar mass distribution at different redshifts, we consider only galaxies above a completeness mass which is redshift dependent. The completeness mass is estimated in each redshift bin as described by Giodini et al. (2009). Briefly we derive the stellar mass ( $M_{\text{lim}}$ ) that each object would have if its apparent magnitude was equal to the sample limit magnitude (i.e.  $i_{AB} = 25$ ) and then we derive the 95% percentile of the distribution in  $M_{\text{lim}}$  for galaxies in the lower 20% percentile in magnitude. We calculate this for each of the redshift bins in which the groups’ sample is divided. Finally a fit to the corresponding envelope as a function of redshift is performed for  $0.2 \leq z \leq 1.0$  in bins of 0.2 in redshift; the ensuing values represent the stellar mass completeness as a function of redshift for our sample. The value of the corresponding completeness mass for each redshift is listed in Table 6. We compute the completeness galaxy stellar mass separately for passive galaxies. Indeed we expect this value to be higher than for the total sample because passive galaxies are less luminous than active ones of similar

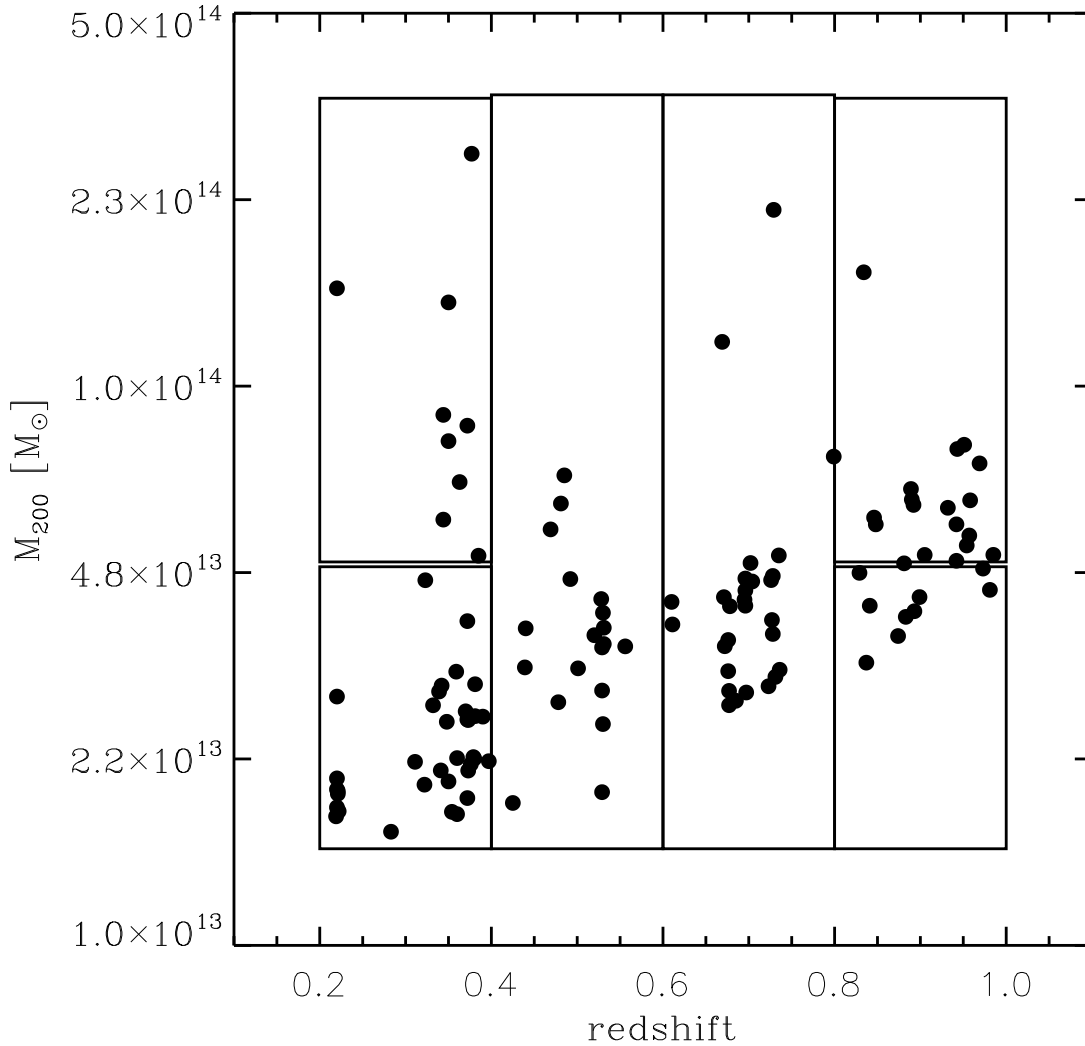


Figure 22: Distribution of  $M_{200}$  as a function of redshift for the 118 X-ray detected groups in the COSMOS field. The rectangles show how the sample is divided in bis of total mass and redshift.

stellar mass. We select the passive galaxies in the photometric catalog as those which have as a best fit to the spectral energy distribution an early type galaxy template. In the COSMOS photometric catalog these galaxies have an SED type between 1 and 8 (for details on the templates see Ilbert et al. 2009 and Polletta et al. 2007). These SED types represent a “quiescent” population consistent with an E/S0/Sa population selected morphologically (Ilbert et al., 2010). The galaxies in this categories overlap at most redshifts with the associated clump of passive galaxies identified in a color-color plot with red  $NUV-R$  and blue  $R-J$  colors, as shown in D09.

The values of the completeness mass for early type galaxies we found are compatible

with those found by Drory et al. (2009) using a maximally high M/L ratio evolution model.

Table 6: Galaxy completeness stellar mass

Redshift	$M_{\text{comp,ET}} [M_{\odot}]$	$M_{\text{comp,all}} [M_{\odot}]$
$0.2 < z < 0.4$	8.9	8.6
$0.4 < z < 0.6$	9.2	9.1
$0.6 < z < 0.8$	9.6	9.5
$0.8 < z < 1.0$	10.1	10.1

## 4.3 Analysis

### 4.3.1 Consistency with the result from the deep fields

In order to have a handle on systematics, we check whether the galaxy stellar mass function that we obtain from our data for the whole COSMOS field, irrespective of the environment, is consistent with the result by D09. These authors compute the galaxy stellar mass function in the COSMOS field and determine the galaxy stellar masses by comparing the multi-band photometry to a grid of stellar population evolutionary synthesis models as described in Drory et al. (2004). They report a bimodal behaviour of the galaxy stellar mass function, represented by a dip in the galaxy stellar mass distribution around  $\sim 10^{10} M_{\odot}$  and a steep upturn at lower masses. This trend is adequately modelled by a double Schechter function. In Figure 23 we present the galaxy stellar mass function computed for the whole COSMOS field, in a similar fashion as shown in D09. Red, blue and black points represent respectively passive, active and the whole galaxy population. The dashed dotted line mark the completeness stellar mass at each redshift. For comparison, we over-plot the double Schechter fit to the GSMF from Drory et al. (2009) to the passive (red dashed line) and active (blue dashed) populations. The only difference in the two GSMs is the method to compute the stellar mass (K-band luminosity versus SED fitting). The two GSMS agree very well: the two curves differ by no more than 0.1 dex in the mass bins above the completeness mass. Thus we are recovering the result from D09 and this excludes any systematic bias between the two samples of galaxies with different stellar mass determination. The GSMFs show a clear dip and upturn towards low masses both for passive and active galaxies, which is hardly compatible with a single Schechter function.

It is important that the global GSMFs measured here, and based on the K-band derived masses, are in such good agreement with the recent determination by D09

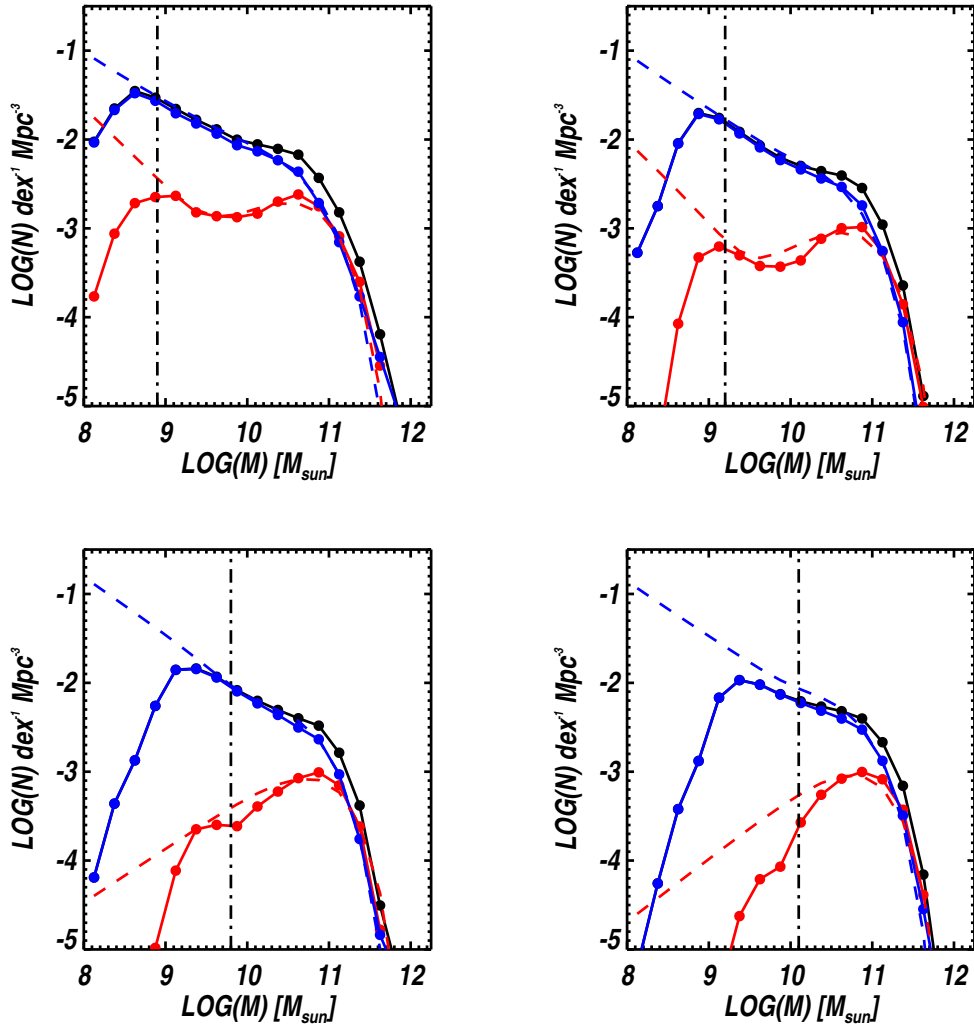


Figure 23: GSMF for all (black points), active (blue) and passive (red) galaxies in the COSMOS field, as a function of redshift. The dashed lines are the correspondent best fitting Schechter function presented in D09.. The vertical dashed-dotted line is the stellar completeness mass at the corresponding redshift.

since, as shown by the latter authors, all GSMFs derived from deep field surveys are consistent (see e.g., Baldry et al. 2008; Ilbert et al. 2009; Pérez-González et al. 2008).

### 4.3.2 Galaxy stellar mass function of COSMOS groups

For each bin of redshift and total mass the composite galaxy stellar mass for the COSMOS X-ray selected groups is expressed as:

$$\phi(M) = \frac{1}{V_z} \sum_i^n (N(M)_i - N_b(M)_i) \quad (35)$$

where  $N$  indicates the member galaxies,  $N_b$  the coeval background galaxies,  $V_z$  is the volume sampled by the redshift bin considered and  $n$  is the number of systems in each bin of redshift and total mass. We divide the groups' GSMF by the survey volume, because this enables us to estimate the contribution of the groups to the GSMF of the whole field. The "field" environment comprises all coeval galaxies outside bound X-ray emitting structures.  $N(M)$  is obtained by direct counting of the member galaxies above the completeness mass in bins of 0.25 dex in stellar mass. The stellar mass bin size corresponds approximately to the error on the mass on the individual galaxies.  $N_b(M)$  is the average background GSMF estimated for each system by considering all the galaxies outside the groups'  $R_{200}$  at the system's redshift (field galaxies). The background GSMF is computed by splitting the field area in four quadrants containing equal surveyed areas. The average over the four background GSMF is then scaled down to the group's area. The background uncertainties ( $\delta_b$ ) are estimated from the standard deviation of the four background GSMF. The total uncertainties on  $\phi(M)$  is a combination of field to field variation and small number statistics:

$$\delta\phi(M) = \sum_i^n \delta_{b,i}^2 + \delta_{p,i}^2 \quad (36)$$

where the second term is the poissonian error on the GSMF

$$\delta_{p,i} = \sqrt{N(M)_i} \quad (37)$$

## 4.4 Results

### 4.4.1 The shape of the galaxy stellar mass function

In figure 25 we plot the GSMFs in the four redshift bin and for passive (in red), active (in blue) and all galaxies (in black). Filled circles mark data-points above the stellar mass completeness limit, while open circles mark the part of the GSMF affected by

## 4 The GSMF of COSMOS groups

---

incompleteness. As the plots show, at all redshifts a single Schechter function is not an adequate description for the shape of the total GSMF of groups with  $M_{500} < 5 \times 10^{13} M_{\odot}$  (black points) and active galaxies' stellar mass function. Indeed, in both cases an increasing number density of low mass galaxies is required to define the GSMF's shape. The passive GSMF, instead, shows a hump at high stellar masses, followed by a dip around  $10^{10} M_{\odot}$  and then an upturn at lower masses.

An alternative way to describe the GSMF's shape has been proposed, that is a sum of two Schechter components (double Schechter function; Driver et al. (1994)), where the extra Schechter component models the rise of the faint (low mass) end, as a steep power law. This function has six free parameters, and is expressed as:

$$\begin{aligned}
 \phi(M)dM &= \phi_h(M)dM + \phi_l(M)dM = \\
 &= \phi_h \left( \frac{M}{M_h^*} \right)^{\alpha_h} \exp \left( -\frac{M}{M_h^*} \right) dM + \\
 &+ \phi_l \left( \frac{M}{M_l^*} \right)^{\alpha_l} \exp \left( -\frac{M}{M_l^*} \right) dM.
 \end{aligned} \tag{38}$$

We define  $M_h^*$  and  $M_l^*$  such that  $M_h^* > M_l^*$  thereby identifying the first term,  $\phi_h(M)$ , with a population of massive galaxies and the second term,  $\phi_l(M)$ , with a population of low mass galaxies.

In order to limit the number of free parameters with respect to the data points above the completeness limit, we fix the slope of the faint end and the relative normalization to the values found by D09. In Table 4.4.1 we present the best fitting Schechter parameters obtained by fitting equation 38 with a non-linear least squares curve fitting method (Markwardt, 2009). The table also lists the reduced  $\chi^2$  values for the best fit and that obtained by fitting a single Schechter function to the data ( $\chi_{single}^2$ ). A word of caution is warranted on the fitting performed when the number of degrees of freedom is larger or equal to the number of free parameters.

The parameters we find for the field GSMF are consistent with those reported by D09 within the uncertainties, whereas the groups' massive end at low redshifts is consistent with the results based on SDSS (Yang et al., 2009).

Comparing the value of  $\chi_{double}^2$  to  $\chi_{single}^2$ , we note that in general the fit improves when the field's and groups' GSMF are described by a double Schechter function. In particular the fitting performed with a single Schechter function on the field galaxy population gives particularly high values of  $\chi_{single}^2$ , in agreement with the finding of D09. However, our analysis does not establish the need for a second Schechter function for the high mass groups (the  $\chi^2$  value doesn't improve by adding a second Schechter component). This suggests that the deviation from a single Schechter function may

become less prominent in massive bound systems.

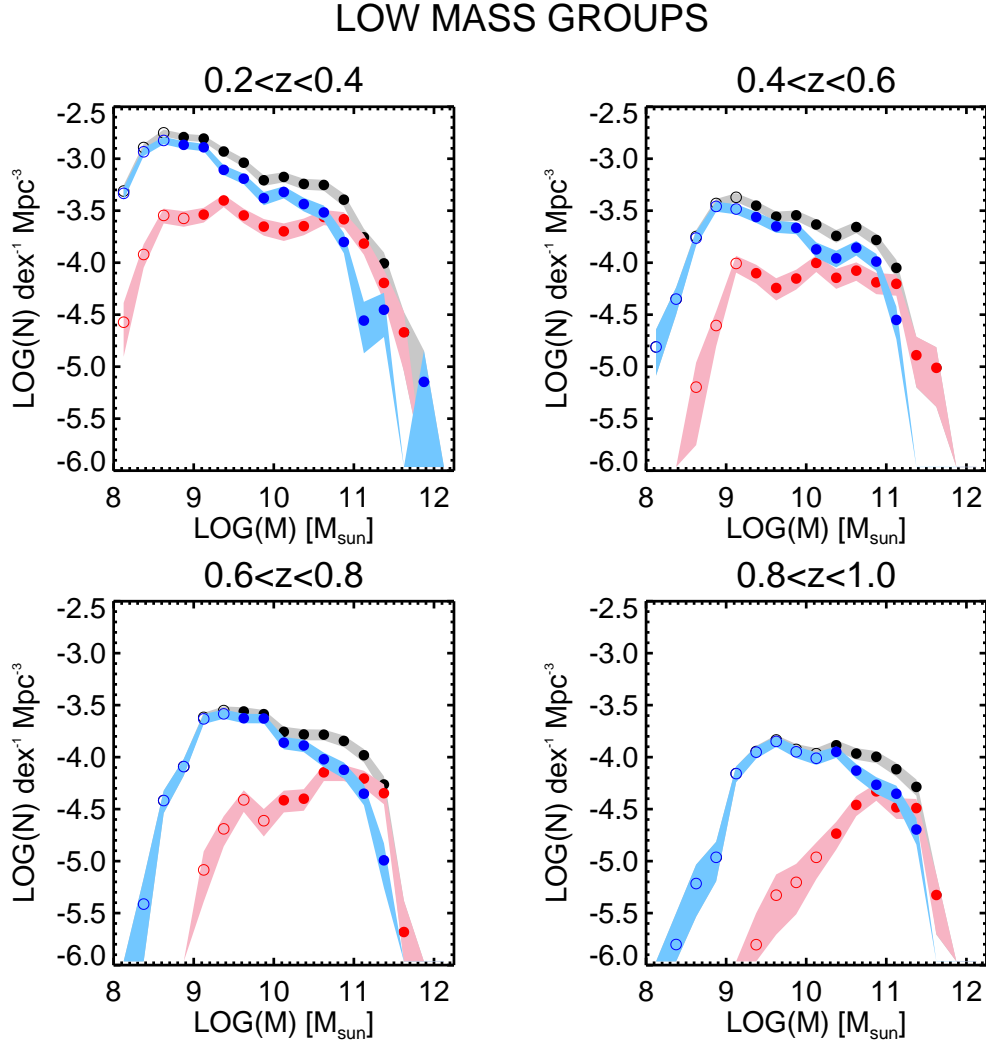


Figure 24: GSMF for all (black), active (blue), passive (red) galaxies within the COSMOS X-ray selected groups, as a function of redshift for objects with  $M_{500} < 5 \times 10^{13} M_{\odot}$  (low-mass groups). Filled circles mark the points above the completeness stellar mass. The band represents the uncertainties on the GSMF, computed by a combination of field to field variation and small number statistics (see text).

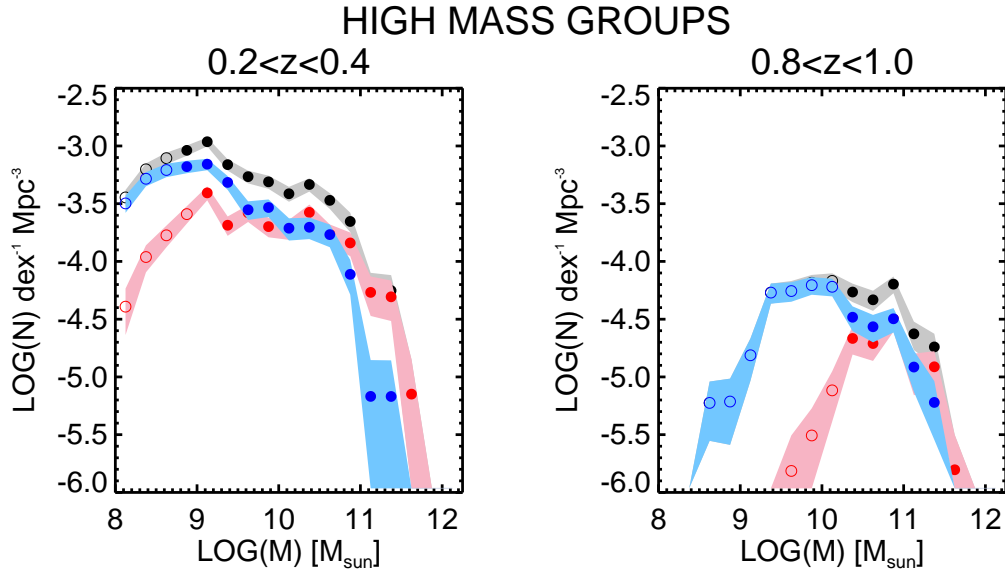


Figure 25: GSMF for all (black), active (blue), passive (red) galaxies within the COSMOS X-ray selected groups, as a function of redshift for objects with  $M_{500} > 5 \times 10^{13} M_{\odot}$  (high mass groups). Filled circles mark the points above the completeness stellar mass. The band represents the uncertainties on the GSMF, computed by a combination of field to field variation and small number statistics (see text).

#### 4.4.2 Environmental Dependence

In order to assess the environmental dependence of the GSMF, we compare its shape across three environments: field, X-ray selected low and high mass groups<sup>1</sup>. In Figure 26 and 27 we show the GSMF for passive and active galaxies in groups and the field (light orange/cyan line) in each redshift bin. When possible we distinguish between more massive (dark red/blue line) and less massive (light red/blue line) groups.

From the plot, we note that the dip is a clear feature in the field, and its amplitude decreases toward lower redshifts. A dip and upturn is found also for low mass groups, whereas it becomes less evident in more massive groups. This finding is enforced by the comparison between the  $\chi^2$  for double and single Schechter fitting performed in section 4.4.1. In particular, moving towards the most massive environment, the hump at high stellar mass becomes less prominent, while the dip gets shallower. Unfortunately we

<sup>1</sup>High and low mass groups differ by a factor of 4 in total mass in the 0.2–0.4 redshift bin, but only by a factor of 2.5 at redshifts 0.8–1.0. On the other hand the median mass of low mass groups increases by only a factor of 2 from  $0.2 < z < 0.4$  to  $0.8 < z < 1.0$ .

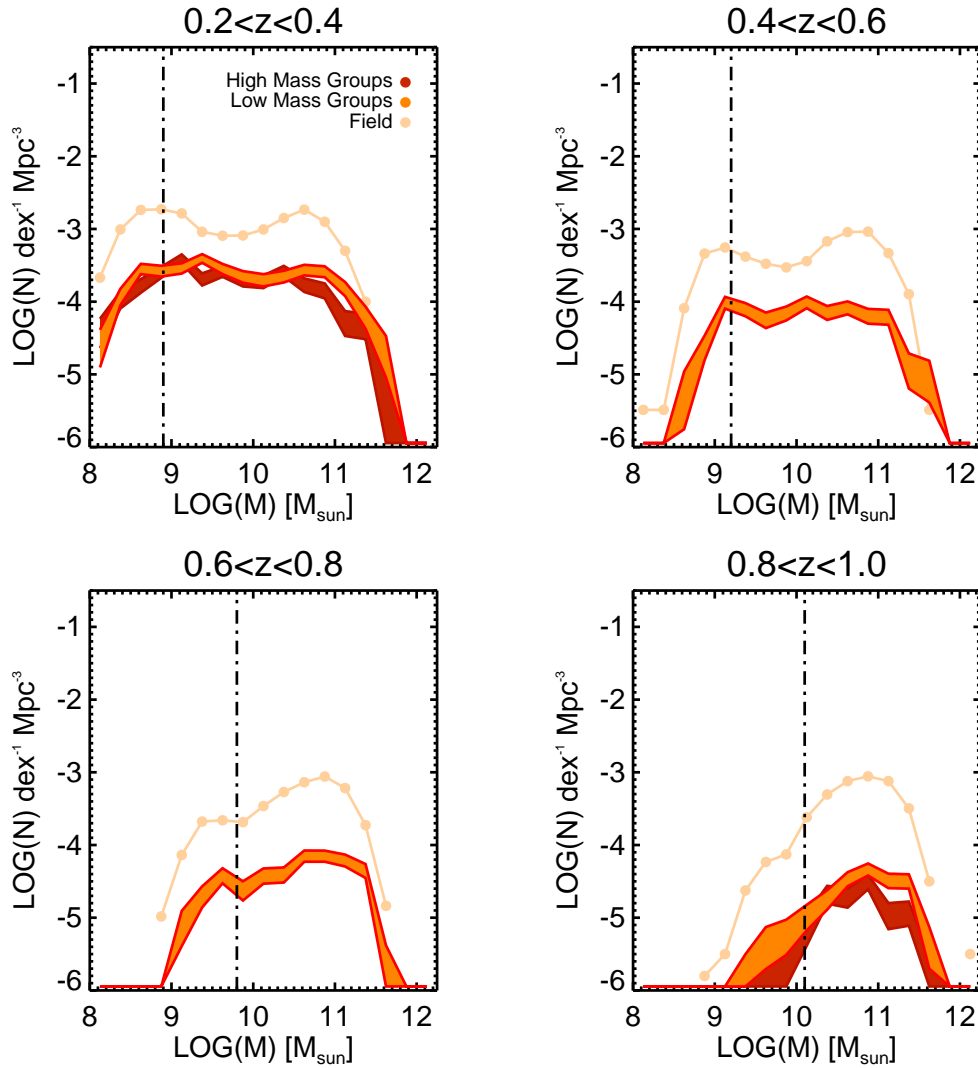


Figure 26: Passive galaxies: evolution with the environment.

cannot appreciate this at all redshifts, because of the lack of smaller groups at high redshifts and the evolution of the completeness mass with redshift, but evidence for a hump in the GSMF of groups exists also at the largest redshifts.

In order to statistically test the difference between the GSFs in different environments, we perform a  $\chi^2$ -two-sample test to check whether the two mass distribution (above the completeness mass) are drawn from the same common distribution (null hypothesis). In order to ensure the validity of this test, we consider only the stellar mass bins where the composite GSMF contains more than 5 galaxies. We perform the test on the galaxy stellar mass distributions of groups and clusters and groups and field and list the results in Table 4.4.2. In the case of passive galaxies at  $z < 0.6$  we obtain a

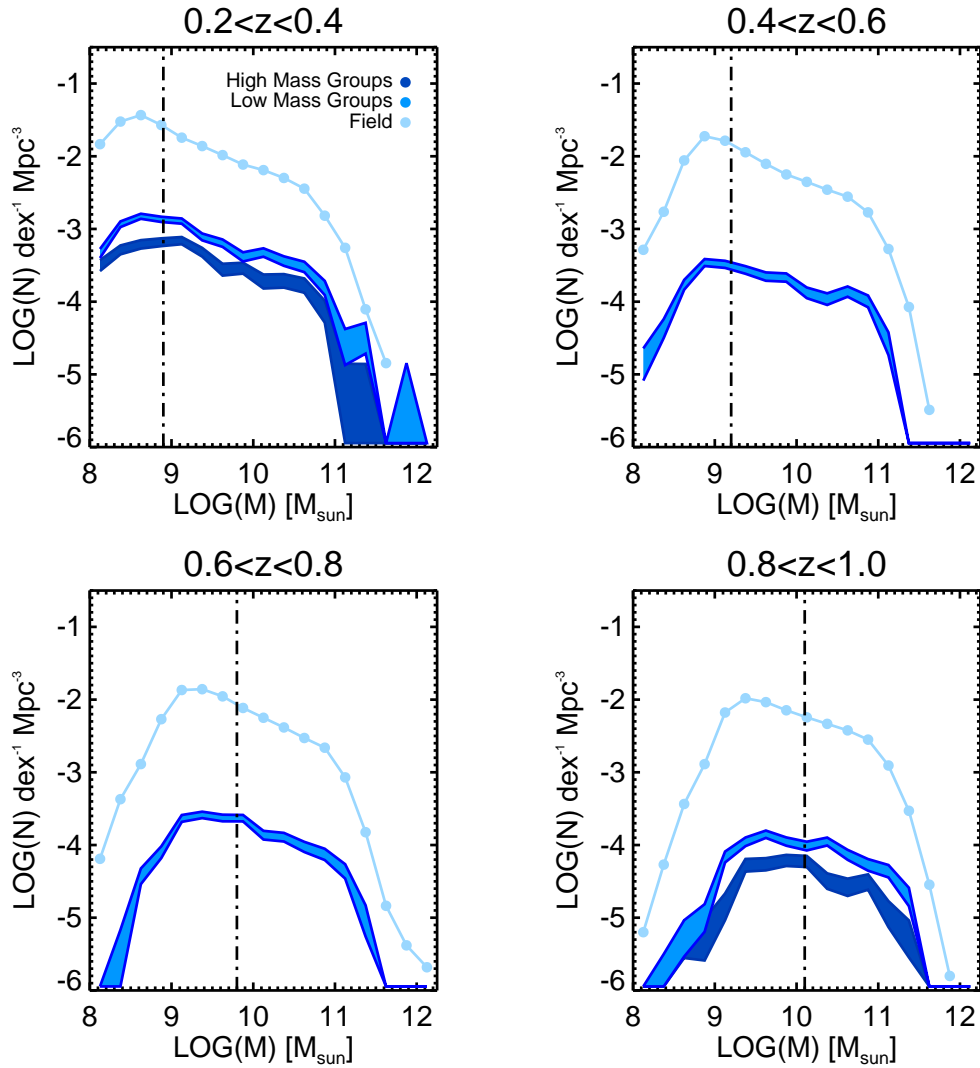


Figure 27: Active galaxies: evolution with the environment.

significant result ( $>2.5\sigma$ ): the passive GSMF of groups differs from both field's and clusters' passive GSMFs. Therefore the passive GSMF at  $z < 0.6$  strongly depends on the environment.

At higher redshift, instead, the distributions do not show a compelling evidence for a significant difference (i.e. rejecting the null hypothesis).

Differently, for the groups' active GSMF we don't report a strong dependence on the environment, since the significance of rejecting the hypothesis of a common parent distribution between groups at different masses and the field is always less than  $2.5\sigma$  in all but one case. However at  $z=0.4-0.6$  the groups' GSMF for active galaxies differs strongly from the field's GSMF (at  $\sim 5\sigma$ ). It is known that at  $z\sim 0.5$  a strong under-

density is present in the COSMOS field, signalled by a paucity of dense structures (e.g. Meneux et al. 2009 and Figure 8 in Lilly et al. 2009), also confirmed by a drop of a factor of  $\sim 3$  in the characteristic density  $\phi^*$  for the groups' GSMF (Table 4.4.1). Therefore, a difference in this redshift bin may indicate the positive feedback on star formation by environmental processes on groups' galaxies (e.g. Braglia et al. 2009).

In order to better investigate the environmental dependence of the GSMFs across the three environments considered, we produce iso- $\chi^2$  contours obtained by fitting a double Schechter function to the groups and field data. In particular we want to investigate the behaviour of the bright-end slope ( $\alpha_b$ ) and the faint-end characteristic mass ( $M_f$ ). We perform this analysis only at redshifts 0.2–0.4, where we can better constrain the characteristic mass at the faint end. We present the 1, 1.5, 2.5  $\sigma$  contour plots of the best fit double Schechter  $\alpha_b$  and  $M_f$  in Figures 28a and 28b, for passive and active galaxies respectively.

In general, we don't find a strong correlation between the best fit slope of the massive end  $\alpha_h$  and the characteristic mass of the low mass end  $M_f^*$ .

For passive galaxies (Figure 28),  $\alpha_h$  is consistent between groups and clusters, while it is inconsistent with that of the field at  $> 2.5\sigma$  level, as determined from the likelihood contours. The difference is that the groups GSMF has a much more negative (flatter) massive-end slope ( $\sim -0.2$  against  $\sim -0.8$ ), which results in a less prominent dip. The value of  $M_f$  does not exhibit a strong dependence on the environment (the  $1\sigma$  error contours overlap in this direction), though it becomes larger towards more massive systems.

The value of  $\alpha_h$  for active galaxies (Figure 28b), instead, is roughly consistent across the environments, and settles to a more negative slope than the one required for the passive GSMFs of groups at different masses ( $\sim -1.1$  against  $\sim -0.8$ ). The behaviour of  $M_f$ , despite only within the  $1\sigma$  error contours, suggests a trend across the environments, inverse to the one reported for passive galaxies:  $M_f$  decreases in higher mass systems, while it is higher in the field.

### 4.4.3 Evolution

In Figure 29 and 30 we illustrate the evolution as a function of redshift of the parameters  $M_h^*$  and  $\alpha_h$ , which describe the massive end of the best fitting Schechter function. We mark in red and blue passive and active galaxies, respectively. For low mass groups we indicate the locus of the SDSS groups at redshift  $0.01 < z < 0.2$  (Yang et al., 2009).

In general we notice a lack of evolution in the field, whereas we find a weak evolution-

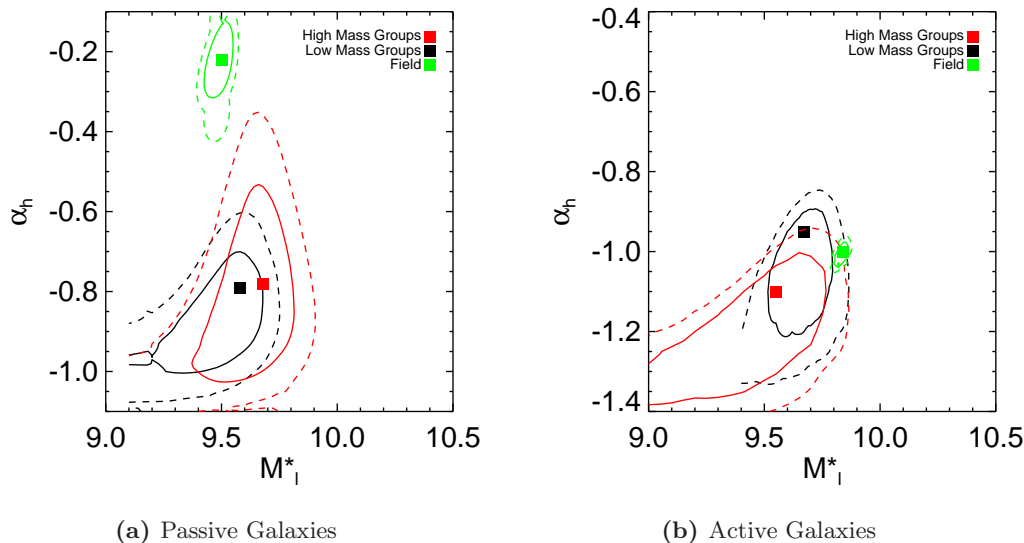


Figure 28: (a) 1,1.5 and 2.5 $\sigma$  contours of the best fit Schechter parameters for passive GSMF in low/high mass groups and field. (b) 1,1.5 and 2.5 $\sigma$  contours of the best fit Schechter parameters for active GSMF in low/high mass groups and field.

ary trend in groups between redshift 0.2 and 1.0. Furthermore, the evolutionary trend in low mass groups is analogous to that in high mass groups and the behaviours for the passive and the active populations are analogous.

In particular for groups:

- For the active population  $M_h^*$  decreases going from  $z=1.0$  to 0.2<sup>2</sup>. This may suggest that a population of active massive galaxies is being transformed into passive ones throughout the cosmic time. It is encouraging that, extrapolating this trend to redshift zero, we find good agreement with the values found by Yang et al. (2009) for the best fit GSMF in the SDSS groups.
- For passive galaxies,  $\alpha_h$  becomes more negative towards lower redshifts. This may indicate that below  $z\sim 1$ , we are witnessing the build up of a passive, intermediate mass population ( $M\sim 10^{10} M_\odot$ ) within X-ray detected systems. Consistently, the dip in the GSMF of passive galaxies gets shallower in amplitude.
- We don't find a significant redshift evolution in the value of  $M_h^*$  for passive galaxies in different environments, suggesting that the high mass end of the passive GSMF is already in place at redshift 1.0 whatever the environment.

<sup>2</sup>We spent a word of caution on the point at  $0.8 < z < 1.0$  for the groups/clusters' active GSMF parameters: the degrees of freedom are less than the free parameters (see Table 4.4.1), therefore we don't draw any conclusion based only on the behaviour of this point.

- While in groups and clusters the characteristic mass  $M_h^*$  is higher for passive than for active galaxies at all redshifts, in the field the values of  $M_h^*$  for the passive GSMF are systematically lower than those for the active one. This indicates that there is a lack of very massive ( $M > 10^{11} M_\odot$ ) passive or quiescent galaxies in the field. This implies that the formation of the most massive early type galaxies is likely the outcome of environmental effects (such as merging) that don't occur in the field, where mass grows mostly by star formation.
- Active and passive field GSMF show very different values of  $\alpha_h$ , the latter being more negative for active than for passive galaxies. This relates to what is shown in Figure 28 and 29, the significant difference in the field passive and active galaxies GSMF. Here we confirm that this holds also at higher redshifts.

## 4.5 Discussion

### 4.5.1 Passive galaxies: environmental dependence

We investigated the environmental dependence of the GSMFs among three environments (low-mass groups, high-mass groups and field), for passive and active galaxies. Both populations show a clear dependence on the environment, and the effect is larger for passive galaxies. In particular we show that the shape of the GSMF is adequately described by a double Schechter function in the field and in low-mass groups, whereas a single Schechter function may hold in high mass groups.

From Figure 26, scaling the field GSMF to the same normalisation of the groups, we can clearly see that a “dip” at low stellar mass ( $10^9$ – $10^{10} M_\odot$ ) is present in the passive GSMF for the field. From Figure 28a we can see how this feature depends on the environment at redshifts 0.2–0.4. The slope of the bright end of the double Schechter function describes the strength of the “dip” in the GSMF. The need for a much less negative slope for the field indicates that the dip is a marked feature in this environment. A more negative  $\alpha_h$  describes a less evident dip in groups, which suggests the presence of a population of passive intermediate-mass galaxies which is not present in the field. Indeed, comparing the GSMF in the different environment, this effect is driven by an excess of passive galaxies between  $10^9$ – $10^{10} M_\odot$  in the groups environment. A similar finding, i.e. the existence of a significant difference between the infrared luminosity function in clusters relative to the field, mostly due to non-emission line galaxies, was reported by Balogh et al. (2001).

Furthermore our result echoes that obtained by Iovino et al. (2010) using zCOSMOS data: these authors suggest that at  $z < 1$  the transition of low mass galaxies from the

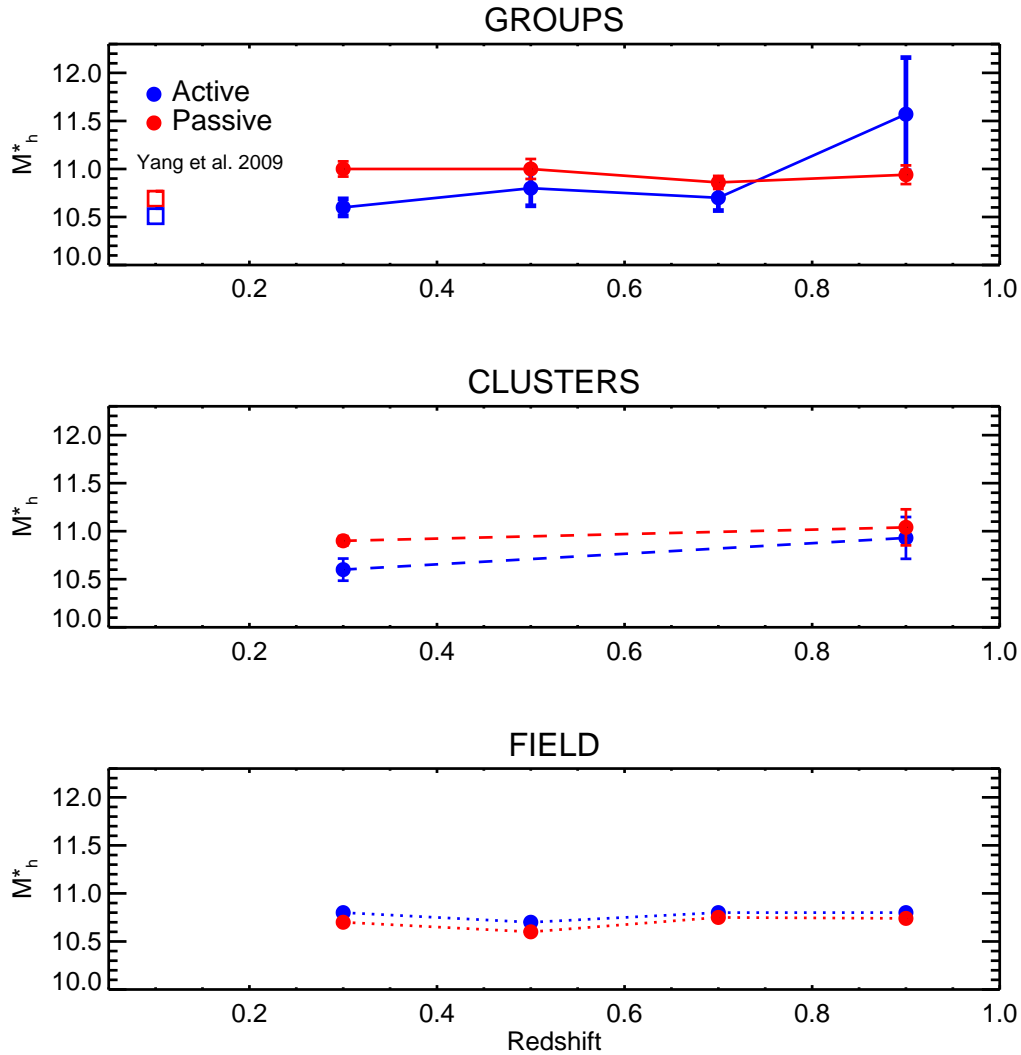


Figure 29: Evolution of the characteristic mass for the massive Schechter component ( $M_h^*$ ) as a function of the redshift in groups, clusters and in the field.

blue to the red cloud is more efficient in groups than for isolated galaxies. They suggest the emergence of a nurture-driven red galaxy population, in contrast to the nature-driven massive red galaxies ( $M > 10^{10.8} M_\odot$ ), which are already in place in all the environments at  $z \sim 1$ . This population makes the difference from the GSMF of the field at similar stellar masses.

The mechanism driving the excess of the passive intermediate/low mass galaxies in structures ought to be efficient already at the low mass groups regime, suggesting that ram-pressure stripping is not the likely process. Indeed the effectiveness of stripping

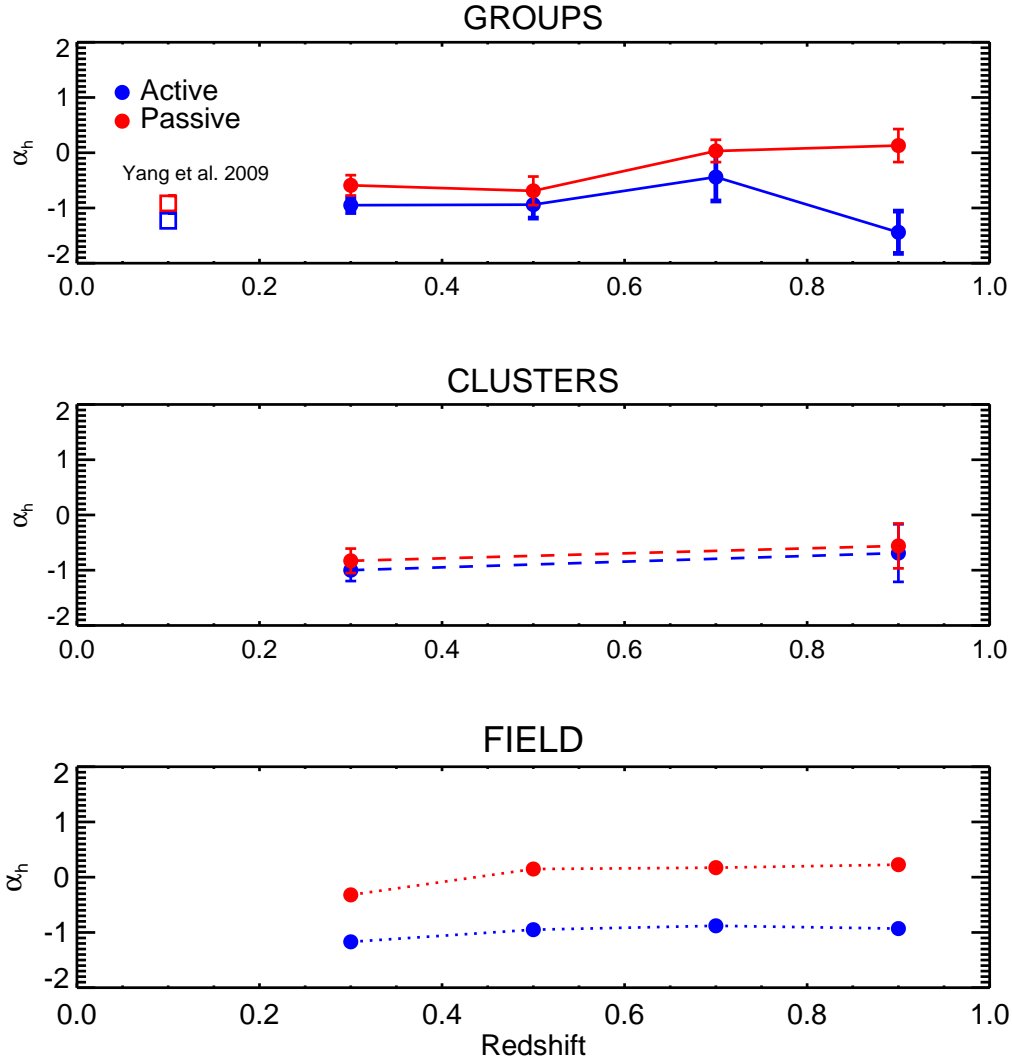


Figure 30: Evolution of the slope for the massive Schechter component ( $\alpha_h$ ) as a function of the redshift in groups, clusters and in the field.

by ram–pressure depends on the relative velocity of galaxies to the ICM, and this varies greatly between high and low mass groups. Finn et al. (2008) come to a similar conclusion analyzing the star formation rate from the  $H_\alpha$  line emission in local groups and clusters (but see also Bolzonella et al. 2009).

However,  $M_1^*$  for the passive GSMF increases passing from low–mass to high mass groups, implying that it is easier to quench galaxies down to lower stellar masses in massive systems.

## 4 The GSMF of COSMOS groups

---

Furthermore the value of  $\alpha_h$  for groups of different masses is comparable within  $1\sigma$ , suggesting that the bulk of the massive passive galaxy population is already formed in systems of  $\sim 10^{13} M_\odot$ .

In this picture, when we consider the GSMF for passive galaxies, the group environment tends to have its own identity with respect to the field and more massive systems.

### 4.5.2 Active galaxies: environmental dependence

The active GSMF is adequately described by a double Schechter mass function across all the environments. This finding is at odds with the interpretation of the bimodal GSMF as due to the dichotomy between active and passive galaxies (e.g. Bolzonella et al. 2009). In this picture red/passive galaxies are responsible for the hump at high mass, while active/blue galaxies define the upturn at lower mass and both populations are adequately described by a single Schechter function. It is possible that a sparser sampling of the high mass end of the active galaxy population in dense environments (likely for studies of spectroscopically selected samples as Balogh et al. 2001 and Bolzonella et al. 2009) could explain why such studies came to this conclusion.

The presence of an extra Schechter component, describing a blue hump at high mass, suggests that the red/blue galaxies dichotomy may not be the only explanation of the observations. For example, the presence of a blue hump is a prediction from the simulations by Faltenbacher et al. (2010). These authors propose an alternative model according to which the differences in the GSMF as a function of the environment stem from those in the underlying mass distribution of halos. In particular the hump in the GSMF is associated with the central group galaxies and the bimodality would be described by that of central/satellites galaxies. In a future paper we will investigate this hypothesis in depth.

Active galaxies show a less pronounced dependence on the environment, as shown by the results of the  $\chi^2$ -two-sample test (Table 4.4.2). This result is consistent with those obtained at low redshift by comparing the shape of the UV luminosity function of clusters and field galaxies (Cortese et al., 2008). According to these authors the overall similarity in the shape of the active galaxy population may be interpreted as follows: active galaxies have only recently fallen into groups/clusters and they have not been affected yet by the surrounding environment (e.g. Tully & Shaya 1984). Therefore active galaxies still maintain the memory of the field mass distribution. However from Figure 28b we report a weak trend for the characteristic mass at the low mass end ( $M_h^*$ ) to decrease in higher mass systems. This trend is likely due to the complementary passage to the passive population of higher mass galaxies in clusters with respect

to groups and the field, reflecting the underlying color–density relation.

### 4.5.3 Evolution

The most interesting result presented in our analysis of the evolution is that the massive end of groups’ passive GSMF evolves in the direction of becoming more similar to the field at high redshift. The massive end slope tends to become more positive, with the result that at redshift  $\sim 1$  the dip at  $10^9$ – $10^{10} M_{\odot}$  dip is more evident in the passive GSMF. Indeed if passive galaxies in this mass range are the product of environmental effects, this would indicate that the environmental mechanism is more effective on those galaxies at lower redshifts. Our result is in line with the prediction by recent simulations (McGee et al., 2009) that by  $z = 1.5$  galaxy groups and clusters will display little to no environmental effects.

## 4.6 Summary

In this paper we investigated the shape of the galaxy stellar mass function and its evolution as a function of the environment and redshift. Combining the photometric and X–ray information in the COSMOS survey we consider galaxies in three different environments: field, low mass groups ( $M < 5 \times 10^{13} M_{\odot}$ ), high mass groups ( $M > 5 \times 10^{13} M_{\odot}$ ). In addition we divide the galaxy sample in active and passive, according to their spectro–photometric type. Our main findings are the following:

1. There is a dip at intermediate stellar masses in the GSMF for field and low mass groups at  $z < 1$ . The feature is present both for active and passive galaxies.
2. The dip is more pronounced for the passive population. The amplitude of the dip for passive galaxies depends on the environment, at least at low redshift ( $z < 0.6$ ). Indeed at low redshift there is a marked difference between low/high mass groups’ and field’ GSMF, namely groups show a much less pronounced dip when compared to the field. We interpret this difference with the presence of an excess of passive galaxies at intermediate mass ( $M \sim 10^{10} M_{\odot}$ ) in groups, likely associated with environmental effects.
3. At high redshift the difference between the passive GSMF for the groups and the field (at  $M > 10^{10.1} M_{\odot}$ ) decreases. On one hand this suggests that the passive galaxies at  $M > 10^{11} M_{\odot}$  are already in place, independently on the environment, in line with the downsizing scenario. On the other hand it also indicates that the

## 4 The GSMF of COSMOS groups

---

environmentally driven growth of the passive population at intermediate mass has not yet taken place at  $z=1$ .

### Acknowledgements

SG acknowledges support by the DFG Cluster of Excellence ‘Origin and Structure of the Universe’. We acknowledge the contributions of the entire COSMOS collaboration; more informations on the COSMOS survey are available at <http://www.astr.caltech.edu/~cosmos>.

Table 7: Schechter best fit parameters to the GSMF

z		$\phi_1$	$\alpha_1^a$	$\log(M_1^*)$	$\phi_h$	$\alpha_h$	$\log(M_h^*)$	$\chi_{double}^2{}^b$	dof	$\chi_{single}^2{}^c$
HIGH MASS GROUPS										
0.2-0.4	Passive	0.083± 0.012	-1.85	9.55± 0.07	0.333± 0.048	-0.83± 0.22	10.90± 0.05	1.24	6	0.90
	Active	0.190± 0.067	-1.73	9.50± 0.13	0.324± 0.114	-1.00± 0.20	10.60± 0.12	1.74	7	1.80
0.8-1.0	Passive	-	-	-	0.050± 0.020	-0.56± 0.41	11.04± 0.19	-	3	1.40
	Active	-	-	-	0.062± 0.030	-0.69± 0.52	10.93± 0.22	-	2	0.70
LOW MASS GROUPS										
0.2-0.4	Passive	0.136± 0.014	-1.85	9.88± 0.03	0.545± 0.056	-0.59± 0.18	11.00± 0.08	0.33	6	2.00
	Active	0.362± 0.088	-1.73	9.58± 0.09	0.615± 0.149	-0.95± 0.13	10.60± 0.09	1.97	8	2.50
0.4-0.6	Passive	0.047± 0.007	-1.84	9.46± 0.09	0.160± 0.000	-0.69± 0.26	11.00± 0.10	1.24	5	0.90
	Active	0.181± 0.079	-1.71	9.57± 0.12	0.200± 0.087	-0.94± 0.24	10.80± 0.18	2.39	4	2.10
0.6-0.8	Passive	-	-	-	0.211± 0.021	0.03± 0.20	10.86± 0.07	-	4	1.40
	Active	0.237± 0.051	-1.61	10.00± 0.10	0.237± 0.051	-0.44± 0.43	10.70± 0.13	0.48	3	1.50
0.8-1.0	Passive	-	-	-	0.117± 0.013	0.13± 0.30	10.94± 0.10	-	3	1.00
	Active	-	-	-	0.034± 0.053	-1.44± 0.38	11.57± 0.59	-	2	0.50
FIELD										
0.2-0.4	Passive	0.952± 0.034	-1.85	9.47± 0.01	3.808± 0.135	-0.32± 0.04	10.70± 0.10	3.06	7	19.00
	Active	3.314± 0.130	-1.73	9.78± 0.01	5.634± 0.220	-1.17± 0.04	10.80± 0.10	4.18	9	16.00
0.4-0.6	Passive	0.726± 0.024	-1.84	9.46± 0.01	2.460± 0.083	0.15± 0.03	10.60± 1.00	2.14	6	14.00
	Active	5.728± 0.161	-1.71	9.72± 0.01	5.728± 0.161	-0.95± 0.03	10.70± 0.10	1.48	7	30.00
0.6-0.8	Passive	-	-	-	2.289± 0.059	0.17± 0.05	10.75± 0.01	-	4	0.40
	Active	6.258± 0.361	-1.61	9.98± 0.02	6.258± 0.361	-0.88± 0.03	10.80± 0.10	2.89	7	16.00
0.8-1.0	Passive	-	-	-	2.277± 0.055	0.23± 0.06	10.74± 0.01	-	3	0.40
	Active	5.096± 0.281	-1.66	9.98± 0.03	6.115± 0.338	-0.93± 0.03	10.80± 0.10	6.08	5	9.40

<sup>a</sup>Fixed to the value for the correspondent redshift found in D09<sup>b</sup>Reduced  $\chi^2$  for a fit with a double Schechter function<sup>c</sup>Reduced  $\chi^2$  for a fit with a single Schechter function

Table 8: Result of the  $\chi^2$ -two sample test on the passive and active GSMF of low/high mass groups and field.

$z$	$\chi^2_{low-mass,high-mass}$	$\sigma$	$\chi^2_{low-mass,field}$	$\sigma$	$N_{bins}$
PASSIVE GALAXIES					
0.2–0.4	20.9	$2.5\sigma$	34.9	$4.0\sigma$	10
0.4–0.6	–	–	26.5	$3.5\sigma$	8
0.6–0.8	–	–	11.3	$1.7\sigma$	7
0.8–1.0	1.98	$0.33\sigma$	6.14	$1.3\sigma$	5
ACTIVE GALAXIES					
0.2–0.4	5.89	$0.6\sigma$	13.1	$1.8\sigma$	8
0.4–0.6	–	–	39.0	$4.8\sigma$	8
0.6–0.8	–	–	13.6	$2.36\sigma$	6
0.8–1.0	1.89	$0.3\sigma$	9.23	$1.9\sigma$	5

# Bibliography

- Arnouts, S., et al. 2007, *A&A*, 476, 137
- Balogh, M. L., Christlein, D., Zabludoff, A. I., & Zaritsky, D. 2001, *ApJ*, 557, 117
- Baldry, I. K., Glazebrook, K., & Driver, S. P. 2008, *MNRAS*, 388, 945
- Bolzonella, M., et al. 2009, [arXiv:0907.0013](https://arxiv.org/abs/0907.0013)
- Braglia, F. G., Pierini, D., Biviano, A., Böhringer, H. 2009, *A&A*, 500, 947
- Capak, P., et al. 2007, *ApJS*, 172, 99
- Cortese, L., Gavazzi, G., & Boselli, A. 2008, *MNRAS*, 390, 1282
- Driver, S. P., Phillipps, S., Davies, J. I., Morgan, I., & Disney, M. J. 1994, *MNRAS*, 268, 393
- Drory, N., Bender, R., Feulner, G., Hopp, U., Maraston, C., Snigula, J., & Hill, G. J. 2004, *ApJ*, 608, 742
- Drory, N., et al. 2009, *ApJ*, 707, 1595
- Faltenbacher, A., Finoguenov, A., & Drory, N. 2010, [arXiv:1002.0844](https://arxiv.org/abs/1002.0844)
- Finoguenov, A., et al. 2007, *ApJS*, 172, 182
- Finn, R. A., Balogh, M. L., Zaritsky, D., Miller, C. J., & Nichol, R. C. 2008, *ApJ*, 679, 279
- Giodini, S., et al. 2009, *ApJ*, 703, 982
- Ilbert, O., et al. 2009, *ApJ*, 690, 1236

## Bibliography

---

- Ilbert, O., et al. 2010, *ApJ*, 709, 644
- Iovino, A., et al. 2010, *A&A*, 509, A260000
- Leauthaud, A., et al. 2010, *ApJ*, 709, 97
- Lilly, S. J., et al., 2007, *ApJS*, 172, 70
- Lilly, S. J., et al. 2009, *ApJS*, 184, 218
- Markwardt, C. B. 2009, *Astronomical Society of the Pacific Conference Series*, 411, 251
- McGee, S. L., Balogh, M. L., Bower, R. G., Font, A. S., & McCarthy, I. G. 2009, *MNRAS*, 400, 937
- Meneux, B., et al. 2009, *A&A*, 505, 463
- Pérez-González, P. G., et al. 2008, *ApJ*, 675, 234
- Polletta, M., et al. 2007, *ApJ*, 663, 81
- Salpeter, E. E. 1955, *ApJ*, 121, 161
- Schechter, P. 1976, *ApJ*, 203, 297
- Tully, R. B., & Shaya, E. J. 1984, *ApJ*, 281, 31
- White, S. D. M., & Rees, M. J. 1978, *MNRAS*, 183, 341
- Yang, X., Mo, H. J., & van den Bosch, F. C. 2009, *ApJ*, 695, 900

# Chapter 5

## Final Remarks and Future Outlook

In this thesis I have addressed a number of aspects related to the baryonic matter component of galaxy groups. Taking advantage of the unique multiwavelength dataset of the COSMOS 2° survey, I have studied the behaviours of the baryonic components (stars and gas) as separate pieces of a jigsaw puzzle, and then gathered the results to obtain and interpret the global picture.

In Chapter 2 I found that the behaviour of the stellar-to-total mass ratio in COSMOS groups and in 27 local clusters is anticorrelated with the total mass of the system. The global trend between  $f_{500}^{\text{stars}}$  and  $M_{500}$  is consistent with that observed in clusters at  $z < 0.3$  using much smaller samples. I extended previous results to the low mass regime by one order of magnitude and to higher redshifts.

The difference in the number of stars formed per unit of halo mass between groups and clusters can be interpreted in terms of a dependence of the star formation efficiency on the total mass of the system. A possible explanation for such a variation in the star-formation efficiency has been proposed in terms of cooling flows being less efficient in shutting off star formation in groups. An alternative scenario is that clusters are formed not only by merging of groups but also accrete a large fraction of their galaxies (with a low stellar mass fraction) from the field. None of these suggestions provides a satisfactory explanation yet, and a thorough investigation of the cause of the varying galaxy formation efficiency remains an important task for the future.

In a future work I will investigate the nature of the large scatter in the  $f_{500}^{\text{stars}}-M_{500}$  relation. Indeed it is of compelling interest to understand if there is a significant difference between systems with high and low stellar mass fractions at similar total masses, which can reflect a difference in the physical processes connected with their formation and evolution. Furthermore, I plan to extend the groups sample to lower

## 5 Final Remarks and Future Outlook

---

masses at high redshifts, in order to obtain a large sample complete in total mass at  $z \geq 1$ , and further investigate the stellar mass fraction evolution (deeper XMM–Newton observations of the COSMOS field will be proposed to this purpose).

As a further main result, the combination of measured values of the stellar mass fraction with values of the gas mass fraction estimated from an average relation obtained for a local sample of groups and clusters revealed that  $f_{500}^{\text{stars+gas}}$  increases by 25% from groups to clusters. After the introduction of appropriate corrections for gas depletion and ICL contribution, the total baryonic mass fraction at the groups regime still differs from the WMAP5 value at  $3.3\sigma$ . I interpret the origin of this discrepancy as a lack of gas (by 33%), which can be caused either by feedback (supernovae and/or radio–mode AGN heating) or by “filamentary heating”. Therefore I confirm that a “missing baryon” problem does exist in galaxy groups.

In Chapter 3 I explored the radio–mode AGN feedback solution to the “missing baryon” problem, using VLA observations of the COSMOS field. Supported by the results from recent simulations, I studied the energetics of radio galaxy feedback in X–ray detected galaxy groups and estimated the effect of the energy injection. Thanks to the large survey of galaxy groups I was able to find that black hole activity is capable of outweighing the capacity of a group to hold its gas, removing a significant part of it. No similar effect is observed in more massive galaxy clusters, where the gravitational binding energy of the underlying dark matter halo restrain the gas from being removed.

New multi–frequency VLA observations of the groups considered in this work are already scheduled, in order to constrain the mechanical output of radio–galaxies with higher accuracy, and to further investigate the interplay between the radio–AGN and the surrounding intra–group gas.

In Chapter 4 I investigated the stellar mass assembly in galaxy groups over the cosmic time: I constructed the galaxy stellar mass function of X–ray detected COSMOS groups and found that the stellar mass function for passive galaxies shows a “dip” at intermediate masses ( $\sim 10^{10} M_{\odot}$ ). The amplitude of the dip decreases at higher redshift. This feature appears more marked in the field, but it is less evident in high–mass groups. I interpreted this finding by the presence of an excess of passive galaxies at intermediate mass, likely the product of environmental effects.

Furthermore, I showed that the galaxy stellar mass function for passive galaxies (at least the high mass end) in groups becomes more similar to that of the field at increasing redshifts. On one hand this suggests that the passive galaxies at  $M > 10^{11} M_{\odot}$  are already in place, independently of the environment, in line with the downsizing sce-

---

nario. On the other hand it also indicates that the environmentally driven growth of the passive galaxy population at intermediate stellar mass has not yet taken place at  $z=1$ .

In the future I intend to extend this investigation by studying the morphological mix of this intermediate stellar mass population in more detail.

Another interesting finding that I have not fully explored yet is the presence of an extra Schechter component for active galaxies, which describes a blue hump at high stellar masses. This suggests that the red/blue galaxies dichotomy, traditionally used to explain the shape of the bimodal galaxy stellar mass function, may not be the only explanation to the observation. For example, the presence of a blue hump is one of the prediction from the simulations of Faltenbacher et al. (2010). These authors propose an alternative model: the differences in the GSMF as a function of the environment stem in these simulations from the underlying mass distribution of dark matter haloes. In particular the hump in the GSMF would be associated with the central group galaxies and the bimodality could be described by that of central/satellite galaxies. In a further paper I will investigate this hypothesis in depth.

A clear picture emerges from my research: groups are very intriguing objects, and not only scaled down versions of clusters. In particular they are excellent cosmic laboratories to study the interplay of physics with the different baryonic components. In general I found that galaxy groups, even if formed from the same ingredients as galaxy clusters (i.e. dark matter, gas and stars), show remarkable differences from the latter when considering the relative contributions to the total mass, the distribution of the individual components, the energetics, and the evolution.

Thanks to the multiwavelength approach used in this research, together with a careful statistical analysis of the results, I was able to offer direct and stringent constraints on models for galaxy/structure formation and evolution. This thesis has demonstrated the importance and the power of such a detailed survey approach for studies of galaxy groups and galaxy evolution.



# Acknowledgements

Finally I would like to thank all the people that made this thesis possible.

First of all thanks to my supervisor Hans Böhringer, for your invaluable advices and continuous encouragement during these three years. Every time I entered your office I knew I could find not only irreplaceable scientific support, but also a remarkable person. This thesis would not be the same without the precious support of Daniele Pierini, which with infinite patience thought me so many things about optical astronomy and life. Thanks to Alexis Finoguenov for having thought me a great deal about science, science politics and salsa dancing. Now I can handle the “waterfall of ideas”. A special thanks goes to Gigi Guzzo for his always present unconditional support: I would not be where I am without having met you. Thanks to Gabriel Pratt for advices and teaching me some English (wait, Irish?). Thanks to Hannelore Hämmerle for the last minute translation of my summary into German...so kind!

In these three years I met so many wonderful persons which I would like to thank, simply for the fact of existing. Thanks to Marcella, Angela Nico and Mara for all the nice moments, coffee breaks and friendship. Thanks to Betta, for your friendship and the shopping together. Thanks to my officemate Veronica for tolerating my mess. Thanks to all the people I had party with: I had so much fun over these three years! A special thanks to my best friends of so many years: Cri, Fra, Mone, Simo and Claudio. Life is so much happier knowing you're there.

Very special thanks go to my family. Many of the things I have done in life would have not been possible without your help, support, and encouragement. *Grazie per aver sempre sostenuto le mie scelte con fiducia ed incoraggiamento. Questa tesi, che é dedicata a voi, é solo un piccolissimo segno dell' affetto che nutro nei vostri confronti.* And last, but not least, special thanks to Rasmus, for just being what you are, for the joy and the serenity you gave me. You're right: the rainbow won't wait while I do the work.



# Curriculum Vitae

## Stefania Giodini

Max Planck Institut  
für Extraterrestrische Physik  
Giessenbachstrasse, D-85748  
Garching bei München

Phone: (089) 30000-3340  
Fax: (089) 30000-3569  
Email: [giodini@mpe.mpg.de](mailto:giodini@mpe.mpg.de)

### Personal

- Date of birth: August 6, 1982.
- Place of birth: Erba (CO), Italy
- Italian Citizen.
- Gender: Female.
- Marital Status: Single

### Education

- B.S. Physics, Universita' degli Studi Milano-Bicocca, 2004.
- M.A. Astrophysics, Universita' degli Studi Milano-Bicocca, 2006.
- Ph.D. Physics, Ludwig Maximilian Universität München, 2010.

Last updated: June 2, 2010

<http://www.mpe.mpg.de/~giodini/Stefania@MPE.html>



# Publication List

## First Author Refereed Journal Articles:

- **Giodini, S.**, and 15 colleagues 2010. Radio galaxy feedback in X-ray selected groups from COSMOS: the effect on the ICM. ArXiv e-prints arXiv:1002.4212.
- **Giodini, S.**, and 26 colleagues 2009. Stellar and Total Baryon Mass Fractions in Groups and Clusters Since Redshift 1. *Astrophysical Journal* 703, 982-993.
- Giodini S. et al., The Galaxy Stellar Mass Function of COSMOS X-ray detected groups: evolution and dependence on the environment. To be submitted.

## Other Refereed Journal Articles:

- Oklopčic, A., Smolčić, V., **Giodini, S.** and 8 colleagues, 2010. Using WAT radio galaxies to identify dynamically young galaxy clusters: a case study in the COSMOS field at  $z=0.53$  accepted for publication to *Astrophysical Journal*
- Civano, F. and 41 colleagues including S. Giodini, 2010. A Runaway Black Hole in COSMOS: Gravitational Wave or Slingshot Recoil?. ArXiv e-prints arXiv:1003.0020.
- Leauthaud, A. and 20 colleagues including S. Giodini, 2010. A Weak Lensing Study of X-ray Groups in the COSMOS survey: Form and Evolution of the Mass-Luminosity Relation *Astrophysical Journal* 709, 97-114.
- Finoguenov, A., and 32 colleagues including S. Giodini 2007. The XMM-Newton Wide-Field Survey in the COSMOS Field: Statistical Properties of Clusters of Galaxies. *Astrophysical Journal Supplement Series* 172, 182-195.